Reactions of molecular dications in the gas-phase

Nurun Tafadar

Thesis submitted for Degree of Doctor of Philosophy

2001

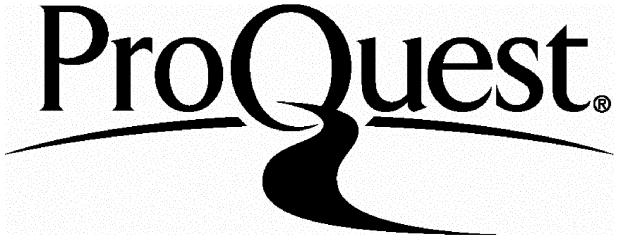

Abstract

This thesis presents the results from a series of experiments investigating the reactivity of gas phase molecular dications with neutral collision partners, at collision energies between 3 and 13 eV in the laboratory frame using a crossed-beam apparatus. The experiments involve measurement of product ion intensities, which are determined by means of time of flight mass spectrometry. The experimental methodology, together with relevant theory is described in the thesis. The relative intensities of product ions formed are a powerful probe of the reaction mechanism. Where appropriate, the reactions are examined for isotope effects by using the isotopic analogue of the neutral collision partner.

Our investigation of the CF_3^{2+}/Ar collision system shows neutral loss and electron transfer dominating the product ion yield. The variation of the neutral loss ion yield with collision energy provides a first estimate of the bond energy of the weak CF_2^{2+}-F bond. *Ab initio* calculations indicate the ground state of CF_3^{2+} adopts a C_{2v} equilibrium geometry. We further conclude that at least two electronic states of CF_3^{2+} are present in the dication beam.

Intramolecular isotope effects in the reactions of CO_2^{2+} and CF_3^{2+} with HD indicates the operation of an intramolecular isotope effect, favouring the formation of the deuterated products DCF_2^+ and DCO^+. However, for the CF_3^{2+}/HD system our data reveals no isotope effect for the formation of HF^+ and the DF^+ within our experimental uncertainty. Statistical effects have been suggested as an alternative to the orientational model previously used to explain these effects.

In our investigation of the $CF_3^{2+}/H_2/D_2$ and $CO_2^{2+}/H_2/D_2$ collision systems, experiments indicate that no intermolecular effects are in operation and the observed collision energy dependence is symptomatic of the absence of a barrier to reaction. In the $CF_3^{2+}/H_2/D_2$ system we observe the formation of the XF^+ product ion; a reaction channel that has not been observed before.

Contents

Acknowledgements

I would like to thank my supervisor, Stephen Price, for his support and assistance and for being my mentor throughout my undergraduate and postgraduate years at UCL. I am very grateful to him for being patient with me and for being an excellent supervisor despite setting the lab on fire and for being responsible for various other disasters.

I would like to acknowledge the people who have helped and worked with me in the lab; Nikolas Kaltsoyannis, Dominic Kearny, Karl Newson, Natalie Love, Sarah Harper, Robin Mukherji and James Perry. Thanks also to the technical staff in the Chemistry Department at UCL and to the EPSRC for funding my research.

I would like to thank all my friends and family for their support. Finally I would like to say a big thank you to my mum and dad for their unwavering support.

Publications

"Single and double electron-impact ionisation of chlorine dioxide", Caroline O'Connor, Nurun Tafadar and Stephen D. Price, *Journal of the Chemical Society- Faraday Transactions*, **94** (1998) 1797-1803

"Bond-forming and electron transfer reactivity in the collisions of CF_2^{2+} with NH_3", Karl A. Newson, Nurun Tafadar and Stephen D. Price, *Journal of the Chemical Society- Faraday Transactions*, **94** (1998) 2735-2740

"Electron transfer and neutral loss reactions in the collisions of CF_3^{2+} with argon", Nurun Tafadar, Nikolas Kaltsoyannis and Stephen D. Price, *International Journal of Mass Spectrometry*, **192** (1999) 205-214

"Intramolecular isotope effects in the reaction of CF_3^{2+} and CO_2^{2+} with HD", Nurun Tafadar, Dominic Kearney and Stephen D. Price, *International Journal of the Chemical Society- Faraday Transactions*, submitted

Chapter 1

Introduction

1.1 Gas phase reactions of molecular dications

This thesis discusses the gas phase reactions of doubly charged molecular ions (molecular dications) with neutral target species. Molecular dications are molecular species that have undergone a double ionisation event by means of either electron impact ionisation[1-15] or photon impact ionisation.[16-22] Over recent years experimental developments have made it possible to perform detailed studies of the structure, spectroscopy and dynamics of monocations; thus a substantial amount of data now exists on these species. However, the fact that, in the gas phase, dipositive ions formed from simple molecules are, highly energized and often highly unstable species possessing markedly different properties from the corresponding singly charged ions, has resulted in these species being less well characterized.

The first detection of a gas phase molecular dication (CO^{2+}) was made in the 1930's.[23] Despite these early observations, molecular dications were generally considered a mass spectrometric curiosity and, as mentioned, were rarely the targets of experimental investigations. However, over recent years, the properties of molecular dications have been the subject of a steadily increasing number of experimental studies.[3-11,13-22,24-37] This increase is in part, due to several new experimental techniques that have been developed to probe these short-lived species. With the development of these new experimental techniques, many experimental groups are currently investigating the properties of molecular dications and, as a result, a much clearer picture is now emerging of the energetics and fates of several diatomic and a small handful of triatomic dications in low-lying electronic states. Indeed, in some cases information is now available concerning the energies and dynamics of the vibrational levels supported in dication metastable electronic states.

As with any poorly characterized species, the majority of experimental investigations have concentrated on probing the properties of molecular dications in an isolated environment. However, stimulated by the success of these experiments, attention has recently begun to be focused on the reactivity of molecular dications following 'collisions' with neutral species or photons.

At first glance, the study of molecular dications may be considered esoteric and of little relevance outside the specialized field of ion chemistry. However, the properties of dications may influence several areas of gas-phase physical chemistry. So, an understanding of the properties of such species is important if we wish to enhance our ability to understand a variety of environmental phenomena (e.g., atmospheric and ionospheric chemistry). For example, the double photoionisation of molecular species has been proposed as a source of energetic ions in planetary atmospheres including the Earth's ionosphere.[38] In addition following the observation of IR emission, doubly charged polycyclic aromatic hydrocarbons (PAH) have been proposed as existing in the interstellar medium.[39-41] Furthermore, in addition to these practical applications the modeling of molecular dications and their spectroscopic properties is also a theoretical challenge. Consequently, comparative experimental data is an essential requirement in assessing the applicability of any new theoretical methodologies.

The fact that little is known of the consequences of the interactions of molecular dications with other atoms and molecules particularly at low collision energies, has prompted a number of experimental groups to embark on programmes designed to study the interactions of molecular dications with atoms, molecules and photons. It is such studies that are the objective of this thesis, and other contributions to this field of work will be discussed where appropriate.

This thesis presents the results from an investigation of the collision-induced reactivity of several gas-phase molecular dications. Chapters 2, 3 and 4 discuss the experimental and theoretical approach used and the method of data analysis. Chapters 5, 6, 7 and 8 present the results of the experimental work carried out. The bulk of this thesis involves the presentation of the results of the experimental work. Such results are displayed in graphical and tabular format, together with a discussion of the results and the appropriate conclusions drawn from the experimental data. However, in order to place the results and conclusions discussed in this thesis into context, it is first necessary to begin with an introduction to the properties of singly and doubly charged ions, together with a brief overview of ionisation, dissociation and the relevant experimental techniques used to investigate charged species.

1.2 Properties of Doubly charged Ions

In contrast to monocations, the majority of dication electronic states are thermodynamically unstable with respect to dissociation, lying at energies above the asymptote for charge separation. As a result, upon formation, most molecular dications undergo immediate fragmentation to give a pair of singly charged ions[42] (equation 1.11) and in some cases, additional neutral products (equation 1.12)

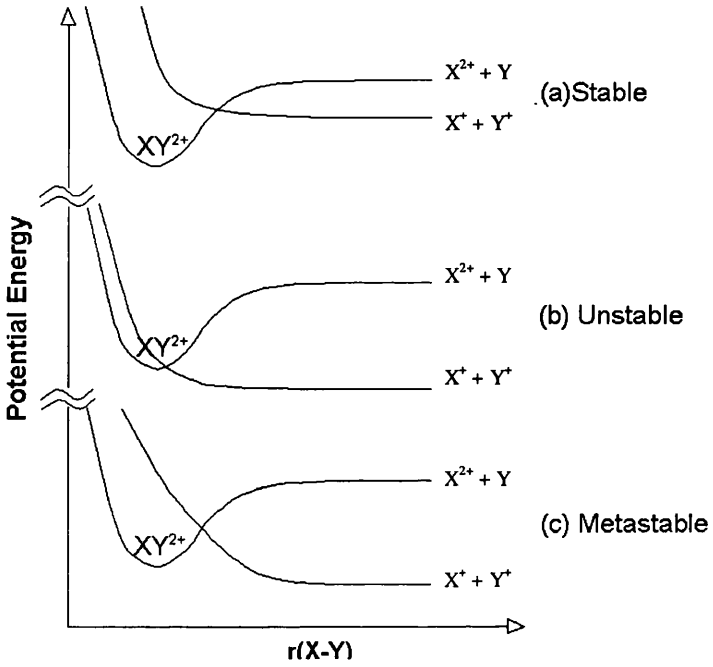

Figure 1.1 Schematic potential energy curves for diatomic dications XY^{2+}: (a) thermodynamically stable dication, (b) thermodynamically unstable dication and (c) metastable dication.

$$XY^{2+} \rightarrow X^+ + Y^+ \qquad 1.11$$

$$XY_2^{2+} \rightarrow X^+ + Y^+ + Y \qquad 1.12$$

As shown above in Figure 1.1, the stability of any molecular species depends upon the form of its potential energy surface. The majority of the electronic states of molecular dications are unstable due to the Coulombic repulsion between the two positive charges. These singly charged fragment ions usually possess considerable kinetic energy, a typical value being 6 eV for an ion pair formed from a diatomic dication. Such energy releases are equivalent to a reaction exothermicity of *ca.* 600 $kJmol^{-1}$, a value comparable with many of the chemical reactions used to propel rockets.

Lifetimes of these unbound states of molecular dications are in the sub-nanosecond range[18,43] and are discussed further below.

The fact that molecular dications, such as CO^{2+}, were first identified using mass spectrometric experiments, where ions must survive for at least 1 μs in order to be detected, clearly indicate that electronic states of dications exist which are sufficiently long-lived to be detected. For many dications at least one long-lived electronic state exists as a result of a barrier in the potential energy surface correlating with the charge separation asymptote. The presence of the barrier arises from a localized minimum in the potential energy surface. As can be seen in Figure 1.2, the energy of the localized minimum is often higher than the asymptote for charge separating dissociation. Consequently, the dications trapped in the potential well formed by the minimum are energetically unstable with respect to dissociation and are termed 'metastable'.

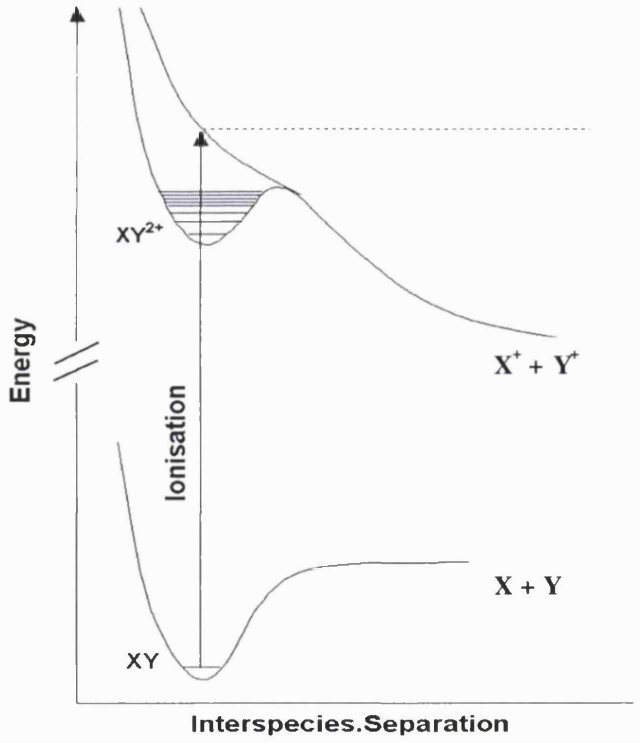

Figure 1.2 Schematic potential energy curves for a diatomic dication.

In some cases the potential well may be deep enough to support many vibrational levels,[44-46] and since dissociation can occur via tunneling through the potential barrier, the lifetimes of these metastable electronic states are dependent on factors such as the height and width of the barrier. Thus, the lifetime of a molecular dication will depend upon its degree of vibrational excitation, since a molecule at a higher lying vibrational

state will be able to tunnel through the barrier with greater ease than one lying in a lower vibrational state. Lower lying vibrational states are relatively long-lived since they are effectively trapped behind the barrier. Such behavior is indeed observed experimentally, and storage ring experiments have determined that dications in low-lying vibrational states live significantly longer than 1s.[47] In fact, because the potential energy surface of the metastable state varies approximately with r^{-1}, at large r, the barrier to charge-separating decay rapidly becomes very broad as the vibrational excitation of the dication decreases. Hence, tunneling appears to be a significant predissociation pathway only for vibrational states which lie very close to the top of the barrier, and predissociation via curve crossings to repulsive states, provides the common decay mechanism for lower lying vibrational states.

Currently there are two interpretations proposed as to the origin of the barrier in the potential energy surface which gives rise to dication metastable states. The first of these interpretations considers these states as arising, as illustrated in Figure 1.3, from an avoided crossing between an electronic state converging at large interspecies separations to a fragmented dication plus neutral ($X + Y^{2+}$), and a purely repulsive electronic state correlating with the charge separating asymptote ($X^+ + Y^+$).

Such avoided crossings can give rise to a potential well whose depth and width are sufficient to allow for the existence of metastable molecular dications.

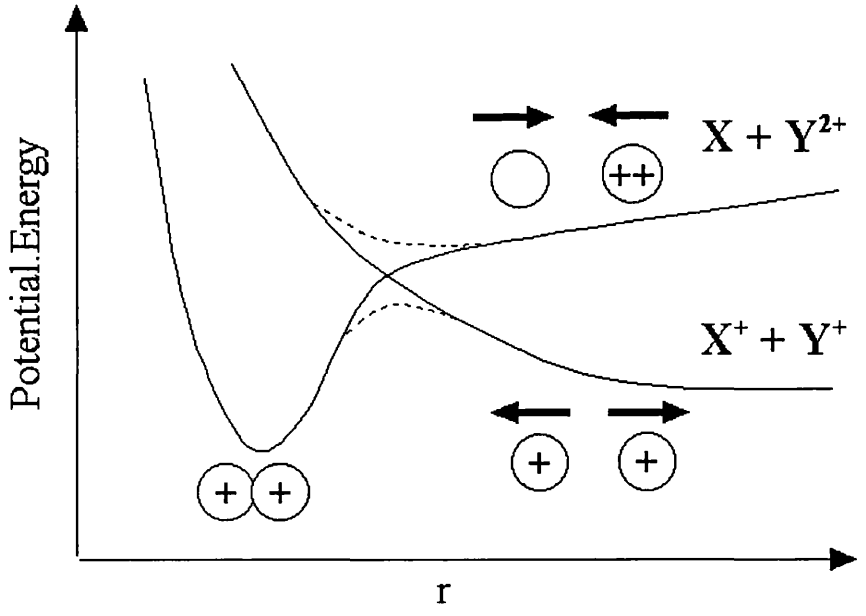

Figure 1.3 Schematic potential-energy curves illustrating how metastable dication states can arise from the avoided crossing (dashed lines) of potential-energy curves which correlate with the charge-separated ($X^+ + Y^+$) and neutral-loss ($X + Y^{2+}$) asymptotes.

O'Neil *et al* [48] following their theoretical investigation of the electronic states of the fluorine molecular dication, have proposed an alternative explanation for the existence of low-lying molecular dications. They found that the potential energy curves of this dication could be well reproduced by taking the well-established curves for the isoelectronic neutral species (O_2) and simply adding a Coulomb repulsion potential. Thus, it was proposed that dication states can be thought of as arising from the combination of the chemical binding potential of the isoelectronic neutral molecule and the Coulomb repulsion of the constituent ion pair, and metastable states will exist when the strength of the chemical bond is sufficient to overcome the repulsion between the two positive charges.

$$V_{XY}^{2+} = V_{bond} + e^2/R \qquad 1.13$$

However, in some heteronuclear diatomic dications, such as HCl^{2+}, this additive model is unsuitable since, at small internuclear distances, both positive charges reside on the same atom. [35]

1.3 Ionisation

Molecular dications may be formed by the double ionisation of a suitable neutral precursor molecule, such as the double ionisation of CF_4, which will subsequently fragment to give CF_2^{2+} or CF_3^{2+}. In order to achieve this double ionisation of neutral molecules, there are two methods that are commonly used: electron impact ionization and photon impact ionisation.

1.3.1 Electron impact ionisation

Electron impact ionisation is a long established method of ion generation and is still widely used in experiments investigating the formation and fragmentation of ions. The principal advantage of electron impact ionisation is the relative simplicity and robustness of the apparatus required to produce ions in usable quantities. The time of interaction between a bombarding electron and a molecule is usually very short and ionisation takes place by a 'vertical' process. That is to say, the electron energy measured as the minimum necessary to produce ionisation is the energy necessary to remove an electron while keeping all nuclei in the positions corresponding to their instantaneous positions in the neutral molecule.

When large amounts of energy are transferred, sufficient to expel an electron from the molecule, a molecular ion is formed. The probability that this will occur is a function of the kinetic energy of the bombarding electron. If sufficient energy is transferred from the bombarding electron to the molecule, two or more electrons can be removed, resulting in ions carrying multiple charges. The process for formation of doubly charged molecular ions by electron bombardment may be represented by:

$$M + e^- \rightarrow M^{2+} + 3e^- \qquad 1.14$$

For the majority of neutral species the electron impact double ionisation cross-section is not usually greater than 5% of the single ionisation cross-section, although a few molecules such as CS_2 [49] and larger molecules[50] have significantly larger double ionisation cross-sections. Hence, to produce a usable beam of doubly charged ions; the efficient mass selection of the reactant beam is a vitally important process.

1.3.2 Photon impact ionisation

In contrast to electron impact, the widespread use of photoionisation as a means of generating ions is a comparatively recent phenomenon. However with the increasing availability of synchrotron radiation sources and improved laser technology, photoionisation is now a frequently used method of ionisation. The double ionisation of a neutral molecule M using photon impact involves the interaction of a photon of known energy emitted by a discharge lamp,[16-19] synchrotron radiation source[20,21,51] or laser[52,53] with a neutral target, thus resulting in ionisation.

$$XY + h\nu \rightarrow XY^+ + e^- \qquad 1.15$$

Although, photon impact, as a means to double ionisation requires equipment of significant complexity, the use of this method does offer two significant advantages over electron impact. Firstly, an investigation of the ionisation of various molecules by means of a He discharge revealed that photon impact ionisation produces significantly greater numbers of doubly charged species than the impact of electrons of corresponding energies.[16] The second advantage is that the energy of the incident photon is known and therefore, in contrast to electron impact ionisation, the energy deposition in the target molecule is also known.

1.4 The bimolecular reactivity of molecular dications

A bimolecular chemical reaction involves an exchange or rearrangement of the atoms of the reactants. The prerequisite for reaction is of course the encounter itself (i.e., the collision) of the two reactants. The result of a bimolecular reaction between a doubly charged ion and a neutral collision partner is dependent upon the collision energy and the identity of the two reactants. However, the results of the experiments performed to investigate the reactivity of molecular dications with neutral collision partners at collision energies ranging from thermal to high (keV) energies,[11,13-15,26-28,54,55] have indicated that four main types of reactions have been observed.

1.4.1 Electron transfer:

Electron transfer is usually the most prolific reaction that takes place between collisions of dications and neutrals. During the encounter an electron may be transferred from the neutral to the dication leaving the ionic products in stable electronic states[4-7,26] (non-dissociative electron-transfer as shown in equation 1.16). Alternatively, the resulting ions may be left in a dissociative electronic state, and the excited ion then fragments[4-7] (dissociative electron-transfer as shown in equation 1.17).

Electron transfer (non-dissociative)

$$XY_2^{2+} + M_2 \rightarrow XY_2^{+} + M_2^{+} \qquad 1.16$$

Electron transfer (dissociative)

$$XY_2^{2+} + M_2 \rightarrow [XY_2^{+}]^{*} + M_2^{+} \rightarrow XY^{+} + Y + M_2^{+} \qquad 1.17$$

1.4.2 Collision induced charge separation (CICS) and Collision induced neutral-loss (CINL):

In these types of reaction the transfer of some kinetic energy of the collision to the dication, leaves the dication in a predissociative state. This predissociative state then either fragments to form two singly charged ions (CICS) (equation 1.18) or simply divides with the double charge intact on one of the fragments (CINL)[8,26,32] as shown in equation 1.19.

$$CO_2^{2+} + Ar \rightarrow CO^+ + O^+ \quad 1.18$$

$$CF_3^{2+} + Ar \rightarrow CF_2^{2+} + F + Ar \quad 1.19$$

1.4.3 Chemical rearrangement (bond-forming) reactions:

The data gathered on this type of reactivity to date has been extremely limited. In this type of reaction chemical rearrangement takes place following collision as shown prototypically in equation 1.20 below, which is common in many dication/neutral collision systems.

$$XY_2^{2+} + M_2 \rightarrow MXY_2^+ + M^+ \quad 1.20$$

$$Ar^{2+} + N_2 \rightarrow ArN^{2+} + N \quad 1.21^{56}$$

The investigation of this type of reactive process is the primary objective of this thesis.

1.5 Probing the properties of molecular dications

Numerous experimental methods are available to probe the properties of doubly charged molecular ions. The dissociation of molecular dications are generally investigated using coincidence techniques. In the case of these short-lived species the experimental procedure involves measuring the difference in the flight times of selected dissociation products formed upon dissociative double ionisation in a time-of-flight mass spectrometer. There are several types of coincidence experiments that detect different dissociation products in coincidence with each other.[45,57-59] These experiments can reveal information on the electronic spectroscopy of the dications and on the dynamics of the double ionisation process. The experiments can further give an insight into the dissociation processes such as fragmentation pathways and appearance energies of fragment ions. A brief summary of these experimental techniques is given below.

1.5.1 The ion-ion coincidence and photoion-photoion coincidences (PIPICO) technique

The ion-ion coincidence technique uses an electron impact time-of-flight mass spectrometer to record the coincidences between a pair of fragment ions by measuring the differences in their flight times in the spectrometer, as a result of the dissociation process below.[31,60,61]

$$e^- + XY \rightarrow [XY_2^+ + 3e^-] \rightarrow X^+ + Y^+ + 3e^- \quad 1.22$$

The PIPICO technique is the equivalent method using photoionisation.[17,62,63] These experiments measure the kinetic release upon dissociation and can reveal information of the mechanism of dissociation and branching ratios for various dissociation channels.

However, there are problems associated with the two techniques discussed above. As mentioned above, both these techniques measure the time-of-flight difference between pairs of fragment ions formed upon dissociative double ionisation. If these two techniques are applied to polyatomic dications, ion pairs of equal mass cannot be determined, since the pair will be centered around zero time of flight difference. For complex polyatomic dications, the above two techniques do not unambiguously identify the ions responsible for the coincidence signals, as there are a large number of available fragmentation channels, which yield ion pairs with the same time of flight difference.

1.5.2 Photoelectron-Photoion-Photoion Coincidences (PEPIPICO).

The development of the triple coincidence technique resolved the problems associated with the two-particle coincidence technique. In this triple coincidence technique the time of ion formation is recorded by the detection of one or more of the ejected electrons. This three-particle coincidence technique involves recording photoelectron-photoion-photoion coincidences (PEPIPICO).[64,65] In this technique a single photoelectron and a pair of photoions in coincidence is detected. By measuring the ion pair intensity and the ions' flight times with respect to the photoelectron allows a two dimensional mass spectrum to be produced. The measurement of the actual ion flight times allows the identification of all the fragment ion pairs formed upon dicationic dissociation. The PEPIPICO spectrum gives information analogous to that obtained from the two particle coincidence techniques, however allowing distinction to be made between different dissociation mechanisms, such as Coulomb explosion or a sequential mechanism, by considering the intensity distributions as a function of the initial momenta of the detected ions.

1.5.3 Covariance mapping mass spectroscopy [33,66-68]

Covariance mapping mass spectroscopy is a similar technique to PEPIPICO. In this particular technique the fragmentation of highly charged molecular ions formed in a single laser pulse is investigated.

$$XY_2^{2+} \rightarrow XY^+ + Y^+ \qquad 1.23$$

From the above equation, if the dication formed dissociates to the singly charged ions shown in the above equation and an XY^+ fragment is detected in a TOFMS, then the probability of detecting a Y^+ fragment in the same pulse is enhanced. Calculation of the covariance between the two ion flight times over a large number of laser pulses results in a positive value and the result is a two dimensional map which can be analyzed in a similar manner to the PEPIPICO spectra to identify the fragmentation products and dication dissociation mechanisms.[33,66,67]

1.5.4 Doppler Free Kinetic Energy Release spectroscopy (DFKER) [58]

Although the techniques described above can be used to determine the energy of the dication states responsible for the observed dissociation reactions, they cannot provide detailed information on the electronic or vibrational structures of the dication investigated. DFKER is a relatively newly developed technique that enables the detailed investigation of the electronic structure, as well as the dissociation dynamics of molecular dications. The simultaneous measurement of the energies of the fragment ions produced upon the dissociation of a diatomic dication results in the elimination of Doppler broadening caused by the thermal motion of the parent molecules. This Doppler broadening limits the energy resolution in conventional kinetic energy release spectra, which precludes the observation of electronic and vibrational states. This technique therefore allows detailed investigations of the electronic structure and the dissociation dynamics, of doubly charged diatomics, such as N_2^{2+}, O_2^{2+} and NO^{2+}.[12,24,69]

1.5.5 Threshold Photoelectrons Coincidence (TPESCO) [70]

This technique records the spectra of coincidences between two nearly zero energy electrons, ejected each time a dicationic state is formed within a few meV of its threshold, as the photon energy is scanned across the range of interest. Direct

observation of molecular dicationic states is therefore possible yielding information regarding the energies and relative peak intensities. This particular technique has been used to investigate the properties of doubly charged ions of HCl and Cl_2.[70]

1.6 Experimental techniques for studying ion-molecule reactions.

As discussed earlier the majority of dications are very short lived species and therefore mass spectrometric techniques are limited to the study of relatively long-lived metastable states. To study in detail properties of molecular dications, such as the dicationic lifetimes and fragmentation branching ratios and the kinetic energy release upon dissociation, new experimental techniques have been developed.

Ion-molecule reactions can be investigated using various techniques. A brief description of these techniques namely, the stationary afterglow, flowing afterglow, guided beam techniques and crossed beam apparatus employed to study ion-neutral reactions at low (thermal) collision energies is given below.

1.6.1 Stationary Afterglow (SA) technique

In the Stationary Afterglow (SA) method,[71-73] low concentrations of both the neutral reactant gas and the precursor source gas, from which the reactant ion is derived, are mixed with an inert carrier gas. The mixture of gases is then subjected to a short pulse ionising DC, RF or microwave discharge, which ionizes the source gas

During the time immediately after the switch off of applied energy (that is during the afterglow) various volume and wall processes contribute to the depletion and sometimes replenishment of populations of electrons, ions, and excited species; measurements of the time dependence of these populations provides data from which a whole variety of collision rates may be calculated. Usually the assembly of particles is contained in a vessel whose geometry is conducive to simple solutions of the diffusion equation. This is termed a time-dependent afterglow, although sometimes the term 'static' or 'stationary afterglow' is used, to distinguish it from the 'flowing afterglow'. The disadvantage of this method is that since both the precursor gas and the neutral reactant are subjected to the ionising discharge, could lead to the formation of ions in excited metastable electronic states, which could complicate the assignment of reaction products.

1.6.2 Flowing Afterglow (FA) technique

A flowing afterglow (FA) is one in which the assembly of particles is carried out along in a gas flowing along in a tube.[74,75] The population of the species under study are monitored so that the time variation is converted into a spatial variation along one dimension, pulsed operation is often used.

The advantages of the flowing afterglow derive from the flexibility with which the rate process can be controlled. Unwanted excited species are difficult to avoid in a time-dependent afterglow, because it is not possible to introduce the reactant gas after the excitation energy has been switched off; in a flowing afterglow, a reactant gas is easily introduced downstream. Many of the complications of the time-dependent afterglow are well known, and its limitations are well defined. Some of the most serious can be avoided by substituting a flowing afterglow. However the complications and limitations of the flowing afterglow are less well understood. The presence of the neutral source gas in the reaction zone introduces potential problems due to reactions between the reactant ions and their source gas, which complicates the assignment of product ions and calculation of any rate coefficients. Furthermore, the presence of any electrons in the reaction site may also complicate the analysis of the reaction products as their presence may lead to a reduction in the reactant ion current, distorting the product ion intensities through the dissociative recombination of the reactant ion (XY^+), given in the equation below

$$XY^+ + e^- \rightarrow [XY] \rightarrow X + Y \qquad 1.24$$

It is not suitable to use either the SA or FA techniques to investigate the collisional reactivity of dications, due to the presence of a buffer gas since the dications generated would electron transfer with this buffer gas.

1.6.3 Guided Beam Experiments

This method allows the use of inhomogeneous electric fields to confine and transport ions, creating the possibility of quenching ionic reagent internal excitation, as well as resulting in very efficient product ion collection over broad collision energy ranges. The technique is best suited to quantitative measurements of total cross-sections as a function of collision energy as well as accurate branching ratio measurements in a multichannel reactive system. In general, the ion of interest is prepared by either UV

photoionisation or electron impact ionisation. An octupole structure guides the primary ions through a collision region and on to a detector. The instrument may use a number of interchangeable sources, including in-line and crossed beam ionisers, an electron impact source followed by a drift region through a high-pressure gas cell to thermalize excited states in the beam, and a surface ionisation source. Following mass selection and deceleration, the ion beam enters an electrostatic octupole around which is wrapped a gas cell for the collision partner. The reaction products are trapped by the inhomogeneous electric field where they are transported to a quadrupole mass filter followed by a detector. A computer-controlled data acquisition system allows the measurements of the total cross-sections and branching ratios. Although this technique is perfectly satisfactory for the investigation of monocation reactions, this is not true for dication collision except at high collision energies (40 eV and above in the laboratory frame).

1.6.4 Crossed-Ion-Beam Spectrometry

The early investigations of the collisional reactivity of molecular dications were performed at high (keV) collision energies in conventional mass spectrometers, thus proving the feasibility of dication beam experiments. In order to investigate collisions at more realistic collision energies, specialist spectrometers must be utilized. Thus crossed beam experiments have been developed. The crossed beam method is ideally suited to the study of detailed dynamics of reactive collisions. Generally in these experiments the dication is produced by electron impact or photon impact ionisation in a low-pressure ion source. The reactant molecules are formed into a collimated beam with a narrow velocity distribution, which are then allowed to intersect at right angles in a small region, in which the reactive encounter takes place. The ambient pressure is kept low ($<10^{-6}$ Torr) to ensure single collision conditions, i.e. eliminate secondary collisions. A detector is then used to mass analyze the product ions formed. The detection system can be designed such that it can be rotated at various angles with respect to the beam system and thus measure the angular distribution of the various scattered species (reactants as well as products) in the lab coordinate system. Further refinements can be added for more detailed studies involving the use of seeded supersonic 'accelerated' beams allowing high translational energies E_T and devices for internal state selection of reactant molecules and product state analysis. The crossed

beam apparatus used to collect the data presented in this thesis will be discussed in greater detail in Chapter 2.

1.7 Conclusion

As has been discussed, although the properties of singly charged ions have been thoroughly investigated, this is not true for doubly charged molecular ions. However, advances in new experimental techniques have promoted an increasing interest in the study of doubly charged molecular ions. Despite this interest, the majority of work to date has concentrated on these species in an isolated environment. However, stimulated by the success of these experiments, attention is now being given to the reactivity of molecular dications with neutral molecular collision partners. It is the work done in this field, which this thesis aims to present. Results from a specialist spectrometer employing a crossed beam apparatus, employing time of flight mass spectrometry, will be discussed in the Chapters to follow.

References:

1 D. A. Hagan and E. J. H. D, *Rapid Commun. Mass Spectrom.* **3,** 196 (1989).

2 K. A. Newson, S. M. Luc, S. D. Price, and N. J. Mason, *Int. J. Mass Spectrom. Ion. Proc.* **148,** 203-213 (1995).

3 Z. Dolejsek, M. Farnik, and Z. Herman, *Chem. Phys. Lett.* **235,** 99-104 (1995).

4 K. A. Newson and S. D. Price, *Chem. Phys. Lett.* **269,** 93-98 (1997).

5 S. D. Price, S. A. Rogers, and S. R. Leone, *J. Chem. Phys.* **98,** 9455-9465 (1993).

6 S. A. Rogers, S. D. Price, and S. R. Leone, *J. Chem. Phys.* **98,** 280-289 (1993).

7 M. Manning, S. D. Price, and S. R. Leone, *J. Chem. Phys.* **99,** 8695-8704 (1993).

8 S. D. Price, M. Manning, and S. R. Leone, *Chem. Phys. Lett.* **214,** 553-558 (1993).

9 S. D. Price, M. Manning, and S. R. Leone, *J. Am. Chem. Soc.* **116,** 8673-8680 (1994).

10 H. R. Koslowski, H. Lebius, V. Staemmler, R. Fink, K. Wiesemann, and B. A. Huber, *J. Phys. B.* **24,** 5023-5034 (1991).

11 C. J. Reid, J. A. Ballantine, and F. M. Harris, *Int. J. Mass Spectrom. Ion. Proc.* **93,** 23-47 (1989).

12 M. Lundqvist, D. Edvardsson, P. Baltzer, M. Larsson, and B. Wannberg, *J. Phys. B.* **29,** 499-514 (1996).

13 J. D. C. Jones, A. S. M. Raouf, D. G. Lister, K. Birkenshaw, and N. D. Twiddy, *Chem. Phys. Lett.* **78,** 75 (1980).

14 X. D. Zhou, A. D. Shukla, T. R. E, and F. J. H, *Int. J. Mass Spectrom. Ion. Proc.* **160,** 49 (1997).

15 A. Ehbrecht, N. Mustafa, C. Ottinger, and Z. Herman, *J. Chem. Phys.* **105,** 9833-9846 (1996).

16 B. P. Tsai and J. H. D. Eland, *Int. J. Mass Spectrom. Ion. Proc.* **36,** 143 (1980).

17 D. M. Curtis and J. H. D. Eland, *Int. J. Mass Spectrom. Ion. Proc.* **63,** 241-264 (1985).

18 J. H. D. Eland, *Chem. Phys. Lett.* **203,** 353-362 (1993).

19 S. Leach, J. H. D. Eland, and S. D. Price, *J. Phys. Chem.* **93,** 7575-7583 (1989).

20 P. Millie, I. Nenner, P. Archirel, P. Lablanquie, P. Fournier, and J. H. D. Eland, *J. Chem. Phys.* **84,** 1259-1269 (1986).

21 E. Ruhl, S. D. Price, and S. Leach, *J. Phys. Chem.* **93,** 6312-6321 (1989).

22 T. Masuoka and I. Koyano, *J. Chem. Phys.* **95,** 909-917 (1991).

23 R. Conrad, *Physik. Z.*, 1930, **31**, 888.

24 M. Lundqvist, D. Edvardsson, P. Baltzer, and B. Wannberg, *J. Phys. B.* **29,** 1489-1499 (1996).

25 C. P. Safvan, M. Krishnamurthy, and D. Mathur, *J. Phys. B.* **26,** L837-l843 (1993).

26 S. D. Price, *J. Chem. Soc. Faraday Trans.* **93,** 2451-2460 (1997).

27 E. Y. Kamber, K. Akgungor, C. P. Safvan, and D. Mathur, *Chem. Phys. Lett.* **258,** 336-341 (1996).

28 S. D. Price, Y. Y. Lee, M. Manning, and S. R. Leone, *Chem. Phys.* **190,** 123-130 (1995).

29 P. A. Martin, F. R. Bennett, and J. P. Maier, *J. Chem. Phys.* **100,** 4766-4774 (1994).

30 P. J. Richardson and J. H. D. Eland, *Mol. Phys.* **55,** 957 (1985).

31 K. A. Newson and S. D. Price, *Int. J. Mass Spectrom. Ion. Proc.* **153,** 151-159 (1996).

32 Y. Y. Lee, S. R. Leone, P. H. Champkin, N. Kaltsoyannis, and S. D. Price, *J. Chem. Phys.* **106,** 7981-7994 (1997).

33 D. Mathur, *Phys. Rep.* **225,** 193-272 (1993).

34 M. Larsson, *Comm. Atom. Molec. Phys.* **29,** 39 (1993).

35 F. R. Bennett and I. R. McNab, *Chem. Phys. Lett.* **251,** 405-412 (1996).

36 D. Mathur, L. H. Andersen, P. Hvelplund, D. Kella, and C. P. Safvan, *J. Phys. B.* **28,** 3415-3426 (1995).

37 T. Weiske, W. Koch, and H. Schwarz, *J. Am. Chem. Soc.* **115,** 6312-6316 (1993).

38 S. Prasad and D. R. Furman, *J. Geophys. Res.* **80,** 1360 (1975).

39 S. Leach, *J.Electron Spec. Rel. Phenom.* **41,** 427 (1986).

40 A. Leger and L. d'Hendecourt, *Astron. Astrophys.* **146,** 81 (1985).

41 L. J. Allamandola, A. Tielens, G, and J. R. Barker, *J. Astrophys.* **290,** L25 (1985).

42 P. Kush, A. Hustrulid, and J. T. Tate, *Physical Review* **54,** 1037 (1938).

43 G. Roberts and A. H. Zewail, *J. Phys. Chem.* **95,** 1259 (1986).

44 M. Larsson, P. Baltzer, S. Svensson, B. Wannberg, N. Martensson, A. N. Debrito, N. Correia, M. P. Keane, M. Carlssongothe, and L. Karlsson, *J. Phys. B.* **23,** 1175-1195 (1990).

45 R. I. Hall, G. Dawber, A. Mcconkey, M. A. Macdonald, and G. C. King, *Phys. Rev. Lett.* **68,** 2751-2754 (1992).

46 G. Parlant, J. Senekowitsch, S. V. O'Neil, and D. R. Yarkony, *J. Chem. Phys.* **94,** 7208-7211 (1991).

47 L. H. Andersen, J. H. Posthumus, O. Vahtras, H. Agren, N. Elander, A. Nunez, A. Scrinzi, M. Natiello, and M. Larsson, *Phys. Rev. Lett.* **71,** 1812-1815 (1993).

48 J. Senekowitsch and S. Oneil, *J. Chem. Phys.* **95,** 1847-1851 (1991).

49 M. V. V. S. Rao and S. K. Srivastava, *J. Geophysics Rev.* **96,** 17563 (1991).

50 M. Soloman and A. Mandelbaum, *Chem. Commun.*, 890 (1969).

51 T. Masuka, *J. Chem. Phys.* **98,** 6989 (1993).

52 B. Ernstberger, H. Krause, A. Kiermeier, and H. J. Neusser, *J. Chem. Phys.* **92,** 5285 (1990).

53 Z. Fang and V. H. S. Kwong, *Phys. Rev. A.* **55,** 55 (1997).

54 M. Hamdan and A. G. Brenton, *J. Phys. B.* **22,** L 45-l 50 (1989).

55 P. J. Stephens and K. J. Jalkanen, *J. Chem. Phys.* **91,** 1376 (1989).

56 P. Tosi, R. Correale, W. L. Lu, S. Falcinelli, and D. Bassi, *Phys. Rev. Lett.* **82,** 450-452 (1999).

57 G. Dawber, A. G. McConkey, L. Avaldi, M. A. Macdonald, G. C. King, and R. I. Hall, *J. Phys. B.* **27,** 2191-2209 (1994).

58 M. Lundqvist, P. Baltzer, D. Edvardsson, L. Karlsson, and B. Wannberg, *Phys. Rev. Lett.* **75,** 1058 (1995).

59 D. M. Szaflarski, a. S. Mullin, K. Yokoyama, M. N. R. Ashfold, and W. C. Lineberger, *J. Phys. Chem.* **95,** 2122-2124 (1991).

60 B. Brehm and de. Frenes, *Int. J. Mass Spectrom. Ion. Proc.* **26,** 251 (1978).

61 K. E. McCulloh, T. E. Sharp, and H. M. Rosenstock, *J. Chem. Phys.* **42,** 3501 (1965).

62 G. Dujardin, S. Leach, O. Dutuit, P. M. Guyon, and M. Richardviard, *Chem. Phys.* **88,** 339 (1984).

63 N. J. Mason, *J. Chem. Phys.* **98,** 1750-1751 (1993).

64 L. J. Frasinski, M. Stankiewicz, K. J. Randall, P. A. Hatherly, and K. Codling, *J. Phys. B.* **19,** L819 (1986).

65 J. H. D. Eland, F. S. Wort, and R. N. Royds, *J. Electron Spectrosc. Relat. Phenom.* **41,** 297-309 (1986).

66 M. R. Bruce, L. Mi, C. R. Sporleder, and R. A. Bonham, *J. Phys. B.* **27,** 5773-5794 (1994).

67 D. A. Card, D. E. Folmer, S. Sato, S. A. Buzza, and A. W. Castleman, *J. Phys. Chem. A* **101,** 3417-3423 (1997).

68 L. J. Frasinski, A. J. Giles, P. A. Hatherly, J. H. Posthumus, M. R. Thompson, and K. Codling, *J. Electron Spectrosc. Relat. Phenom.* **79,** 367-371 (1996).

69 D. Edvardsson, M. Lundqvist, P. Baltzer, B. Wannberg, and S. Lunell, *Chem. Phys. Lett.* **256,** 341-347 (1996).

70 A. G. McConkey, G. Dawber, L. Avaldi, M. A. Macdonald, G. C. King, and R. I. Hall, *J. Phys. B.* **27,** 271-282 (1994).

71 D. Smith, A. G. Dean, and N. G. Adams, *J. Phys. D.* **7,** 1944 (1974).

72 E. W. McDaniel and E. A. Mason, *The Mobility and Diffusion of Ions in Gases*, (1973).

73 *Techniques for the study of ion-molecule reactions*, Vol. XX, edited by J. M. Farrar and W. H. Saunders (John Wiley, New York, 1988).

74 E. E. Ferguson, F. F. C, and Schmeltekopf, **5,** 1 (1969).

75 F. C. Fehsenfeld, *Int. J. Mass Spectrom. Ion. Proc.* **16,** 151 (1975).

Chapter 2

Experimental Details

2.1 Introduction

As mentioned in Chapter 1, a wide variety of experimental techniques are available to study the consequences of ionic collisions with atoms and molecules.[1] As also detailed in the preceding Chapter, this thesis reports the results of experimental work to study the gas-phase reactions of doubly charged molecular ions following their collisions with neutral molecules. The experiments were performed using a crossed beam apparatus.[2-11] The charged products of the interaction are identified and quantified using time-of-flight mass spectrometry (TOFMS).[2,6,12,13] A complete diagram of the experimental apparatus is shown in Figure 2.1. In this Chapter the experimental arrangements employed and the implementation of the techniques used are described in detail.

2.2 Ion Source

The experiments carried out in this thesis were performed by intersecting a continuous beam of mass selected molecular dications with an effusive jet of the neutral target species. The dications are generated in an ion source. The arrangement of the electron bombardment ion source is shown in Figure 2.2. The source block is cubic in shape and is constructed from stainless steel so as to be able to withstand the harsh environment of the ionisation plasma. The ion source consists of the basic block together with a thermionic tungsten filament which produces a beam of ionising electrons, an electron trap employed to regulate the filament current in order to maintain a constant rate of ion production, and an extraction electrode, which is used to extract the newly formed ions from the source block. The precursor gas enters the back of the source block via a flexible PTFE tube, passing through a narrow channel before reaching the central chamber.

Both dications and monocations are generated by electron impact ionisation from the selected precursor molecule. This is achieved by directing a focused beam of electrons with energy of the order of ~150 eV onto a perpendicularly orientated jet of precursor gas inside the ion source block. To raise the filament to its emission temperature

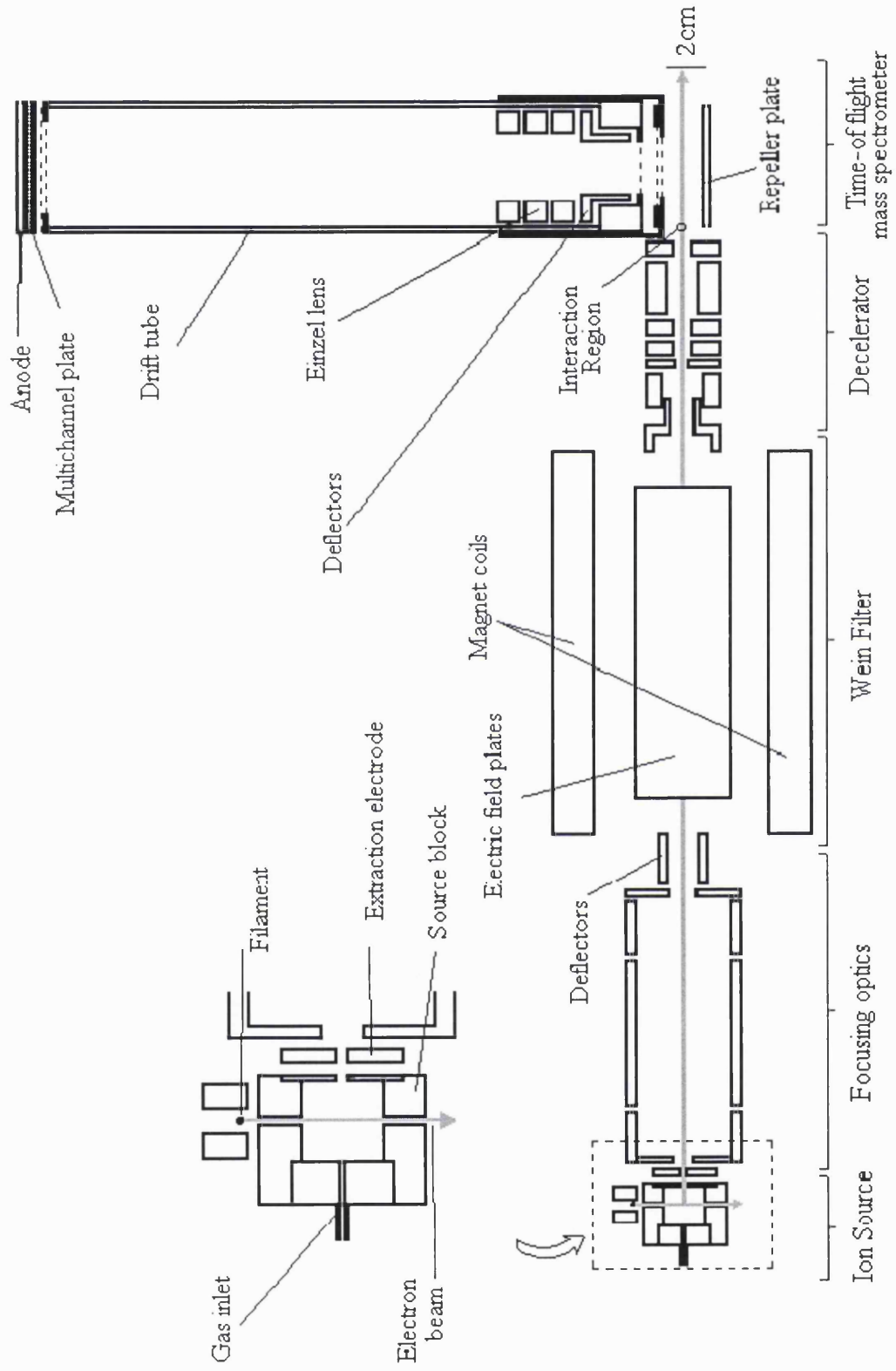

Figure 2.1 Experimental apparatus setup

requires a current of the order of 3A passing through the thermoionic tungsten filament, which produces an ejected electron current typically between 10-20 μA. The kinetic energy of these electrons can be varied simply by changing the potential difference between the filament and the ionisation chamber.

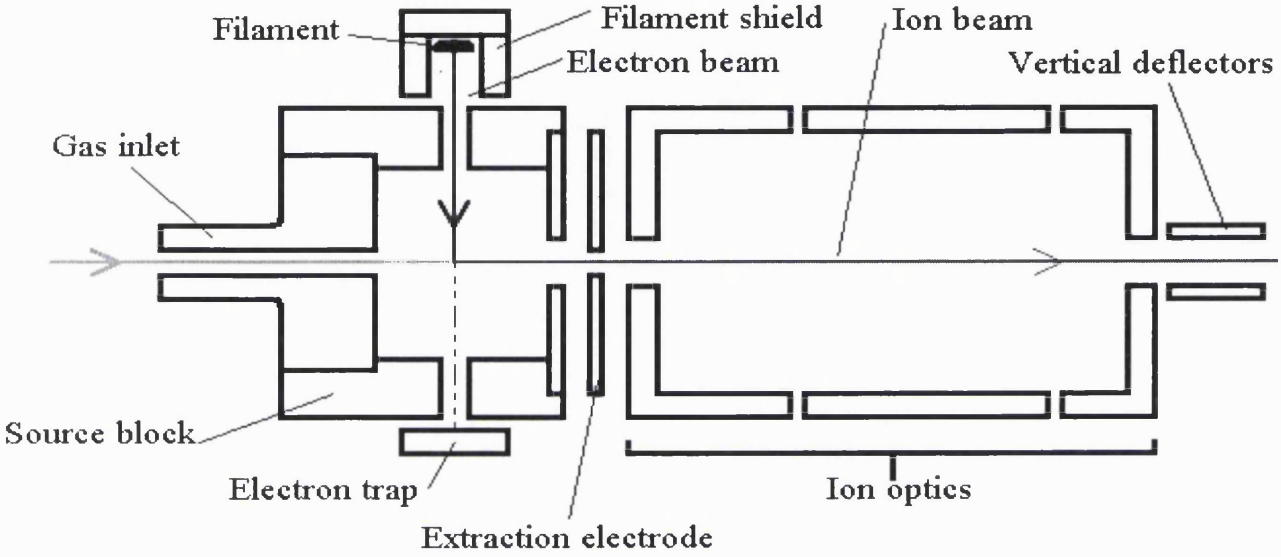

Figure 2.2 Schematic diagram of the ion source block and extraction electrode arrangement

The pressure in the source region is kept low (< 4.0 x 10^{-6} Torr) to ensure that the number of collisions taking place between the neutral precursor molecules and the dications or other ions, are minimal. Any reactions such as those shown in equations 2.11 and 2.12, taking place would result in a lower generated dication current reaching the interaction region of the time of flight mass spectrometer through various collision induced reaction channels. It is expected that the number of dications generated would be proportional to the number density of the neutral collision gas, and indeed this behavior is observed; as an increase in the precursor gas pressure gives an increase in the dication current. However, as the precursor gas pressure is increased above some optimal value, the dication current is observed to fall with increasing pressure. This decrease in the dication current may be explained as arising from the increase in the number of collision induced charge separating or charge transfer reactions taking place in the source block under these elevated pressures e.g.

$$CF_3^{2+} + CF_4 \rightarrow CF_2^+ + F^+ + CF_4 \qquad 2.11$$

$$AB_2^{2+} + XY_3 \rightarrow AB^+ + B^+ + XY^3 \quad 2.12$$

Therefore, in order to keep these adverse effects to a minimum, the background pressure is kept low. In the apparatus three diffusion pumps are used. The source region, the main chamber and the detector region are continuously pumped so that low pressures are maintained. As mentioned above the ions are generated inside the central chamber, where ionising electrons are directed perpendicularly to the trajectory of the jet of precursor gas from which the reactant dication is formed. Although the electron beam is not mono-energetic, it has a small spread of energies about the mean value, the design of the ion source ensures that the beam of ionising electrons is very narrow. The electric field within the ionisation chamber is kept very small, so that the ions formed within the narrow beam of electrons are produced at points of the same electrical potential. Therefore, as the ions are formed in a very small volume of the source block and have uniform electric potential, the kinetic energy of the charged species in the ion beam is also uniform, being defined solely by the potential at which the source block is held. In addition, the design of the source also leads to the efficient extraction of ions aided by means of an extraction electrode; this prevents an excessive build up of space charge inside the source block.

An array of electrostatic ion optics, consisting of a secondary extraction lens, a pair of vertical deflecting plates and other focusing elements are employed to extract the ions from the ion source block and collimate them into a beam. Since dications have short life times it is necessary to get the dication beam to the interaction region in the shortest possible time, therefore the ions are accelerated to a relatively high kinetic energy (200q eV). Furthermore accelerating the ions to a higher kinetic energy results in the relative uncertainty to be small before the ions pass into the velocity filter.

2.3 Mass selection and the velocity filter

In order to use the beam for collision experiments, the ion beam issuing from the accelerating region needs to be mass selected to separate out the doubly charged ions, since the ion beam at this stage comprises of both dications and monocations. The desired dications are a relatively small component of this beam.

Mass separation is accomplished by the use of a Coultron velocity filter,[14] which is based on a Wein velocity filter[15,16] consisting of a pair of electrostatic plates and an electromagnet. The deflection plates are mounted such that the magnetic field (B) lies in

a direction perpendicular to the direction of the electric field (E) as shown in Figures 2.3 and 2.4 below. An ion of mass m, charge q and velocity v injected into a magnetic

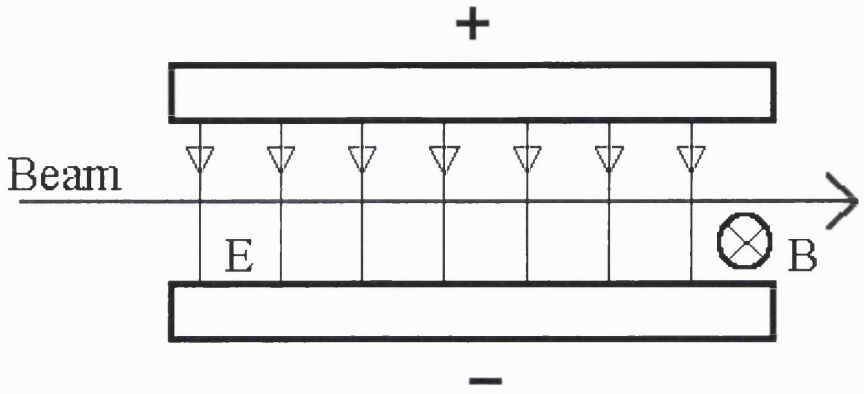

Figure 2.3 Arrangement of the electrostatic plates giving rise to the electric field in the velocity filter. As indicated the B field is going into the plane. The view is perpendicular to the ion beam direction.

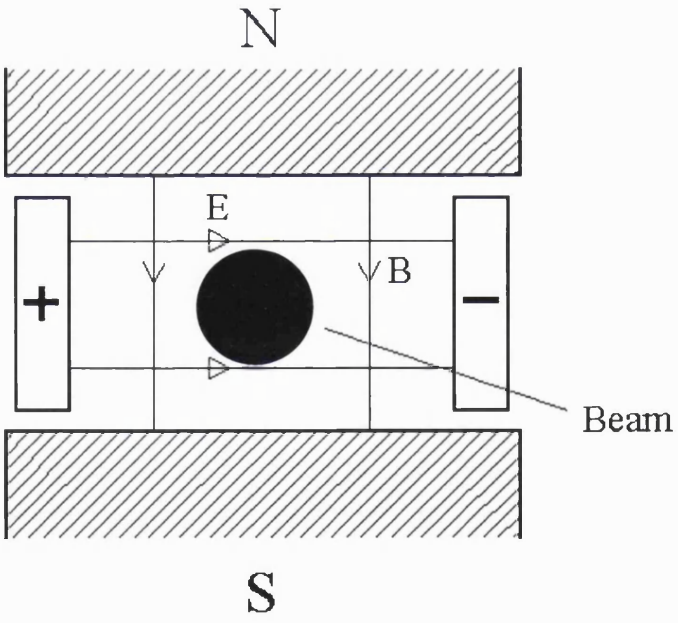

Figure 2.4 The electromagnet arrangement inside the velocity filter. The view is along the axis of the ion beam

field (B) has a force F_B acting on it given by:

$$F_B = Bqv \qquad 2.13$$

Similarly the force F_E on a particle of charge q in an electric field of strength E is given by:

$$F_E = Eq \qquad 2.14$$

The combination of the magnetic and electric fields results in the two forces F_E and F_B being in opposition. Hence, an ion passing through the velocity filter will be deflected out of the beam unless the two opposing forces are equal in magnitude. Such a balance in both these forces occurs for a unique ion velocity v_o where,

$$v_o = E_o / B_o \qquad 2.15$$

Thus, if the magnetic flux density and the electric field intensity are set at values B_o and E_o respectively, then any ions not having velocity v_o will be deflected from the beam.
The ions are extracted from the source region and are accelerated into the velocity filter by an accelerating potential V. Therefore all ions of charge q will be accelerated to the same kinetic energy qV, allowing the ion's velocity to be expressed in terms of its mass,

$$v = \left(2qV/m\right)^{1/2} \qquad 2.16$$

Thus equating equations 2.15 and 2.16 we can obtain an expression for an ion of particular mass m_o remaining undeflected by the opposing magnetic and electric fields for a given set of operating parameters, B, E and V.

$$m_o = 2qVB_o^{\,2} / E_o^{\,2} \qquad 2.17$$

an ion of mass other than m_o will be deflected out of the ion beam. The Coultron velocity filter achieves its maximum resolution at high values of B and in practice, the magnetic flux density is kept constant to minimise the effects of hysteresis losses and detrimental effects of the magnet heating or cooling which would result from the current supplied to the electromagnet coils being adjusted. Mass selectivity of the velocity filter is therefore

accomplished by varying the electric field strength, which is achieved in practice by scanning the voltage applied to the electrostatic plates.

One problem with the basic velocity filter concerns the natural focusing effect of the crossed electric and magnetic fields.[14-19] Ions in the centre of the ion beam will be undeflected on passing through the filter if the beam and filter are well aligned. However, ions away from the centre of the beam will be drawn to a central focal point, at some distance beyond the filter. This unwanted effect is eliminated by the inclusion of additional plates placed between the electrostatic plates. These additional plates are biased with respect to the electrostatic plate potentials and are connected to potentiometers to allow the sensitive adjustment of their potentials. When correctly biased, the electric field is altered, making the electric field weaker at the positive electrostatic plate and stronger at the negative plate. This produces an electric field shape that compensates for the inherent focusing tendency of the velocity filter.

2.4 Ion deceleration

After traversing the velocity filter at $200q$ eV in the laboratory-frame, the kinetic energy of the ion beam must be substantially reduced before the ions encounter the neutral molecules. The necessity for accelerating the ions to such a high translational energy before the ions enter the velocity filter, is that the lifetimes of dicationic species are often of the order of microseconds or less. In order to minimise the loss of dicationic species from natural unimolecular decay, the ions are accelerated so as to reduce the transit time from the ionisation region to the collision region. Furthermore, high-energy beams are easier to use, as perturbing effects of any stray electric fields are less significant. Despite this, the beam energy in our experiments are limited to an upper value of 13 eV in the laboratory frame. The experiments reported here were performed at low collision energies to maximise the yield of bond-forming reactions. At these lower collision energies we expect the bond-forming reaction to be favoured due to the increase in the interaction time between the dication and neutral. Furthermore, at higher beam energies in excess of 12 eV laboratory frame energy, we expect a deterioration of the detection efficiency of the TOFMS as a result of the product ion's significant transverse velocity component. The detection efficiency will be discussed in further detail in Chapter 3. Hence, deceleration of the ion beam is required and is achieved using further ion optics with subsequent refocusing. This procedure results in a dication beam of 1-500 pA at laboratory-frame energies of 2-20 eV.

The ion optics used in the deceleration process are a commercial assembly. They consist of six independently insulated concentric copper cylinders mounted on a brass plate, which is also independently insulated; a schematic layout of the decelerator assembly is shown in Figure 2.5. Cylinders 1,2 and 3 are held at approximately the same potential as the accelerated ion beam. Cylinder 5 is held at 0 V. Cylinders 4 and 6 are held at lower potentials and can be controlled by the use of potentiometers. The final cylinder, 7, is held at ground potential. The aim of this is to gradually reduce the beam energy.

The process of deceleration can cause strong divergence of the ion beam. This divergence arises due to the fact that the decelerator is only able to reduce the ion's longitudinal velocity component, leaving the ion's transverse velocity unaffected by the deceleration process. Hence, a quadrupole mass filter is not used in this apparatus to select the dication beam as low collision energies are required, although this method is perfectly satisfactory at high collision energies above 40 eV in the laboratory frame. The significant transverse velocity components imparted to the dications by the quadrupole filter would not result in practical dication beam intensities at low collision energies.

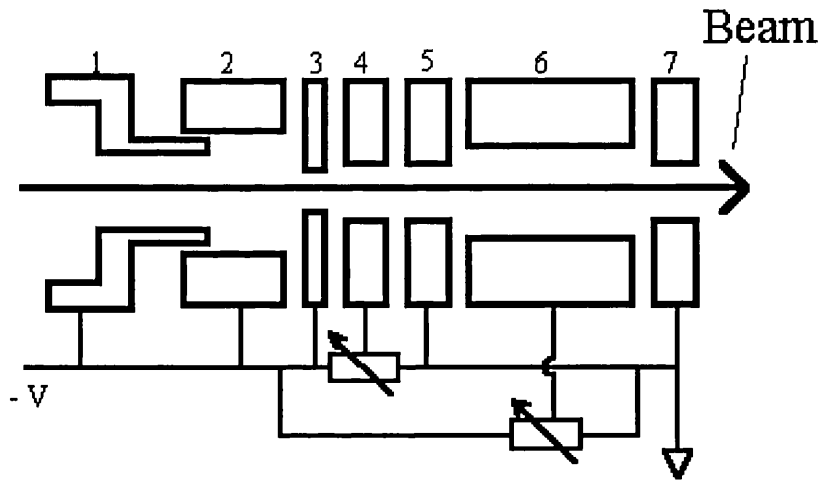

Figure 2.5 Schematic layout of the decelerator assembly. Labels are explained in the text

Element 6 is an Einzel lens, which has a cylindrical focusing capability, which enables the ion beam to be refocused before it reaches the interaction region. Varying the potential on elements 4 and 6 by means of adjusting the potentiometers controls beam focusing. On leaving the deceleration optics, the collimated beam of molecular dications, now at the desired collision energy, enters the interaction region, which is inside the source region of the time-of-flight mass spectrometer.

2.5 Time-of-flight mass spectrometry

On leaving the decelerator, the dication beam intersects an effusive beam of the neutral collision partner in the collision region, which doubles as the source region of the TOFMS. The product ions that are formed following the collision of the dication beam and the neutral target gas, are detected and identified using mass spectrometry; specifically time of flight mass spectrometry (TOFMS).

TOFMS is now a widely used experimental technique,[20] and is conceptually simple relying on the principle that ions of differing mass when accelerated to equal kinetic energies by a set of electric fields, have different velocities. Due to these different velocities the time of flight of ions with differing mass over a set path length will be different. The flight time of an ion in a TOFMS can be derived using a combination of Newtonian mechanics and electrostatics. It can be shown that the time of flight of an ion in a series of electric fields (τ_{tof}) is given by:

$$\tau_{tof} = k\sqrt{m} \qquad 2.18$$

where k is a constant that is determined from the internal dimensions of the spectrometer and the magnitude of the electric potentials used to accelerate the ions.

The increased interest and use of TOFMS is due to a large number of advantages over conventional mass spectrometry.[20] These include the ability to detect ions of all masses simultaneously and high speeds, which enable the collection of a complete spectrum in a few microseconds. These properties enable accurate measurements of relative intensities to be made despite fluctuating source conditions, making time of flight mass spectrometry a highly reliable experimental technique that is ideal for analysing pulsed or spatially limited ionisation events. The simplicity of the design of a time of flight mass spectrometer is also a significant advantage, as other mass spectrometric techniques rely heavily upon the accuracy of mechanical alignment and require costly apparatus design and construction.[12]

The TOFMS used in the experiments reported in this thesis is an implementation of the commonly used two field device constructed to the standard Wiley-McLaren design,[12] with a first order space focus. A schematic diagram of this is shown in Figure 2.6 below.[13] This design of TOFMS contains a source region, which in the experiments

performed here is also the interaction region of the dication and neutral gas, a second acceleration region and a drift region which is free of electric fields. These regions of the TOFMS are traditionally assigned lengths of $2s_o$, d and D respectively. After the reactive encounter all the ions are extracted from the interaction region by a pulsed positive voltage V_o applied to the repeller plate. The ions then enter the second acceleration region where they undergo further acceleration before entering the field free drift region and eventually impinge on the detector. Therefore in order to record a time of flight mass spectrum the flight time of an ion between the source region and the detector must be measured.

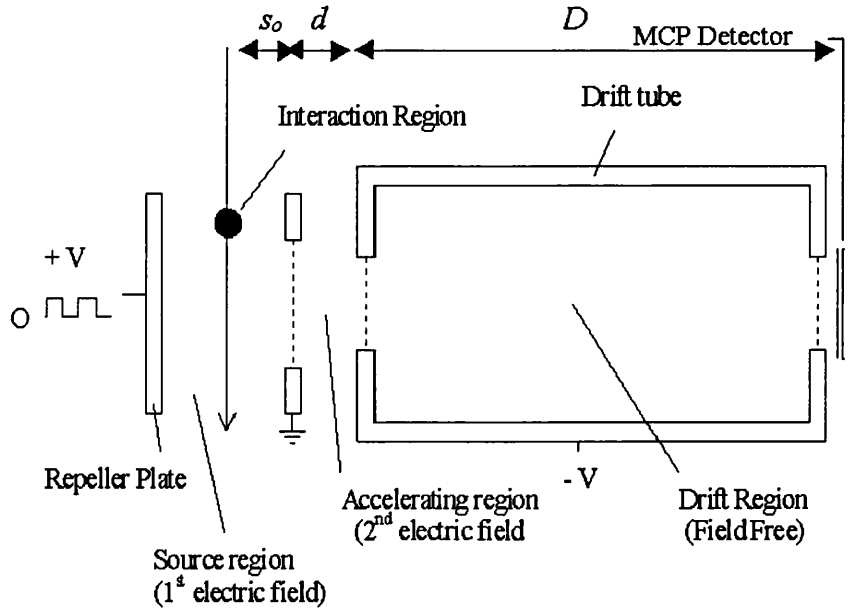

Figure 2.6 Schematic diagram of a twin electric field time-of-flight mass spectrometer, including the source/interaction region.

With such an experimental arrangement, it is expected that all ions of the same mass will have equal flight times in the TOFMS. However, when the electric field is applied to the source region, the ions present have some spatial distribution. Therefore the final energy of the ions after acceleration will not be uniform since the ions will have an initial potential energy dependent on their positions. As a result, ions of the same mass will have different flight times depending on their initial positions in the interaction region. In an attempt to overcome, or at least reduce, this detrimental effect, the spectrometer is designed so that the ions are focused. Focusing attempts to ensure that, irrespective of the

above effects, ions of a given mass arrive at the ion detector at the same time.[12] A situation in which the ions are focused may be described mathematically:

There is no variation in the ion's flight time t, with the ions initial position about s_o in the source region.

$$\left(dt_{tof}/ds\right)_{s=s_o} = 0 \qquad 2.19$$

If this mathematical condition is applied to the equation for the total flight time of an ion in a two-field TOFMS, the following expressions are obtained

$$D = 2sk^{3/2}\left[1 - \frac{1}{k + k^{1/2}}\frac{d}{s}\right] \qquad 2.20$$

$$k = \left[\frac{sE_s + dE_d}{sE_s}\right] \qquad 2.21$$

Where E_s and E_d are the strength of the electric fields in the source and accelerating regions respectively. Therefore, for a two field TOFMS, this differential tells us that space focusing can be achieved by simply adjusting the ratio of E_d/E_s.[12] Thus, a first-order space focus can be achieved for a two-field device with a wide variety of s_o, d and D parameters, in contrast to a single-field TOFMS which has a purely geometric space focus.

Improved space focusing in a two-field TOFMS can be achieved using second-order focus conditions,[21] which calls for the lengthening of the acceleration region for a given total length of flight path. The use of a TOFMS with a second-order focusing is advantageous when diffuse ion sources are employed and also in the study of energetic and heavy ions. However, for the experiments discussed here, first-order focusing of the TOFMS is sufficient.

In practice the ion peaks in the mass spectrum have finite half widths corresponding to a range of ion flight times; this is a physical consequence of the ions having a distribution of kinetic energies together with the fact that the ions are formed over a range of positions in the source region and that the focusing is not perfect. Although focusing can help to reduce the spread of the ions flight times of a given mass arising because of the

ion's initial position, it is very much more difficult to reduce the detrimental effects of the ions having differing initial velocities. Hence, in addition to having differing initial speeds, the ions' initial trajectories may be in different directions; this further complicates the problem of focusing since ions with initial trajectories directed away from the detector will require a finite time for the electric field to change the direction of their motion. This additional time is known as the 'turn around time' and adds to the width of a given mass spectral peak. Perhaps the most important feature of the Wiley-McLaren design of twin electric field TOF mass spectrometer is the relative ease of achieving focus as discussed above.[12] The focusing is achieved by simply adjusting the ratio of the electric fields.

In general, ions are generated in the source region of the spectrometer either by electron impact or photon impact ionisation of the precursor gas sample. Alternatively, ions may be produced in a separate ion gun, as in the case of the crossed beam spectrometer, prior to being transported to the interaction region. The mass spectrum is recorded by periodically pulsing on a positive potential to the repeller plate in the spectrometer's source region, while simultaneously a START signal is sent to an electrical timing device. The positive voltage pulse applied to the repeller plate creates an electric field in the source region. This electric field extracts the positively charged ions from the source region. A second electric field accelerates the ions further before they pass into a field free drift region. After the drift region the ions reach the detector, where the arrival of the ion results in a STOP signal being sent to the electronic timing device. The ion's time of flight is simply the difference between the start and stop times.

Although the TOFMS part of the apparatus is based upon the Wiley-McLaren twin field design, the TOFMS used in the experiments described in this thesis incorporates a number of refinements,[2,6-10,19] as shown in Figure 2.1. These refinements include an Einzel lens and ion deflectors, both of which are situated at the start of the spectrometer's drift tube. These electrostatic elements are only useful at large laboratory-frame collision energies, and for the work reported in this thesis they were not used and were held at the same potential as the drift tube. A further addition to the design is a grid situated between the grounded acceleration grid and the drift tube grid, and is held at a low positive potential (2-5V) which prevents stray ions from entering the acceleration region during that part of the cycle of the TOFMS when the repeller plate is held at ground potential. A Faraday cup is situated beyond the source region, allowing the dication beam intensity (current) to be measured independently of the TOFMS.

2.6 Recording spectra

The target gas pressure is rigidly maintained at a constant value, typically 4 x 10^{-6} Torr during the course of recording a mass spectrum. The pressure is kept sufficiently low to guard against the possibility of multiple collisions in the interaction region. Multiple collisions would unnecessarily complicate the identification of the reaction channel leading to the formation of a given product ion, as the same product ion could be formed in two or more different reaction processes.

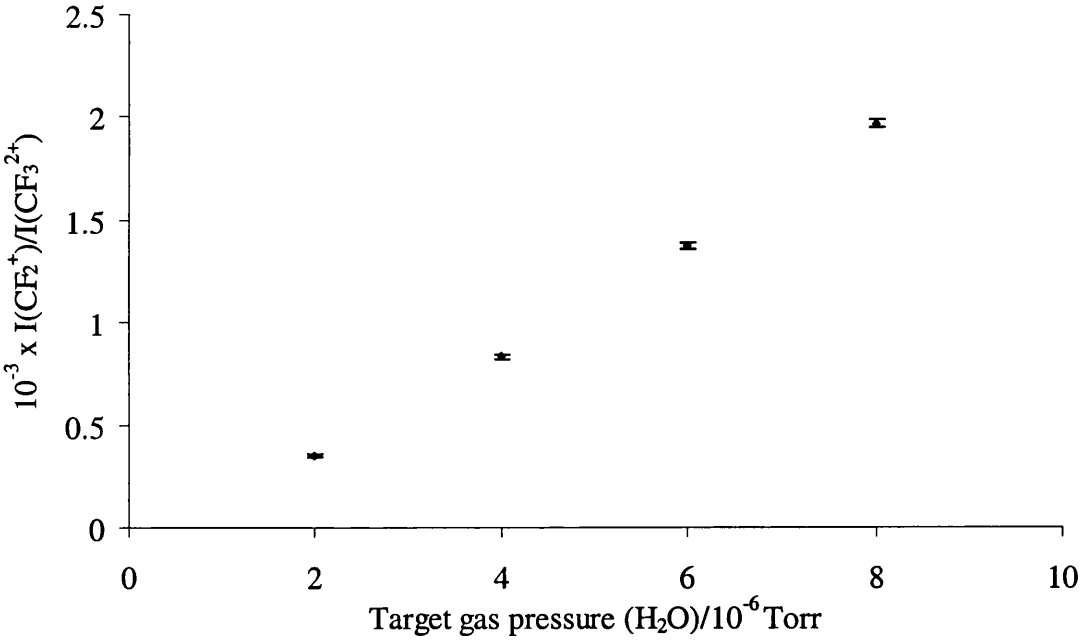

Figure 2.7 Graph of the relative product ion (CF_2^+) intensity produced following collisions between CF_3^{2+} and H_2O as a function of target gas pressure. The linear relationship is indicative of single collision conditions.

The conditions are carefully tested to ensure that multiple collisions are not occurring by measuring the product ion intensity as a function of the target gas pressure. A linear relationship, such as that shown in Figure 2.7, confirms the presence of single collision conditions.[22]

As mentioned above the product ions, which are formed following the collisions, are extracted out of the source region by the application of an extraction pulse. These ions pass through the drift region and finally impinge on the detector. Timing of the ion's flight time is achieved by measuring the difference in the times of a START signal to initiate the ion's transit from the source region and a STOP signal is generated by the ion when it reaches the detector. As shown in Figure 2.8 the start signal is generated by a pulser unit, which then delivers a +400 V pulse to the repeller plate of the TOFMS, which initiates the extraction of the ions from the spectrometers source region. Simultaneously the pulse generator sends the same START signal to a Lecroy TDC (time to digital converter). The START pulse is sent after the extraction pulse is applied to the repeller plate so any RF noise resulting from the application of the +400 V will not be detected. The pulse is sent from the pulse generator to the TDC via a LeCroy 3420 constant fraction discriminator (CFD) to convert the NIM pulse produced by the pulse generator to the ECL pulse required for the operation of the TDC. The arrival of the ion at the front plate of the detector generates a STOP signal, this signal is

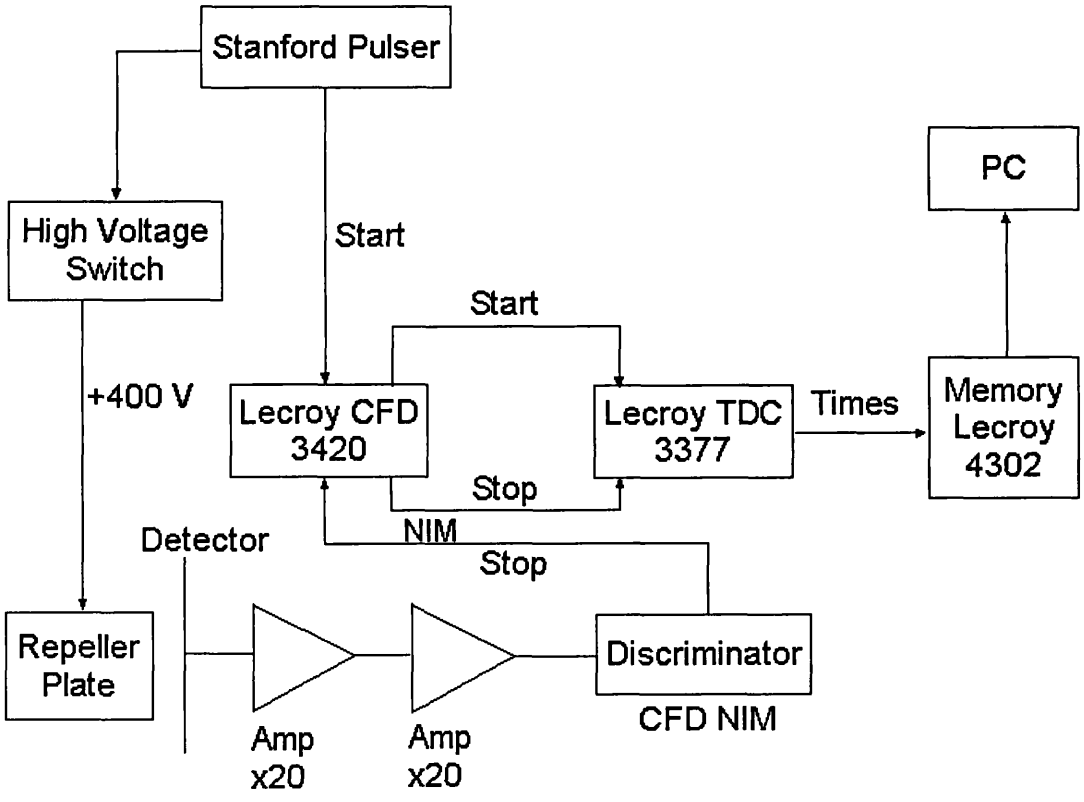

Figure 2.8 Schematic diagram of the data collection electronics.

amplified and discriminated to remove electronic noise before reaching the same LeCroy TDC, thus ending the timing cycle. The ion times recorded are transferred from the TDC

to memory (LeCroy 4302), using the FERA (Fast Encoding and Readout ADC) system, designed for fast conversion of analogue information into a digital format.

The data acquisition procedure is repeated until the memory is full (16K of data) and the contents are then extracted by the custom written data acquisition algorithm and transferred via a SCSI port to a PC. The data acquisition algorithm is coded in Visual Basic, and allows the time-of-flight mass spectra to be recorded. Upon extraction of the data from the memory, the flight times recorded are added to a histogram of the number of ions versus t_{tof}. The complete histogram can then be displayed on the PC.

2.7 Operational Parameters

Typical operating parameter are listed in the tables below

Table 2.1 Typical spectrometer operating parameters

Parameter	Typical Value
Laboratory frame collision energy	3-12 eV
Repeller plate pulsing frequency	50 kHz
Precursor gas pressure	4×10^{-6}
Neutral target pressure	3.0×10^{-6}
Electron energy	150eV
Repeller plate potential	Pulsed to +400V from 0V
Drift tube potential (TOF deflectors/Einzel lens)	-1230 V
MCP detector front plate voltage	-2050 V
MCP detector back plate voltage	40V
Sandwich grid potential	~2.2 V
Accelerating potential	250 V
Filament voltage	150 V
Electromagnetic current	2.2 A
Decelerator element potential	0 to –150 V

2.8 Conclusion

This Chapter describes the implementation and modifications of the spectrometer used to investigate the reactivity of molecular dications with neutral species. The operational methodology and conditions have been discussed. All experiments reported in this thesis have been carried out under single collision conditions.

References:

1 *Techniques for the study of ion-molecule reactions*, Vol. XX, edited by J. M. Farrar and W. H. Saunders (John Wiley, New York, 1988).

2 K. A. Newson and S. D. Price, *Chem. Phys. Lett.* **269,** 93-98 (1997).

3 C. Y. Ng, T. Baer, and I. Powis, *Unimolecular and Bimolecular Ion-Molecule Reaction Dynamics*, (John Wiley and sons Ltd, New York, 1994).

4 T. Baer and C. Y. Ng, *State selected and State-to State Ion-Molecule Reaction Dynamics Part 2 (Theory)*, (John Wiley and sons Ltd, Inc, New York, 1992).

5 *Molecular Reaction Dynamics and Chemical Reactivity*, edited by R. D. Levine and R. B. Bernstein (Oxford University Press, Inc, 1987).

6 S. D. Price, *J. Chem. Soc. Faraday Trans.* **93,** 2451-2460 (1997).

7 M. Manning, S. D. Price, and S. R. Leone, *J. Chem. Phys.* **99,** 8695-8704 (1993).

8 S. D. Price, S. A. Rogers, and S. R. Leone, *J. Chem. Phys.* **98,** 9455-9465 (1993).

9 S. D. Price, M. Manning, and S. R. Leone, *J. Am. Chem. Soc.* **116,** 8673-8680 (1994).

10 S. A. Rogers, S. D. Price, and S. R. Leone, *J. Chem. Phys.* **98,** 280-289 (1993).

11 S. D. Price, M. Manning, and S. R. Leone, *Chem. Phys. Lett.* **214,** 553-558 (1993).

12 W. C. Wiley and I. H. McLaren, *Rev. Sci. Inst.* **26,** 1150 (1955).

13 K. A. Newson, S. M. Luc, S. D. Price, and N. J. Mason, *Int. J. Mass Spectrom. Ion. Proc.* **148,** 203-213 (1995).

14 L. Wahlin, *Nuclear Instruments & Methods in Physics Research Section B-beam Interactions with Materials and Atoms* **27,** 55 (1964).

15 W. Wien, *Ann. Physik.* **65,** 440 (1898).

16 M. L. Oliphant, E. S. Shire, and B. M. Crowther, *Proc. Royal Soc. (London)* **A146,** 922 (1934).

17 O. Klemperer and M. E. Barnet, *Electron Optics*, (Cambridge University Press, Cambridge, 1971).

18 M. Szilagyi, *Electron Optics*, (Plenum, New York, 1988).

19 A. R. Kip, *Fundamentals of Electricity and Magnetism*, (McGraw-Hill, Singapore, 1969).

20 D. Price and G. J. Milnes, *Int. J. Mass Spectrom. Ion. Proc.* **99,** 1-39 (1990).

21 J. H. D. Eland, *Meas. Sci. Tech.* **4,** 1522-1524 (1993).

22 K. Yamasaki and S. R. Leone, *J. Chem. Phys.* **90,** 964-976 (1989).

Chapter 3

Data Analysis

3.1 Introduction

Monitoring the gas phase reactivity of doubly charged molecular ions involves recording flight times, in a TOFMS, of product ions that are formed following collisions. The analysis procedure uses the raw data from the time of flight mass spectra, to derive information about the reactivity. This analysis procedure will be discussed in this Chapter.

3.2 The time of flight mass spectrometer

As discussed in the previous Chapter the computer receives the raw experimental data from a memory unit (LeCroy 4302), via a SCSI port. From the flight times of the detected ions, the computer assigns each of the counts to a time channel, and builds up a histogram of these flight times, each time channel corresponding to a point on a mass scale. The number of ions in each channel is a measure of the intensity of ions of that particular mass and a complete histogram represents the mass spectrum. As mentioned in Chapter 2, the flight time of an ion is dependent on the square root of its mass m. Therefore, following calibration of the TOFMS with a well characterized gas, the identity of the ions present in the time of flight mass spectrum can be determined. The minimum and maximum times of the array of time channels are variable parameters, allowing various product ions to be represented in a mass spectrum over a wide mass range.

3.3 Data Analysis

As mentioned before the raw data for analysis consists of the intensities of the ion signals from the recorded mass spectra, such as shown in Figure 3.1. Since the computer assigns each count to a time channel, this provides a distinct advantage for analysis, since the intensities of the ion signals are determined simply by summing the

counts for each of the channels making up a peak, thus avoiding unnecessary complicated numerical procedures.[1] The computer program is written in Visual Basic and allows the

intensities of the peaks to be rapidly calculated given the minimum and maximum mass or channel numbers, corresponding to the desired peak.

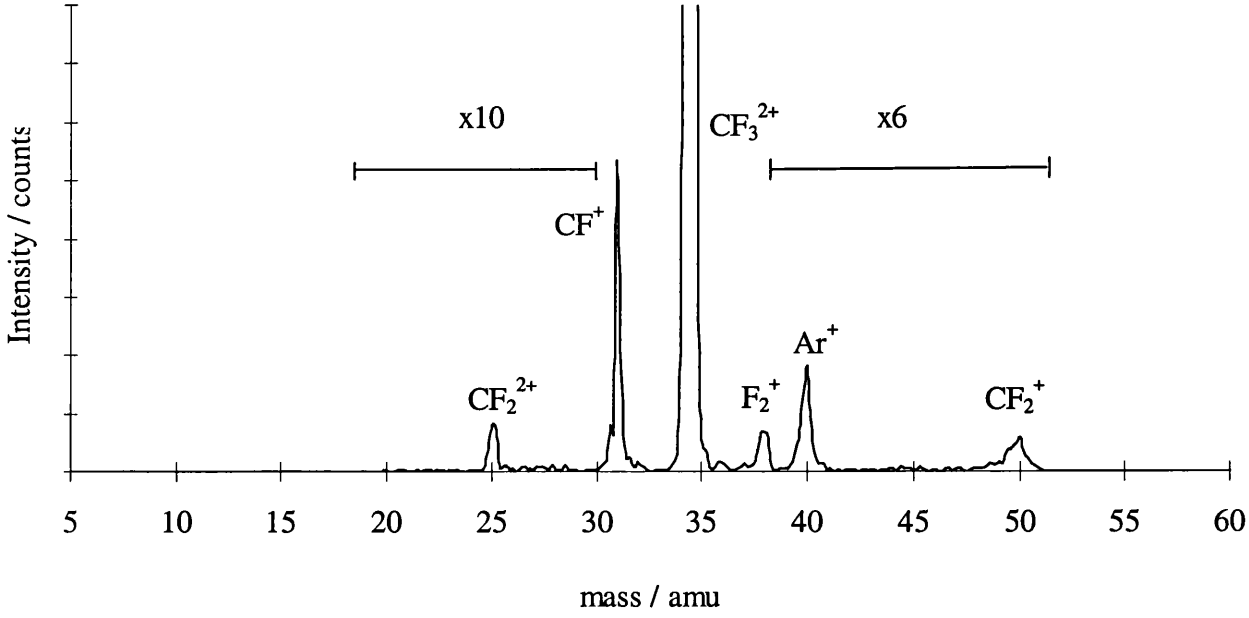

Figure 3.1 Time of flight mass spectrum showing the product ions formed in collisions between CF_3^{2+} and Ar atoms at collision energy of 3.3 eV in the centre-of-mass frame.

As will be discussed below the raw data needs to be corrected for both background and impurity ions. To remove background contribution, since it may be important where the reaction cross-sections are low such as for bond-forming reactions,[2-6] an appropriate background area, close to the peak in consideration, is taken and the following formula is used to give the background subtracted ion count of the peak. The average number of counts per channel in the background is subtracted from each channel of the product ion count.

$$Bg corrected counts = Raw counts - \left(\left(\frac{Bg counts}{total channels in Bg} \right) \times total channels in peak \right) \qquad 3.11$$

The major source of any impurity ion contribution to the spectra is the dication beam itself. Although dication beams of high purity (> 99%) can be achieved, the dication beam will always contain a number of contaminant ions that traverse the velocity filter. Furthermore, unimolecular decay of the dicationic species is another possible source of impurity ions.[7-9] e.g.

$$CF_2^{2+} \rightarrow CF^+ + F^+ \qquad 3.12$$

As shown in Figure 3.2, a total of five mass spectra are collected at each beam energy. The first spectrum is a mass spectrum of the product ions formed as a result of collisions between the reactant dications and neutral target molecules i.e. in the presence of the neutral collision gas. A spectrum is then collected in the absence of any collision gas keeping all other conditions exactly the same as the product ion mass spectrum.[10]

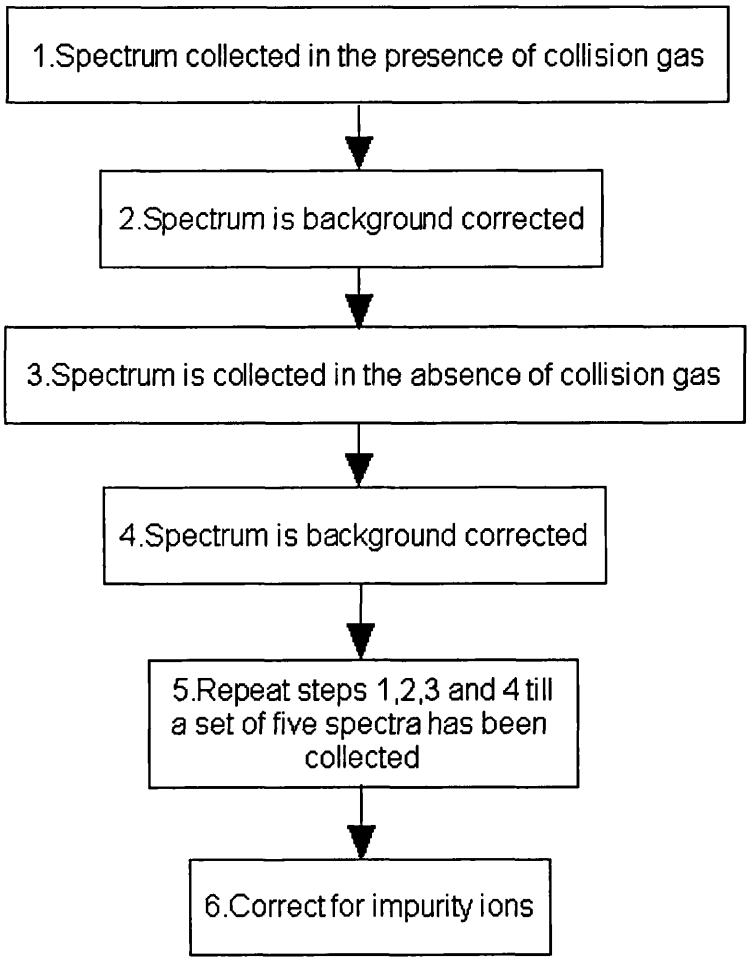

Figure 3.2 Flow diagram of data collection procedure

This procedure is repeated until the complete set of mass spectra are collected, resulting in the set of spectra containing three spectra in the presence of collision gas and two spectra without. The data is then corrected to remove the contribution of impurity ions and collisions with residual molecules that maybe be present, by subtracting corresponding ion counts obtained from the spectra collected in the absence of collision

gas, and averaged, allowing us to obtain the product ion signals due solely to the desired interaction process.

The net product ion signals are then corrected, for any mass discrimination effects to obtain the product ion yields for a given reacting system. Mass discrimination effects will be considered in the next section. This procedure is repeated at least 3 times to give an average product ion yield and an associated standard deviation.

3.4 Product ion efficiency

If a reaction occurs during a collision between the reactant dication and the neutral collision partner, the dynamics of the reaction may result in a significant release of kinetic energy due to the large Coulombic repulsion between the pair of singly charged ions that are formed in close proximity. In addition each reaction channel may have a different average kinetic energy release (KER) and a different distribution of kinetic energy releases.[6] This KER, in the centre-of-mass frame, changes the translational energy of the reaction products in the laboratory frame. Hence, the different product ions may have different velocities across the source region of the time of flight mass spectrometer (TOFMS). Owing to these different transverse energies, the product ions may travel different distances as they fly down the TOFMS to reach the

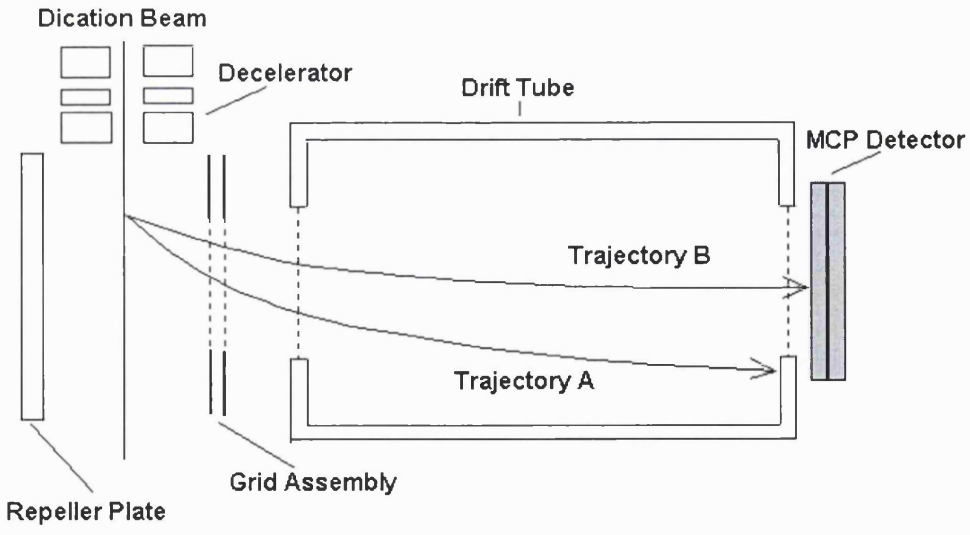

Figure 3.3 Schematic diagram of the TOFMS showing the trajectories of product ions formed at the same point in the interaction region. Trajectory A represents the path taken by an ion formed in a reactive encounter in which there is a large kinetic energy release, whilst trajectory B represents the case where the kinetic energy release is significantly smaller.

multichannel plate (MCP) detector. Those ions that posses a larger transverse kinetic energies in the laboratory frame will travel a greater distance away from the central axis

of the spectrometer than less energetic product ions. Hence, the length of the source region in the direction of the ion beam that is imaged onto the MCP detector varies with the total kinetic energy of the product ion. Therefore, in order for us to allow for this discrimination effect the background corrected ion count must be further adjusted, to yield the true relative ion intensities. A schematic diagram of the ion trajectory range in the TOFMS, which gives rise to the mass discrimination effect, is shown in Figure 3.3 above.

As mentioned above, the product ions formed will have a component of velocity perpendicular to the longitudinal axis of the TOF spectrometer which is due to the fact that the reactant dications are delivered to the source region, in a direction perpendicular to the longitudinal axis of the TOF mass spectrometer. Furthermore due to the highly energetic reaction processes of these species the product ions may, as a result of reactive scattering, have enhanced transverse velocity components.

Those ions with a higher transverse velocity component will not be efficient in reaching the detector compared to those product ions that have a relatively low transverse velocity component. This is viewed as a reduction of the detection efficiency and in order to correct the detected ion intensities, it is necessary to consider the ion's mass, its time of flight and, in the case of a product ion, the distribution of the kinetic energy released on reaction.

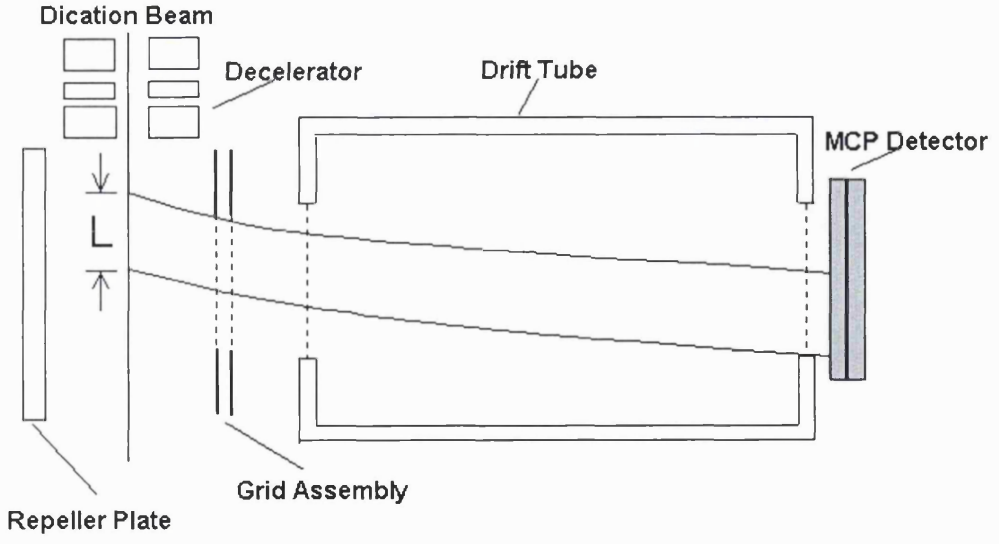

Figure 3.4 Schematic diagram of the TOFMS showing the distance 'L' between the trajectories reaching the front plate of the ion detector.

In principle, the transverse velocity of the product ions in the laboratory frame can be calculated given the value of the KER for the reaction and the laboratory-frame

collision energy using basic kinematics. However, due to the scarcity of data many of these energetics are not available in the literature and product ion KER distributions have to be estimated. This is not a major approximation as, undoubtedly, the KER of the chemical reaction channels are dominated by the Coulombic repulsion between the singly charged product ions. In fact the relative correction factors we calculate as are shown in Chapters 5, 6, 7 and 8, are not a strong function of the KER, supporting this approach. To use these representative KER values to determine the average product ion velocity we also assume that the dynamics of the collision system predominantly involve forward scattering.[6] Again, this is an assumption, but angularly resolved investigations of dication reactivity indicates that forward scattering is the dominant reaction mechanism in dication chemical reactions.[6]

The intensity I of an ion signal reaching the detector is proportional to the ion density n in a volume V of the interaction region that is imaged onto the detector in the TOFMS:

$$I = nVj \qquad 3.13$$

Where j is a mass-independent ion detection efficiency and is an intrinsic property of the ion detection electronics. The flux F of a product ion is related to its velocity v across the ion source region and the ion density n:

$$F=nv \qquad 3.14$$

By considering Equations 3.13 and 3.14 it is possible to obtain an expression for the relationship between the ion flux and the detected ion intensity:

$$F = \frac{Iv}{Vj} \qquad 3.15$$

The volume V of the interaction region/source region imaged onto the detector may be expressed in terms of its cross-sectional area A and length L giving:

$$F = \frac{Iv}{ALj} \qquad 3.16$$

The cross-sectional area of the volume imaged onto the detector depends upon the internal bore of the decelerator assembly and its focussing characteristics. Hence, the

cross-sectional area A is constant for any reaction process, and for two such processes denoted A and B, the relative ion fluxes are given by:

$$\frac{F_A}{F_B} = \frac{I_A}{I_B}\frac{v_A}{v_B}\frac{L_B}{L_A} \qquad 3.17$$

The relative cross-sections for the reaction processes are proportional to the relative product ion fluxes. Therefore the relative cross-sections for reaction processes A and B can be determined from the mass spectrometric product ion intensities by:

$$\frac{\sigma_A}{\sigma_B} = \alpha\frac{I_A}{I_B} \qquad 3.18$$

In the above correction L is the effective length of the source region of the TOFMS that is imaged onto the detector. The length L is dependent upon the internal geometry of the spectrometer, the transverse velocity v of the product ion and the ion's time-of-flight. The value v is given by the centre-of-mass velocity (collision energy) and the energy imparted to the ion in the reaction process.[2]

Comparison of previous work using this procedure[2] with results in the literature for the $CF_2^{2+}/H_2/D_2$ collision system shows good agreement with alternative procedures used,[11] and confirms the validity of this approach.

3.5 Conclusion

The analysis procedure that is performed on the data correct the ion intensities for background ion contribution, detection efficiency and provides a simple and accurate means of obtaining the relative cross-sections of reaction processes.

References:

1 W. C. Wiley and I. H. McLaren, *Rev. Sci. Inst.* **26,** 1150 (1955).

2 K. A. Newson and S. D. Price, *Chem. Phys. Lett.* **269,** 93-98 (1997).

3 S. D. Price, M. Manning, and S. R. Leone, *J. Am. Chem. Soc.* **116,** 8673-8680 (1994).

4 S. D. Price, *J. Chem. Soc. Faraday Trans.* **93,** 2451-2460 (1997).

5 K. A. Newson and S. D. Price, *Chem. Phys. Lett.* **294,** 223-228 (1998).

6 Z. Dolejsek, M. Farnik, and Z. Herman, *Chem. Phys. Lett.* **235,** 99-104 (1995).

7 C. Y. Ng, T. Baer, and I. Powis, (John Wiley and sons Ltd., New York, 1994).

8 T. Baer and C. Y. Ng, (John Wiley and sons Ltd., Inc, New York, 1992).

9 *Molecular Reaction Dynamics and Chemical Reactivity*, edited by R. D. Levine and R. B. Bernstein (Oxford University Press, Inc, 1987).

10 S. A. Rogers, S. D. Price, and S. R. Leone, *J. Chem. Phys.* **98,** 280-289 (1993).

11 Z. Herman, J. Zabka, Z. Dolejsek, and M. Farnik, *Int. J. Mass Spectrom.* **192,** 191-203 (1999).

Chapter 4

Interactions of molecular doubly charged ions with neutrals: a theoretical perspective

4.1 Introduction

In considering the topic of collisions between molecular dipositive ions (molecular dications) and neutral molecules, one must pay particular attention to the processes that involve the transfer of an electron from one of the colliding partners to the other since electron transfer often dominates dication/neutral collisions. The majority of molecular dications have electronic states that rapidly fragment to form a pair of singly charged ions. However, as mentioned in Chapter 1, a large number of molecular dications possess at least one electronic state which is long-lived owing to a barrier in the charge-separating pathway. These metastable states live long enough for an investigation of their interaction with neutral target atoms or molecules to be undertaken. Electron transfer reactions often dominate dicationic reactivity with atomic collision partners and the considerable state selectivity observed in these charge transfer reactions can be rationalized using the Landau-Zener (L-Z) model of the electron transfer process. A semi-empirical model of the bimolecular electron transfer reactivity of molecular dications with neutral targets[1-5] has been attempted with some success, using an adaptation of the Landau-Zener theory of electron transfer between singly charged atomic ions and neutrals.[6,7] However, the bond-forming (chemical) reactivity occurring in certain molecular dication/neutral collision systems at low laboratory frame collision energies (<13 eV) has not, to date, received significant attention from theoreticians. However, an attempt to model the mechanism of bond forming reactions based on the principles of the L-Z theory has been attempted.[8]

This Chapter examines aspects of the theory relating to gas-phase ionic reactivity that are of primary importance in understanding the experimental work presented in this thesis and explaining the subsequent results. Specifically, a discussion of the Landau-Zener theory of electron transfer and its offshoot, the reaction window theory is presented.

4.2 Reaction window theory and the Landau-Zener model

The Landau-Zener model (L-Z)[6,7] is a semi-classical picture of electron transfer reactivity for purely atomic collision systems and determines the probability of electron transfer between given reactant and product electronic states. The L-Z model has been applied successfully to rationalize electron transfer reactivity in a wide variety of systems and considers the reaction as occurring at the crossing, *r*, of two diabatic potential curves corresponding to the reactants and products. Such a crossing is illustrated in Figure 4.1 for a dication electron transfer reaction.

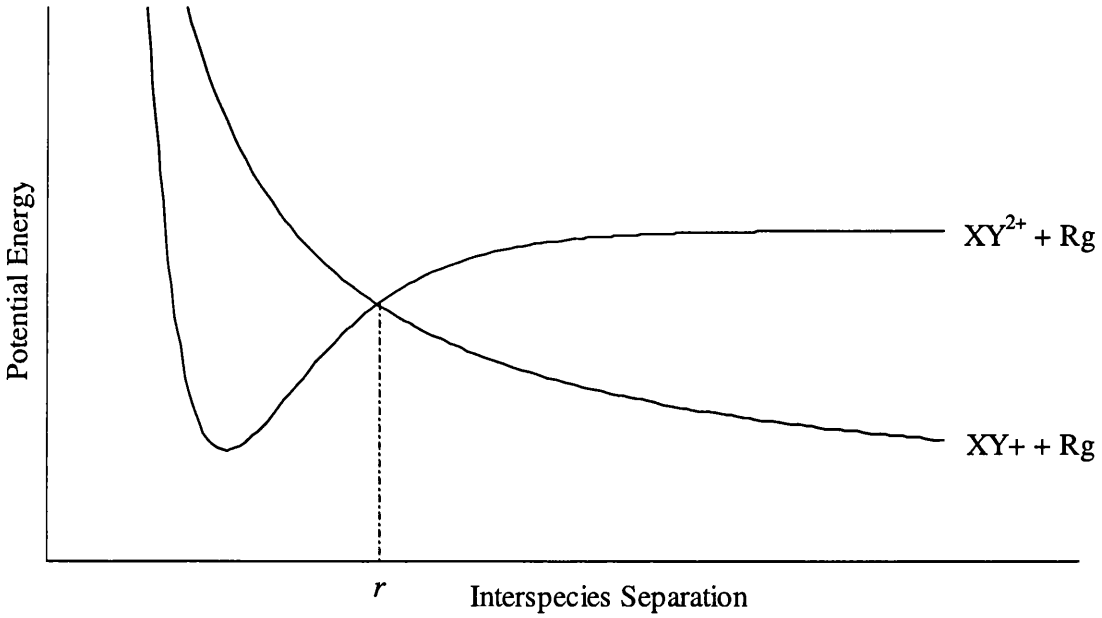

Figure 4.1 Schematic potential energy curves for the crossing of product and reactant potentials for a dication-neutral electron transfer reaction.

To apply the Landau-Zener model to dication-neutral collision systems, the reactants are pictured as approaching each other on a potential-energy curve dominated by polarization attraction. At some interspecies separation, the curve-crossing radius, *r*, this reactant potential may cross the potential-energy curve corresponding to the products of the reaction and an electron can be transferred from the neutral to the dication. The product potential is modeled as being purely repulsive since it is dominated by the electrostatic repulsion between the two singly charged product ions. Qualitatively, the probability of the electron transfer occurring depends on the coupling between the product and reactant surfaces, which in turn depends on the radius of the crossing. If the crossing is at too large an interspecies separation there is little coupling

and therefore little probability of the electron tunneling between the two reactants. If the crossing is at too small an interspecies separation, the interaction between the two surfaces is very large and on one pass through the crossing the probability of the electron being transferred is very high. However, although the system makes two passes through the crossing (as the reactants approach and depart from one another) this strong coupling does not result in a reactive encounter. Between these two limits lies a range of interspecies separation (ca. 3-6 Å), the so-called 'reaction window'. Thus, if the curve crossing for the system under consideration lies in this window, electron transfer is expected to be favored.

As mentioned above, for an electron transfer to occur the curve crossing may occur either on the incoming or outgoing trajectories. Hence, the total probability P for electron transfer is given by:

$$P=2\delta(1-\delta) \qquad 4.11$$

Where δ is the probability of remaining on the curve on one pass through the avoided crossing and can be calculated using the Landau-Zener equation.

$$\delta = exp\left(\frac{-\pi|H_{12}|^2}{2\hbar|V'_p - V'_r|v_b}\right) \qquad 4.12$$

Hence, the quantity δ is a measure of the coupling between the product and reactant potential curves and is a function of $V_1' - V_2'$ which is the magnitude of the difference in the gradients of the two potential energy curves at the crossing radius, r, the relative radial velocity v_b and the electronic coupling matrix H_{12} between the product and reactant electronic states.

To model, qualitatively, the dication electron transfer reactions we have only to construct the appropriate potential energy surfaces, which requires a knowledge of the exothermicity of the reaction and the polarisability of the neutral collision partner, and calculate the interspecies separation of the curve crossing.[2] If the curve crossing lies in the reaction window then electron transfer is expected to be favored.

The potential energy curves are modeled using simple standard electrostatic equations:

$$V_r = -\frac{z^2 e^2 \alpha}{2(4\pi\varepsilon_0 r)^4} + \Delta E \qquad 4.13$$

$$V_p = \frac{e^2}{R} \qquad 4.14$$

The zero potential is defined as the infinite separation between the two singly charged ions. In equation 4.13 the potential of the reactant channel V_r is given as the sum of the standard polarization attraction function that is determined from the polarisability (α) of the neutral target species and reaction exothermicity ΔE. The model does not make any allowance for the repulsive wall encountered at very small values of r. However, this is not a major approximation since this repulsion is only significant at very small interspecies separation, and may therefore be ignored over the range of interspecies separations where the reactant and product curves intersect. The potential V_p (equation 4.14) of the electron transfer product channel is modeled as being purely repulsive, due to the coulombic repulsion between the singly charged product ions. Thus using these potentials we can evaluate the curve crossing radius, and, for a given impact parameter and collision energy, the relative radial velocity. The relative radial velocity v_b may be calculated from the impact parameter b, the initial velocity of the reactants and the energy gained by the collision partner as a result of the polarization attraction between the two reactants approaching the curve-crossing radius. H_{12} is estimated using the empirical equation of Olson *et al.* [9] which has been used previously by several authors and have proved reliable in this role in recent studies.[1-3,10]

The accurate calculation of the electronic coupling matrix H_{12} requires precise details of the electronic wavefunctions of the collision system. The function given by Olsen *et al.*,[9] which we use, gives the electronic coupling matrix element as

$$|H_{12}|^2 = (I_A I_B)(R_c^*)^2 \exp(-1.72 R_c^*) \qquad 4.16$$

Where:

$$R_c^* = \left(\frac{\sqrt{I_A} + \sqrt{I_B}}{\sqrt{2}} \right) R_c \qquad 4.17$$

Given the above parameters we can then evaluate the electron transfer cross-section for forming the electronic state of the product ions for which we derived the exothermicity by integrating P (equation 4.11) with respect to the impact parameter b between $b=0$ and the maximum value of b for which the collision reaches the crossing radius.

Our calculations, which are based on the L-Z theory are approximate.[2,10] Most importantly they neglect any anisotropy in the potential surfaces. However, in the past this model has proved highly successful in the semi-quantitative rationalization of the product ion yields from molecular dication electron transfer reactions. This success is principally due to the fact that electron transfer occurs efficiently at significant interspecies separations where the model potentials provide a good approximation to the real potential energy surfaces.

As mentioned before, to model qualitatively the dication-electron transfer reactions we only have to construct the appropriate potential-energy surfaces. If the curve crossing lies in the reaction window then electron transfer is favored. This simple model immediately indicates the crucial importance of the reaction exothermicity in determining the propensity for electron transfer. If the exothermicity is small, the curve crossing will lie at too large an interspecies separation. Conversely, if the exothermicity is too large the curve crossing will lie at too small a value of the interspecies separation. The applicability of this model has been confirmed by analysis of the electron transfer reactions between molecular dications and rare gas collision partners.[1-5] Here the electron transfer reactions with lighter rare gases (He and Ne) are not favored because the reactions are either endothermic or barely exothermic. However, electron transfer reactions are observed with the heavier rare gas targets (Ar, Kr and Xe) which have larger reaction exothermicities, that lie within the reaction window. For a given dication, electron transfer reactions become more exothermic with the heavier rare gases, owing to the decrease in the ionisation potential of the neutral target. Thus, electron transfer reactions are often unfavourable with He and Ne, where the reaction is endothermic or weakly exothermic, whilst dominant with Ar, Kr and Xe.[5]

An additional feature of this application of the reaction window theory is its ability to predict whether an electron transfer reaction will be dissociative or non-dissociative. As mentioned above, the exothermicity of an electron transfer reaction determines the feasibility of the reaction. However, a collision system may have many channels of electron transfer reactivity with each channel having a particular value of exothermicity. Therefore given the window of exothermicities, the electron transfer reactivity of any dication-neutral collision system can be rationalized using the above approach. Thus, the L-Z model is a powerful predictive tool of electron transfer in molecular dication-neutral atomic collision systems.

4.3 The centre of mass system

The reactions of interest in this thesis can be described in the lab system. However, it is advantageous to describe the collision not in terms of the motion of each particle but, rather, in terms of their relative separation and the motion of their centre of mass (c.m.). There are no external forces operating on the system in the interaction region, and so the motion of the c.m. is unperturbed and its kinetic energy is constant throughout the collision. It is therefore convenient to subtract this constant from the total energy and deal with the remainder, which is the kinetic energy of the relative motion. The centre of mass although being conceptually greater in complexity then the laboratory frame system, does however greatly simplify the calculation process.[11]

The centre of mass origin has a position vector R_{cm} with respect to the point of collision, that is the origin in the laboratory frame. The separation of the collision partners r_a and r_b, is given by:

$$\hat{r}_a = \frac{m_b}{m_a + m_b}\left(\hat{R}_a - \hat{R}_b\right) \qquad 4.18$$

Similarly,

$$\hat{r}_b = \frac{-m_a}{m_a + m_b}\left(\hat{R}_a - \hat{R}_b\right) \qquad 4.19$$

Where R_a and R_b are position vectors. The velocity vectors of A and B in the CM frame u_a and u_b are easily obtained by differentiating equations 4.18 and 4.19 with respect to time:

$$\hat{u}_a = \frac{d\hat{r}_a}{dt} = \frac{m_b}{m_a + m_b}(\hat{v}_a - \hat{v}_b) \qquad 4.20$$

And

$$\hat{u}_b = \frac{d\hat{r}_b}{dt} = \frac{-m_a}{m_a + m_b}(\hat{v}_a - \hat{v}_b) \qquad 4.21$$

equation 4.20 and 4.21 can now be used to find the sum of the linear momenta (ΣP_{cm})

$$\Sigma P_{cm} = m_a\hat{u}_a + m_b\hat{u}_b = \frac{m_a m_b}{m_{a+m_b}}(\hat{v}_a - \hat{v}_b) - \frac{m_a m_b}{m_a + m_b}(\hat{v}_a - \hat{v}_b) = 0 \qquad 4.22$$

Hence, the total linear momentum in the centre of mass system is zero
Similarly, the relative kinetic energy of the reactants in the centre of mass system for A and B of centre of mass kinetic energies is given by:

$$T_a = \frac{1}{2}m_a\hat{u}_a^{\,2} = \frac{1}{2}m_a\left[\frac{m_a}{m_a + m_b}(\hat{v}_a - \hat{v}_b)\right]^2 \qquad 4.23$$

$$T_b = \frac{1}{2}m_b\hat{u}_b^{\,2} = \frac{1}{2}m_b\left[\frac{-m_b}{m_a + m_b}(\hat{v}_a - \hat{v}_b)\right]^2 \qquad 4.24$$

Thus, the combined centre of mass kinetic energy is given by:

$$T = T_a + T_b = \frac{1}{2}\frac{m_a m_b}{m_a + m_b}(\hat{v}_a - \hat{v}_b)^2\left(\frac{m_b}{m_a + m_b} + \frac{m_a}{m_a + m_b}\right) \qquad 4.25$$

Simplifying,

$$T = \frac{1}{2}\mu v^2 \qquad 4.26$$

At large separations R, the relative velocities and, hence, the relative kinetic energy T are constant. Therefore the total kinetic energy ET is equal to the relative kinetic energy T at large interspecies separations where any forces between the collision partners are negligible. However, as the two particles converge, the relative kinetic energy is changed as a result of the interaction between the collision partners and only the total collision energy is conserved.

$$E_T = \frac{1}{2}\mu v^2 = T + V(R) \qquad 4.27$$

Where v is the initial value of the relative velocity of the collision partner (i.e. at large values of separation R where $V(R)$ is effectively zero). Hence the relative kinetic energy available at the point of interaction T, is dependent upon the separation R:

$$T = E_T - V(R) \qquad 4.28$$

4.4 Collision cross-sections and impact parameter[11]

For a chemical reaction to take place, the reactant species must come into close enough contact to allow the chemical rearrangement of the collision partners. As a first approximation, the assumption is made that the reactants are hard spheres and must collide before a reaction takes place.

Hence, the interspecies centre-centre separation R upon collision is given by $R=d$. In other words, a collision occurs whenever the centre of one molecule enters a sphere of radius d around the second molecule. For an incident reactant molecule this sphere presents an effective area centered around its collision partner, into which its centre must enter for a collision to occur. The physical size of the collision partners therefore determines the collision cross-section. The collision cross-section σ_c can be defined as

$$\frac{1}{\lambda} = \sigma_c n \qquad 4.29$$

Where λ is the mean free path and n_b is the number density of the collision partner. As can be seen from equation 4.29, increasing the collision cross-section has the effect of increasing the chances of a collision occurring. This is quantitatively observed as a reduction in the distance the reactant travels before colliding (the mean free path). For

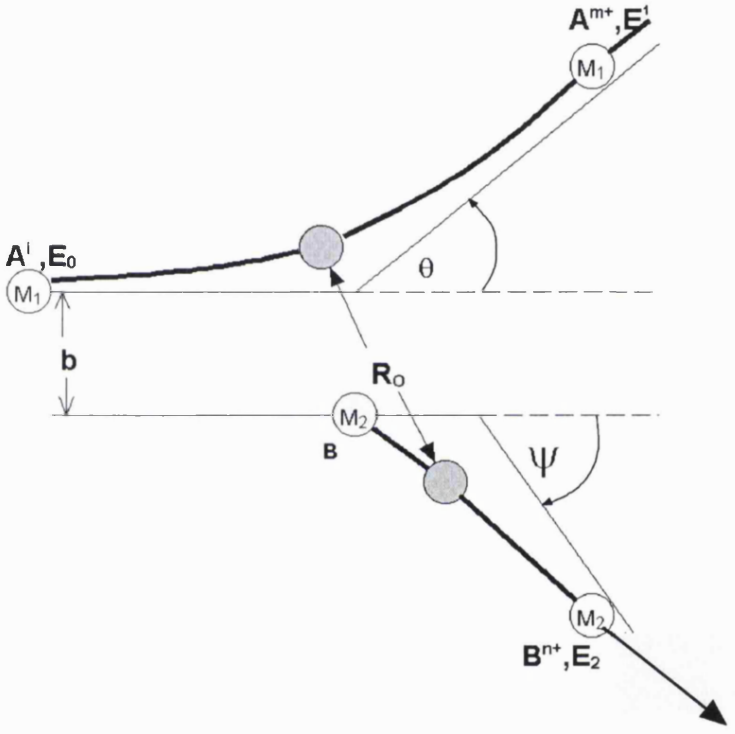

Figure 4.2 Schematic of the collision $A^{i+} + B \rightarrow A^{m+} + B^{n+} + (m+n-1)e$ in the laboratory coordinates. The ion energies E, the scattering angle θ and ψ, and the impact parameter b are indicated. The shaded circles show the position of the ions at the distance of closest approach.

real molecules the collision cross-section can be considered in terms of the impact parameter b. The impact parameter is defined as being the distance of closest approach of the particles in the absence of an interparticle force. If one considers ion trajectories having impact parameters in the range b to $b+db$ and assuming cylindrical symmetry of the ion flux, then the ion trajectories have to pass through an annular volume of radius b and thickness db in a plane perpendicular to the original direction of motion. Hence, this gives an element of the collision cross-section $d\sigma_c$ where:

$$d\sigma_c = 2\pi b db \qquad 4.30$$

Integrating equation 4.30 for all values of the impact parameter up to a maximum (b_{max}) that will result in a collision, at a given collision energy, gives:

$$\sigma_c = \pi b^2_{\max} \qquad 4.31$$

For example, in the hard sphere model b_{max} is equal to the hard sphere diameter d, giving a hard sphere collision cross-section $\sigma_c = \pi d^2$

4.5 The reaction cross-section

The reaction cross-section σ_r governs the rate of those collisions that lead to chemical reaction. It is the measure of the effective size of the molecules as determined by the propensity to react. It is therefore smaller than the collision cross-section, which governs the rate of all collisions, irrespective of their outcome.[11]

Hence when we pass a beam through a scattering cell, the loss of the beam flux due to reactive collisions is given by

$$-\left(\frac{dI_A}{dx}\right) = k(v)N_A N_B = I_A(x)N_B\sigma_r \qquad 4.32$$

Where the beam of the incident reactant A of a number density N_A passing through a reaction cell containing the collision partner B of number density N_B and I_A is the intensity of the beam of reactant species A at position x.

In a simplified model it is possible to estimate the reaction cross-section by assuming that every collision results in a reaction. This is clearly a gross over simplification since there are many possible outcomes of a collision such as non-reactive scattering and electron transfer.

Consequently,

$$\sigma_c > \sigma_r \qquad 4.33$$

As the reactants approach one another at some given energy the initial approach can be characterized in terms of the impact parameter. For a chemical reaction to take place, it

is necessary for the molecules to approach sufficiently close so that 'chemical' forces can operate and the necessary atomic rearrangements can take place. For collisions of high impact parameter the centrifugal barrier keeps the molecules apart. During the collision, the kinetic energy, which is initially wholly translational, is being converted to centrifugal energy. As the two particles approach each other, their centrifugal energy (due to the rotation of their relative separation) increases. The centrifugal energy acts as a repulsive contribution, which is known as the centrifugal barrier, in that it prevents the too-close approach of the colliding particles. We therefore expect that reaction will take place only when b is small that is, of the order of the range of the intermolecular force, and hence that the reaction will fail to occur [i.e. $P(b)=0$] for higher values of b.

4.6 Conclusion

In situations where there is a lack of comparative data, as is the case of the gas-phase reactivity of doubly charged molecules with neutral molecular targets, understanding related theoretical information is of great importance. The subjects discussed in this Chapter are all important in gaining an understanding of reactive processes. The Landau-Zener model described in this Chapter provides a means of gauging the likelihood of electron transfer reactivity and forms the basis for models of bond-forming reactions presented in the following Chapters.

References:

1 M. Manning, S. D. Price, and S. R. Leone, *J. Chem. Phys.* **99,** 8695-8704 (1993).

2 S. A. Rogers, S. D. Price, and S. R. Leone, *J. Chem. Phys.* **98,** 280-289 (1993).

3 S. D. Price, S. A. Rogers, and S. R. Leone, *J. Chem. Phys.* **98,** 9455-9465 (1993).

4 S. D. Price, M. Manning, and S. R. Leone, *J. Am. Chem. Soc.* **116,** 8673-8680 (1994).

5 S. D. Price, *J. Chem. Soc. Faraday Trans.* **93,** 2451-2460 (1997).

6 L. Landau, *Phys. Z. Sowjetunion* **2,** 26 (1932).

7 C. Zener, *Proc. Roy. Soc. Lond. Ser. A* **137,** 696 (1932).

8 K. A. Newson and S. D. Price, *Chem. Phys. Lett.* **269,** 93-98 (1997).

9 R. E. Olson, F. T. Smith, and E. Bauer, *Applied Optics* **10,** 1848 (1971).

10 P. Champkin, N. Kaltsoyannis, and S. D. Price, *Int. J. Mass Spectrom. Ion. Proc.* **172,** 57-69 (1998).

11 *Molecular Reaction Dynamics and Chemical Reactivity*, edited by R. D. Levine and R. B. Bernstein (Oxford University Press, Inc, 1987).

Chapter 5

Electron transfer reactions between CF_3^{2+} and Ar

5.1 Introduction

Experimental investigations have recently focused on the reactions of perfluorinated molecular ions, such as CF_2^{2+} and SiF_2^{2+}.[1-3] For these dications, neutral loss reactions in addition to electron transfer and collision induced charge separation, are observed to occur following collisions with the rare gases.[3,4]

Early experiments to investigate the reactivity of molecular dications involved colliding doubly charged ions formed by non-dissociative double ionisation of stable molecules (e.g. CS_2^{2+}, CO^{2+}) with atomic targets.[1,5-8] These experiments revealed a rich electron transfer reactivity (Equation 5.11) which was rationalized using a simple model based on the Landau-Zener theory which has been discussed in detail in Chapter 4. Some of these observations also showed dicationic charge separation (Equation 5.12) induced by collisional energy transfer.

$$CO_2^{2+} + Ar \rightarrow CO_2^{+} + Ar^{+} \qquad 5.11$$

$$CO_2^{2+} + Ar \rightarrow CO^{+} + O^{+} + Ar \qquad 5.12$$

Later experiments explored the reactivity of fragment dications (e.g. CF_2^{2+}, SiF_2^{2+}), as mentioned above, in collision with atomic targets.[1-3,9] These experiments found, in addition to the electron transfer reactivity observed with other dications, that there was a propensity for the dication to lose neutral species upon collisional excitation.[2,4,10]

This Chapter presents an investigation of the product ions formed following collisions of CF_3^{2+} with Ar. We study the relative yields of the electron transfer reactions and also investigate the collision energy dependence of the neutral loss reactions. The latter part

of the investigation allows us to estimate the C-F bond energy in CF_3^{2+} which will be discussed later on in this Chapter.

5.2 Experimental Details

A detailed account of the experimental methodology employed in the mass spectrometric measurements is given in Chapter 2. As mentioned in Chapter 2, in order to ensure single collision conditions the number density in the TOFMS is carefully controlled, and is confirmed by linear dependence of the product ion yields on the neutral gas pressure. This is achieved by the careful monitoring of the target gas pressure, which is set at 3×10^{-6} Torr in this investigation. The stringent regulation of the target gas pressure at this level not only ensures single collision conditions, but also attempts to avoid pressure-related deviations in the intensities of the product ions. Any deviations in the product ion intensities may then be attributed directly to fundamental changes in the reaction process. The Ar collision partner is obtained from a lecture bottle and stored in a low-pressure reservoir. To ensure that the electronic state distribution in the dication beam is the same throughout the course of the experiment, the operating conditions of the ion source are strictly controlled.[11]

5.3 Results and analysis

Time of flight mass spectra were recorded following collisions between CF_3^{2+} and Ar at lab frame collision energies from 3 to 12 eV. These correspond to centre of mass frame collision energies between 1.8 to 4.4 eV. The centre of mass collision energy is calculated using the initial dication velocity, which is known from the beam potential, and assuming that the velocity of the neutral molecule is negligible with respect to the velocity of the dication. Given that the neutrals are admitted as an effusive beam and that the dication beams have energies between 3 and 12 eV in the laboratory frame this approach is perfectly satisfactory. When the mass spectra are corrected for impurity ions in the dication beam, as discussed in Chapter 3, we clearly see the presence of CF_2^{2+}, CF^+, CF_2^+ and Ar^+ ions resulting from the bimolecular encounters of CF_3^{2+} with Ar. A representative time-of-flight mass spectrum is shown in Figure 5.1

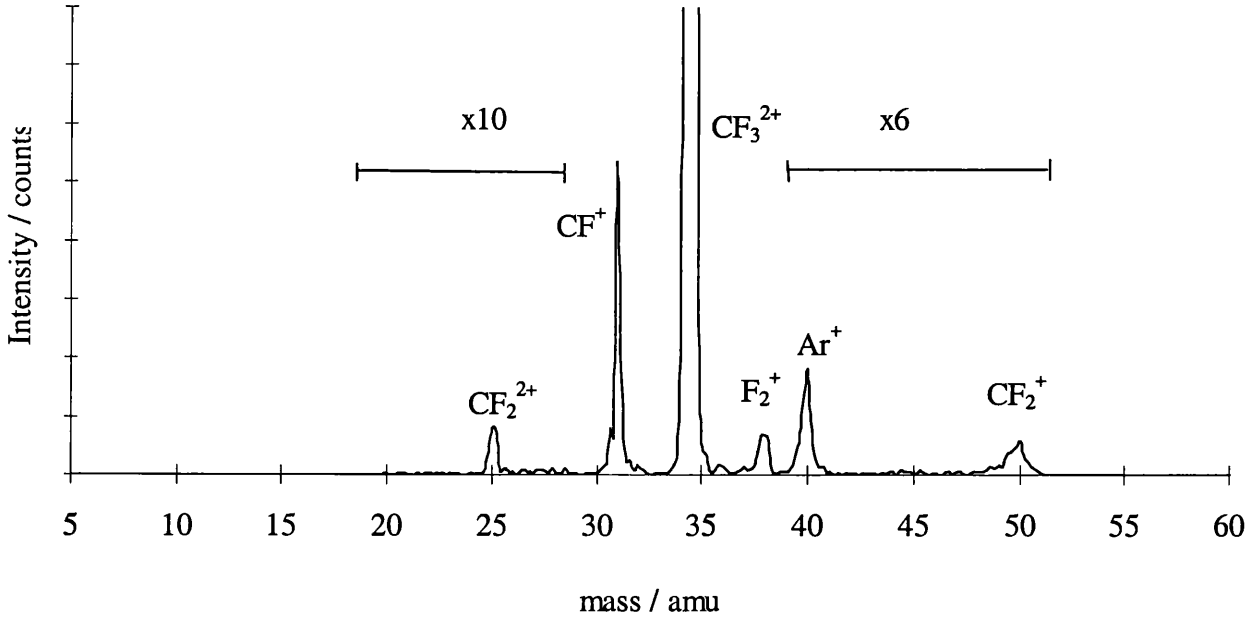

Figure 5.1 Time of flight mass spectrum showing the product ions formed in collisions between CF_3^{2+} and Ar atoms at collision energy of 3.3 eV in the centre-of-mass frame.

5.4 Assignment of product ions

As mentioned above the TOF mass spectra clearly indicate the presence of F_2^+, CF^+, CF_2^{2+}, CF_2^+ and Ar^+. F_2^+ and CF^+ are present in the absence of any collision gas and after analysis to correct for background and impurity ions, as explained in Chapter 4, F_2^+ was found to be an impurity ion. As mentioned above, although CF^+ is also an impurity ion, which is present in the absence of any collision gas, after correction, some of the CF^+ is found to be present as a product ion. CF_2^{2+}, CF^+, CF_2^+ and Ar^+ are clearly formed in bimolecular encounters. Representative values of the background corrected product ion intensities confirming this conclusion are shown in Table 5.1 below, together with their experimental uncertainties.

Table 5.1 Background corrected product ion intensities [in arbitrary units (au)] recorded following collisions of CF_3^{2+} with Ar at collision energy of 3.3 eV in the centre of mass frame. The number in the parentheses gives the uncertainty in the last Figure of the product ion intensity.

Product ions	CF_2^{2+}	CF^+,	Ar^+	CF_2^+	F_2^+
Intensity (au)	64(7)	161(36)	170(14)	201(14)	-1(26)

The identities of these product ions immediately allow considerable insight into the reactivity of the CF_3^{2+}/Ar collision system. Firstly, the CF_3^{2+} product ion can only be formed as a result of collision induced neutral loss (Equation 5.13),

$$CF_3^{2+} + Ar \rightarrow CF_2^{2+} + F + Ar \qquad 5.13$$

The reaction process that leads to the formation of the CF_2^+ and CF^+ product ions that we detect can be formed by either dissociative electron transfer (Equation 5.14) or collision induced charge separation (Equation 5.15)

$$CF_3^{2+} + Ar \rightarrow CF_3^{+*} + Ar^+ \rightarrow CF_2^+ + F + Ar^+ \qquad 5.14$$

$$CF_3^{2+} + Ar \rightarrow CF_2^+ + F^+ + Ar \qquad 5.15$$

However, the absence of any real F^+ signals in the mass spectra eliminates the possibility of CF_2^+ and CF^+ product ions being formed as a result of collision induced charge separation. Hence these ions are assigned as the products of dissociative electron transfer reactions. Indeed, the formation of just CF^+ and CF_2^+ ions from CF_3^{2+} following electron transfer has been reported before.[12]

5.5 Product ion intensities

In common with the results of all the collision experiments reported in this thesis, the intensities of the competing electron transfer and chemical (bond-forming) reaction channels are obtained from suitably background and impurity ion-corrected measurements of the detected intensities of the product ions. In addition to the background ion contribution, the product ion intensities are also corrected for variations in the detection efficiency.

As discussed in Chapter 3, dication reactions may result in a significant release of kinetic energy. This kinetic energy release (KER) in the centre of mass frame affects the product ion translational energy component in the lab frame. Each of the reaction channels may have differing average KER values and differing distributions of the KER. Consequently different product ions may have different transverse velocities. Therefore due to their different transverse velocities, the product ion will travel through different distances across the spectrometer, in a plane perpendicular to its central

(longitudinal) axis, in the transit time between leaving the spectrometer's source region and reaching the MCP detector.

Those ions with larger transverse kinetic energies in the lab frame will travel a greater distance away from the central axis of the TOFMS than less energetic product ions. Owing to this effect, the length of the source region, which is imaged on to the MCP detector, varies with the total kinetic energy of the product ion. Hence, the background and impurity corrected ion count must be further adjusted, to allow for this potential discrimination, to yield the true relative ion intensities. A detailed discussion of the methodology behind the background ion correction and the subsequent corrections for the detection efficiency variability is given in Chapter 3.

In principle, the transverse velocity of the product ions in the laboratory frame can be calculated given the value of the KER for the reaction and the laboratory-frame collision energy using basic kinematics. This approach involves assuming, as has been shown recently to be the case for CF_2^{2+}/D_2 system,[13] that dissociative electron transfer involves the population of unstable states of CF_3^+ which subsequently dissociate to form CF^+ or CF_2^+ with an energy release negligible in comparison to that of the Coulombic repulsion between the Ar^+ and the parent ion. Unfortunately, no data concerning the KER values and distributions for the electron transfer reactions between CF_3^{2+} and Ar are available in the literature. In light of this scarcity of data, the KER data for the electron transfer channels in the CF_2^{2+}/D_2 collision system,[14] has been used in the correction process for the CF_3^{2+}/Ar data presented in this Chapter. Using this datum is not a major approximation, as undoubtedly the KER of the electron transfer channels in both collision systems is dominated by the Coulombic repulsion between the singly charged product ions. In fact the relative correction factors which have been calculated are not a strong function of the KER, which further supports this approach. To use these representative KER values to determine the average product ion velocity we also assume that the dynamics of the collision system predominantly involve forward scattering. Although this is an assumption, angularly resolved investigations indicate forward scattering as the dominant reaction mechanism in dication electron transfer reactions.[13-15]

After using the representative KER values to determine the product ion velocities, the correction formula (Equation 3.13), is applied to the corrected ion intensities to give the true relative ion intensities R for CF_2^+ and CF_3^+. The derivation of the correction formula has been described in detail in Chapter 3.

Table 5.2 Correction factors α calculated by using Equation (3.18) for the relative detection efficiency of CF_2^+ and CF^+ and the resulting relative ion intensities R (CF^+)/R (CF_2^+) derived from the background corrected experimental data.

E_{COM}	α	$R(CF^+)/R(CF_2^+)$
4.4	0.59	0.65
4.0	0.62	0.57
3.7	0.64	0.72
3.3	0.66	0.53
2.9	0.68	0.51
2.6	0.71	0.31
2.2	0.73	0.57
1.8	0.75	0.51

By calculating α for the collision system employed in this work (Table 5.2) it can be seen that the detection efficiency varies only slightly (12%) over the collision energies employed in this work and the CF_2^+ ion is always slightly discriminated against.

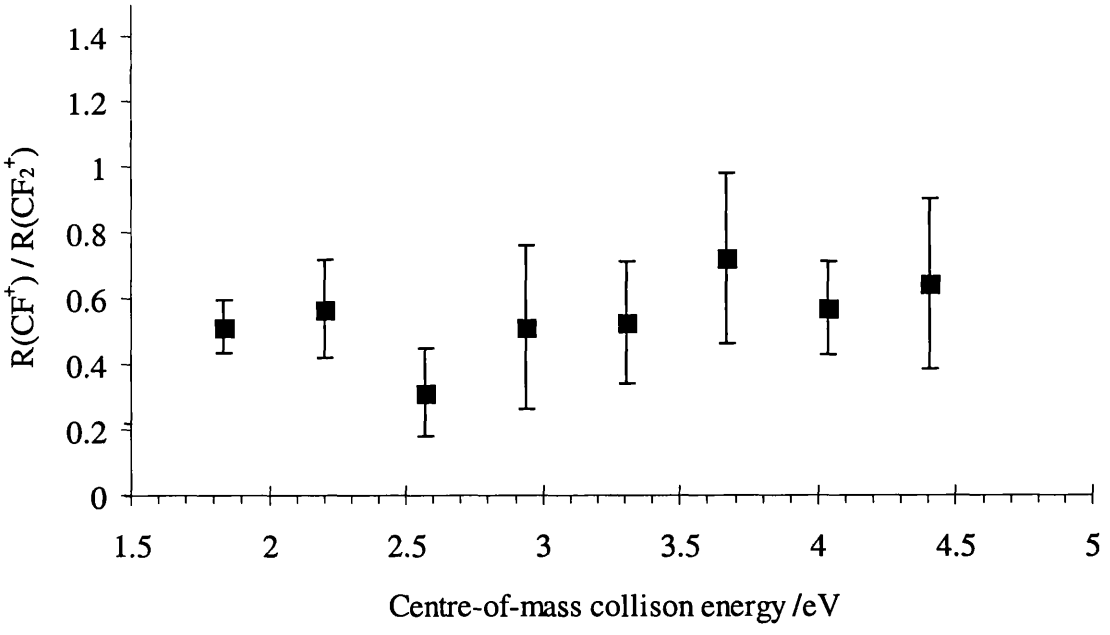

Figure 5.2 Variation of the relative ion intensity of the CF^+ and CF_2^+ product ions, as a function of collision energy, following collisions of CF_3^{2+} with Ar

The discrimination arises from the fact that the velocity of both the CF_2^+ and CF^+ ions across the source region is determined by the initial velocity of the CF_3^{+*} ion, the primary product of the electron transfer reaction. Hence, the heavier CF_2^+ ion has a

large transverse kinetic energy and is less efficiently detected. Correcting our background corrected ion intensities using the values of α (Table 5.2) yields the relative intensities also listed in Table 5.2 and plotted in Figure 5.2. It can be seen from Figure 5.2 that within our error limits the relative cross-sections for forming CF_2^+ and CF^+ are in approximate ratio of 2:1 and do not vary significantly with the collision energy employed in this work.

5.6 Discussion

5.6.1 Neutral-loss reactivity

Figure 5.3 shows the yield of the neutral loss reaction (Equation 5.3) as a function of the centre of mass collision energy. As shown in Figure 5.3, linear extrapolation, by using a least squares analysis of the experimental data, of the CF_2^{2+} yield to the energy axis results in an estimate of the energy required to collisionally dissociate an F atom from CF_3^{2+}. This estimate provides a lower bound on the bond energy as the contribution of any internal excitation in the CF_3^{2+} projectile to breaking the C-F bond is neglected. This estimate of the bond energy indicates, as expected that the CF_3^{2+} dication possesses one extremely weakly bound (~55 kJmol-1) fluorine atom.

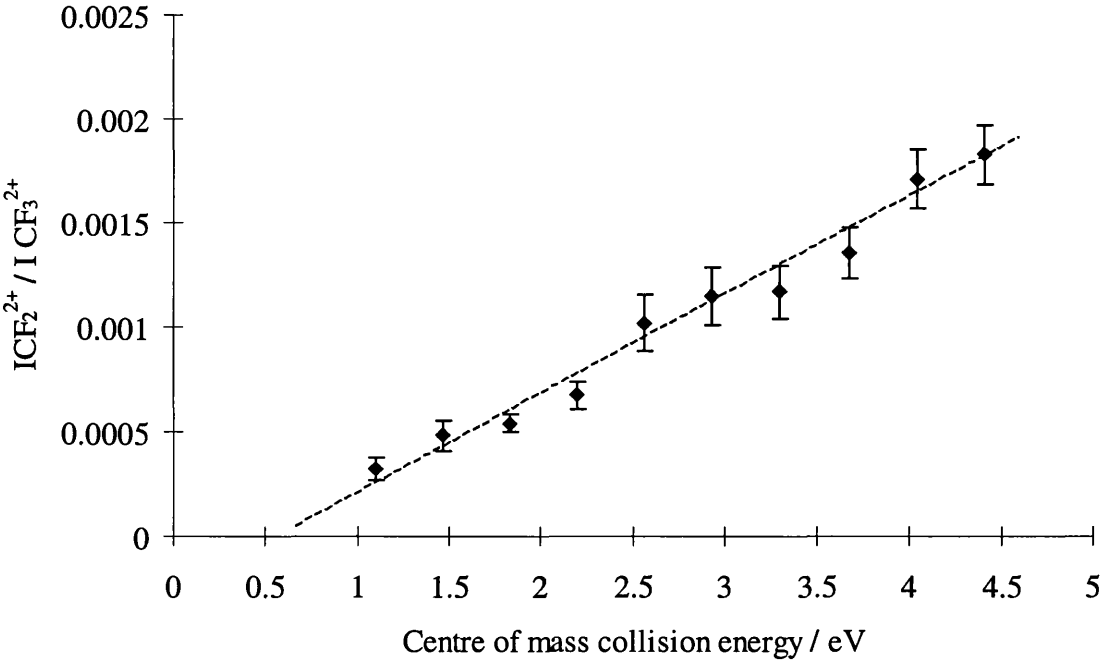

Figure 5.3 Variation of the ion intensity of CF_2^{2+}, relative to the number of unreacted dications, as a function of collision energy following collisions of CF_3^{2+} with Ar. The line is a least-squares fit to the data.

Our *ab initio* calculations described below indicate that the $^2B_2$ ground state of CF_3^{2+} has a T shaped C_{2v} geometry, as illustrated in Figure 5.4, with one long and two short C-F bonds. This calculated structure and its total energy (-335.90 Hartree) are in excellent agreement with very recent calculations of Hrusak *et al.* (total energy = -335.93 Hartree).[16] In previous work, the electron transfer reactivity of molecular dications has been rationalised using a simple model based on the Landau-Zener theory.[5] In order to apply this model to the CF_3^{2+}/Ar collision system we need to know the electronic state energies of CF_3^{2+} and CF_3^+ at the geometry at which the electron transfer occurs. As CF_3^{2+} is the reactant species, we assume the geometry of the electron transfer reaction is that of the equilibrium geometry of the ground state of CF_3^{2+}. Unfortunately the electronic and structural data required for this analysis are not available in the literature and we have calculated the required energetics *ab initio* described below.

Ab initio calculations were carried out by Dr Nikolas Kaltsoyannis at University College London (UCL). The calculations were performed using the GAUSSIAN98 [17] and MOLPRO96.4 [18] program suites. All ground state calculations were carried out at the unrestricted Hartree-Fock level with the correlation consistent valence triple zeta basis set of Kendall *et al.*[19] The geometry of the $^2B_2$ ground state of CF_3^{2+} was calculated using GAUSSIAN98, electron correlation being added at the MP2 level. The electronic states of CF_3^+ at the ground state geometry of CF_3^{2+} were then calculated using the state-averaged complete active space self-consistent field/multireference configuration interaction (CASSCF/MRCI) [18,20-22] approach implemented in MOLPRO. The active space for the CASSCF calculations comprised of the nine highest occupied molecular orbitals (i.e. 18 electrons) and the four lowest unoccupied molecular orbitals. The energies of the lowest three roots of the singlet and triplet states of each of the four spatial symmetries of C_{2v} were calculated.

As mentioned, since electron transfer will result in the formation of CF_3^+ ions with the geometry of the reactant dication, to apply the Landau Zener model, which has been discussed in detail in Chapter 4, to the collision and explain the observed relative yield of CF^+ and CF_2^+ we require the energies of the ground and excited states of CF_3^+ at the dication geometry. The calculated relative energies of the lowest lying states of CF_3^+ at the ground state geometry of CF_3^{2+} are given in Table 5.4 and schematically illustrated in figure 5.6. The C_{2v} geometry CF_3^{2+} has, as in the case of the isoelectronic BF_3^+ ion [23],

been ascribed to a second-order Jahn Teller distortion.[16] The second-order Jahn-Teller distortion is a structural distortion

Table 5.3 The energies (eV) of the lowest lying electronic states of CF_3^+ (relative to the energy of the $^1A_1$ ground state in its equilibrium D_{3h} geometry) at the geometry of the $^2B_2$ ground state of CF_3^{2+}

	Energy (eV)		
State		n=2	n=3
$^1A_1$	0.226	7.605	15.766
$^3A_1$	7.205	8.88	13.542
$^1A_2$	7.428	11.475	15.096
$^3A_2$	7.367	11.356	14.823
$^1B_1$	8.625	8.806	14.033
$^3B_1$	8.031	8.831	14.008
$^3B_2$	7.748	11.085	14.715

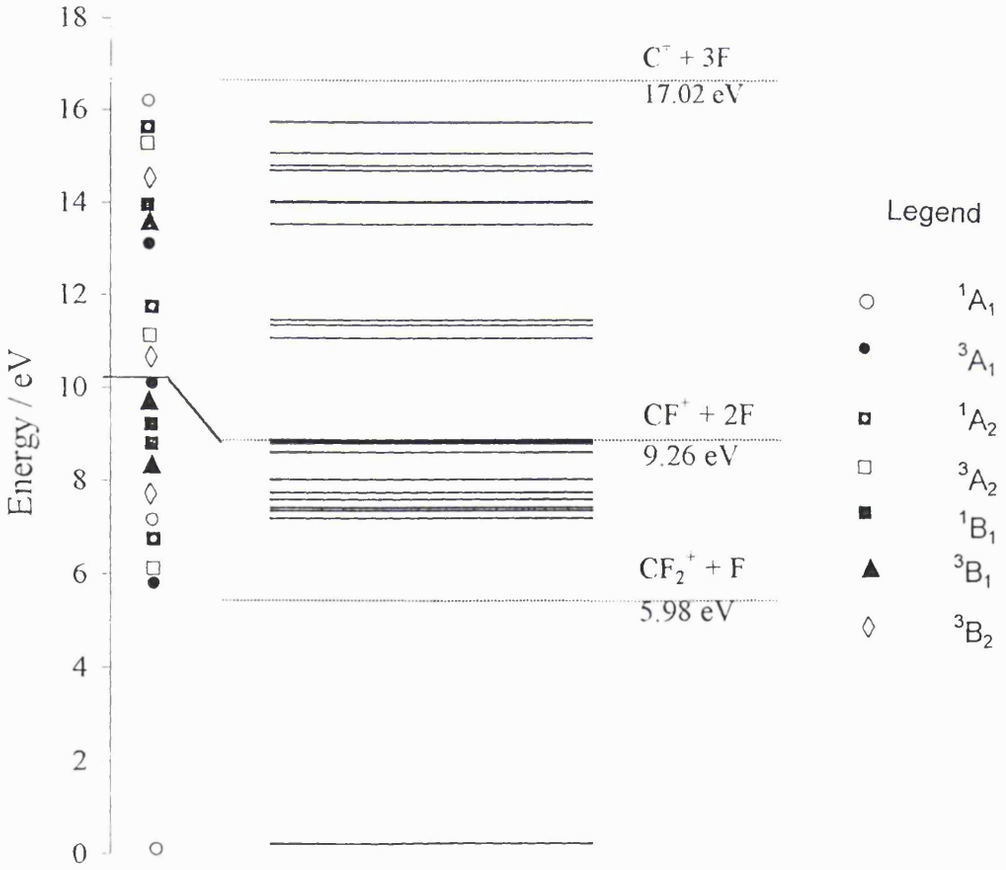

Figure 5.5 Schematic diagram of the energies (eV) of the lowest lying electronic states of CF_3^+ (relative to the energy of the $^1A_1$ ground state in its equilibrium D_{3h} geometry) at the geometry of the $^2B_2$ ground state of CF_3^{2+}

arising from a second-order energy change in the HOMO. Molecules with a small energy gap between the occupied and the unoccupied MOs are susceptible to a structural distortion, which allows intermixing between them. This distortion results in the lowering of the symmetry of the ground state with a lengthening and consequent weakening of one of the C-F bonds. However, the neutral-loss reactivity exhibited in the collision reactions of CF_3^{2+} is no longer an isolated phenomenon. Neutral-loss reactivity contributes significantly to the product ion yield following bimolecular collisions of a wide variety of perfluorinated dications.[2,4,10] Clearly, *ab initio* investigations of the electronic structure of a variety of the perfluorinated dications would be valuable in determining if Jahn Teller distortions are always at the heart of the neutral-loss reactivity of dications, or whether as has been previously proposed,[4] large dications consist of a strongly bound dication core (e.g. CF_2^{2+}) together with one or more weakly bound atoms.

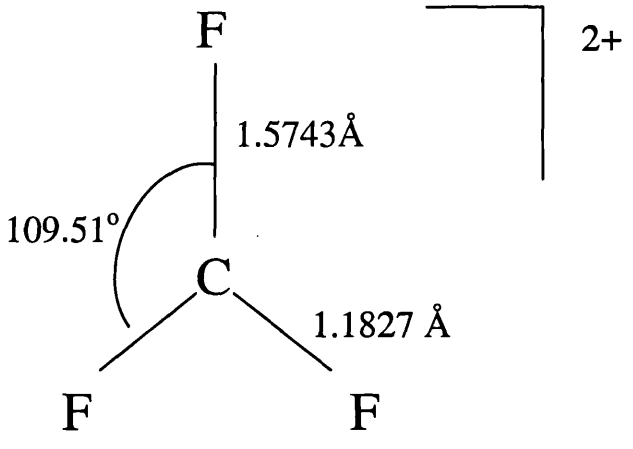

Figure 5.4 The calculated geometry of the $^2B_2$ ground state of CF_3^{2+}

5.6.2 Electron transfer reactivity.

In an attempt to explain the relative ion yields of CF_2^+ and CF^+ (Figure 5.2), the reaction process is rationalised using a 'curve crossing' model based on the Landau-Zener theory of electron transfer. As mentioned above a full account of this approach is given in Chapter 4. Briefly, the model pictures the reactants as approaching each other on a potential energy curve dominated by polarisation attraction. At some interspecies separation, the curve crossing radius, this reactant potential may cross the potential energy curve corresponding to the products of the reaction and an electron can be transferred from the neutral to the dication. The product potential is modeled as purely

repulsive as it is dominated by the electrostatic repulsion between the two singly charged product ions.

Together with this Landau-Zener algorithm, and our calculated state energies, the cross-sections for populating the various low-lying electronic states of CF_3^+ from the ground state of CF_3^{2+} can be calculated. However in order to transform these calculated electron transfer cross-sections into a prediction of the ion yield we need to know the stability of the CF_3^+ states we populate. Unfortunately, again, unlike more common ions (e.g. OCS^+), this information is unavailable. Hence, it is necessary to make a series of assumptions that have been used previously to predict the fate of excited states of molecular ions formed in electron transfer reactions.[1,2,5,6] In this approach we assume that if a CF_3^+ electronic state lies above a thermodynamic dissociation limit, then it dissociates to yield those dissociation products on the timescale of the experiment. If the state is at high enough energy to lie above two dissociation limits, we assume that it dissociates to the closest lying limit. Thus, the population of a CF_3^+ electronic state lying on or above the asymptote for fragmentation into $CF_2^+ + F$ at 5.98 eV [24] (relative to the equilibrium geometry of the 1^1A_1 ground state of CF_3^+ which we use as our energy zero) will result in the observation of CF_2^+ in the product mass spectrum. Similarly, an electronic state of CF_3^+ lying on or above the dissociation asymptote at 9.26 eV [24] will fragment into the $CF^+ + 2F$ channel and a state lying on or above the asymptote at 17.02eV will fragment into $C^+ + 3F$ channel resulting in the observation of CF^+ and C^+, respectively, in the product ion mass spectrum.

Table 5.4 and figure 5.6 show that the calculated cross-sections for the population of electronic states that lie above 15 eV is effectively zero. This arises as the electron transfer exothermicity for populating such high-lying states is sufficiently small that the curve crossing is highly diabatic and no electron transfer occurs. Hence we predict that the electron transfer reactions in this system cannot populate any CF_3^+ state lying above the dissociation asymptote to $C^+ + 3F$. Thus we do not expect to see any C^+ fragments in the product ion mass spectrum, which is in accord with our experimental observations. Also, within our error limits, we observe no CF_3^+ signals that result from bimolecular encounters. The data presented in Table 5.4 are in good agreement with this observation. Table 5.4 shows that we calculate no significant probability for populating the ground state CF_3^+, the only state that lies below the $CF_2^+ + F$ asymptote at this geometry, by electron transfer.

Experimentally CF_2^+ ions are a significant component of the ion yield, and it is clear from the data presented in Table 5.4 that the CF_3^+ states populated by the electron transfer reactions of the ground state of CF_3^{2+} all lie below the asymptote for dissociation to $CF^+ + 2F$ but above the dissociation asymptote leading to $CF_2^+ + F$. Hence we predict a significant CF_2^+ signal in the product ion mass spectrum. Again this is in accordance with our experimental observations. However we see that from Table 5.4 that the ground state of CF_3^{2+} has a low probability of populating any excited states of CF_3^+ which lie high enough in energy to dissociate to $CF^+ + 2F$. This is in conflict with our experimental data (Figure 5.2) which show that, although CF_2^+ is the dominant product ion, CF^+ is also formed in significant quantities. There are several possible explanations for this disagreement. First, it is possible that the calculated relative energy of the ground state of CF_3^{2+} is in error. We feel that this is unlikely, as the energetics from the *ab initio* calculations agree closely with those of other workers.[16] Indeed, a significant error in the energy (~5 eV) would be required to give the ground state of CF_3^{2+} sufficient energy to populate CF_3^+ states that can dissociate to CF^+ via electron transfer. Second, it may be that the ground state CF_3^{2+} ions in the dication beam are not predominantly at their equilibrium geometry which is where we assume the reaction to occur. However the estimated pressure in the ion source is such that we would expect a significant probability for some vibrational relaxation following ionization and, even if some vibrational excitation is not present, the average geometry of the ground state dications should be well represented by the equilibrium geometry. In addition, since the ions must survive for a flight time of several tens of microseconds before they encounter the neutral beam, it is likely that highly excited vibrational states of the ground state will predissociate before they reach the interaction region. Indeed, previous investigations of the electron transfer reaction of polyatomic molecular dications have shown that the observed ion yields are consistent with the dications in the ion beam being well described by the ground state geometry.[2] Thirdly, it is quite possible that the ground state of the dication is not the only electronic state of CF_3^{2+} present in our ion beam. Indeed, previous studies of perfluorinated dications have provided evidence that excited dication states can exist in ion beams.[1,13,25] Our Landau-Zener model predicts (Table 5.4) that a metastable CF_3^{2+} state lying 5 eV above the ground state of the dication would react principally to populate CF_3^{2+} states which dissociate to yield CF^+ rather than CF_2^+ or C^+. We feel that this latter explanation is the most probable and that our ion beam is composed of CF_3^{2+} ions in both ground and

Table 5.4
Calculated electron transfer cross-sections σ (in arbitrary units) for populating the low-lying electronic states of CF_3^+ listed in table 5.4 from (a) the ground state of CF_3^{2+}, which lies 25.184 eV above the equilibrium geometry of CF_3^+ and (b) an excited state of CF_3^{2+} lying 5 eV higher in energy.

CF_3^{2+} state	Product ion	σ(CF_3^{2+} E=25.185 eV)	σ(CF_3^{2+} E=30.185 eV)
$1\,^1A_1$	CF_3^+	0	0
$2\,^1A_1$	CF_2^+	0.18	0.02
$3\,^1A_1$	CF^+	0	0
$1\,^3A_1$	CF_2^+	1.82	0.01
$2\,^3A_1$	CF_2^+	0	0.42
$3\,^3A_1$	CF^+	0	0
$1\,^1A_2$	CF_2^+	0.57	0.02
$2\,^1A_2$	CF^+	0	15.80
$3\,^1A_2$	CF^+	0	0
$1\,^3A_2$	CF_2^+	0.81	0.01
$2\,^3A_2$	CF^+	0	18.45
$3\,^3A_2$	CF^+	0	0
$1\,^1B_1$	CF_2^+	0	0.22
$2\,^1B_1$	CF_2^+	0	0.34
$3\,^1B_1$	CF^+	0	0
$1\,^3B_1$	CF_2^+	0	0.05
$2\,^3B_1$	CF_2^+	0	0.37
$3\,^3B_1$	CF^+	0	0
$1\,^1B_2$	CF_2^+	0.06	0.03
$2\,^1B_2$	CF^+	0	22.02
$3\,^1B_2$	CF^+	0	0

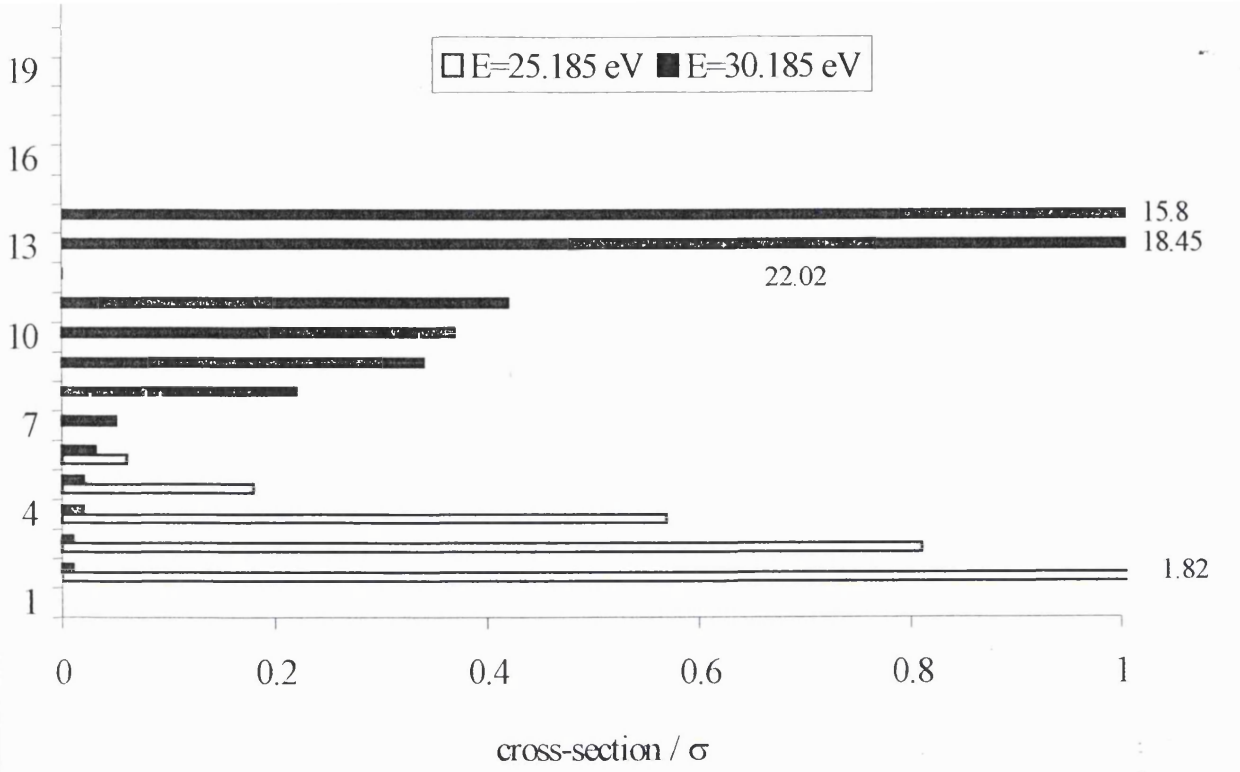

Figure 5.6 Schematic representation of electron transfer cross-sections σ in arbitrary units) for populating the low-lying electronic states of CF_3^+ listed in table 5.4 from (a) the ground state of CF_3^{2+}, which lies 25.184 eV above the equilibrium geometry of CF_3^+ and (b) an excited state of CF_3^{2+} lying 5 eV higher in energy.

excited states. It is reassuring to note that the Landau-Zener calculations predict no dramatic change in the relative electron transfer cross-sections with collision energy, as we observe experimentally.

5.7 Conclusion

This study of the identities and relative intensities of the product ions formed following collisions of CF_3^{2+} with Ar show that electron transfer and neutral-loss reactivity dominates the product ion yield. The variation of the neutral-loss ion yield with the collision energy provides a first estimate for the bond energy of the weak CF_2^{2+} - F bond as 58 $kJmol^{-1}$. *Ab initio* calculations performed to try to rationalize the yield of the electron transfer reactions indicate that the ground state of CF_3^{2+} adopts a C_{2v} equilibrium geometry. Using this *ab initio* calculation, together with calculated energies of the electronic states of CF_3^+ and Landau-Zener theory, we are forced to conclude that at least two electronic states of CF_3^{2+} are present in the dication beam, thus allowing for CF_3^+ states to be populated which can dissociate to give our observed product ions. The ground state of CF_3^{2+} is predicted to react via electron transfer to form predominantly $CF_2^+ + Ar^+$. An excited state of CF_3^{2+} lying approximately 5eV above the ground state is, hence, required to explain the formation of CF^+.

References:

1 M. Manning, S. D. Price, and S. R. Leone, *J. Chem. Phys.* **99,** 8695-8704 (1993).

2 P. Champkin, N. Kaltsoyannis, and S. D. Price, *Int. J. Mass Spectrom. Ion. Proc.* **172,** 57-69 (1998).

3 Y. Y. Lee, S. R. Leone, P. H. Champkin, N. Kaltsoyannis, and S. D. Price, *J. Chem. Phys.* **106,** 7981-7994 (1997).

4 S. D. Price, M. Manning, and S. R. Leone, *Chem. Phys. Lett.* **214,** 553-558 (1993).

5 S. D. Price, S. A. Rogers, and S. R. Leone, *J. Chem. Phys.* **98,** 9455-9465 (1993).

6 S. A. Rogers, S. D. Price, and S. R. Leone, *J. Chem. Phys.* **98,** 280-289 (1993).

7 C. E. Melton and G. F. Wells, *J. Chem. Phys.* **27,** 1152 (1957).

8 Z. Herman, P. Johnathon, A. G. Brenton, and J. H. Beynon, *Chem. Phys. Lett.* **41,** 433 (1989).

9 Y. Y. Lee and S. R. Leone, *J. Phys. Chem.* **99,** 15438-15443 (1995).

10 S. D. Price, *J. Chem. Soc. Faraday Trans.* **93,** 2451-2460 (1997).

11 A. Ehbrecht, N. Mustafa, C. Ottinger, and Z. Herman, *J. Chem. Phys.* **105,** 9833-9846 (1996).

12 S. D. Price, M. Manning, and S. R. Leone, *J. Am. Chem. Soc.* **116,** 8673-8680 (1994).

13 J. Zabka, M. Farnik, Z. Dolejsek, and Z. Herman, *Int. J. Mass Spectrom. Ion. Proc.* **192,** 165 (1999).

14 Z. Dolejsek, M. Farnik, and Z. Herman, *Chem. Phys. Lett.* **235,** 99-104 (1995).

15 Z. Herman, *Int. Rev. Phys. Chem.* **15,** 299-324 (1996).

16 J. Hrusak, N. Sandig, and W. Koch, *Int. J. Mass Spectrom.* **187,** 701-706 (1999).

17 M. J. Frisch, G. W. Trucks, H. B. Schlegel, G. E. Scuseria, M. A. Robb, J. R. Cheeseman, V. G. Zakrzewski, J. A. M. Jr., R. E. Stratmann, J. C. Burant, S. Dapprich, J. M. Millam, A. D. Daniels, K. N. Kudin, M. C. Strain, O. Farkas, J. Tomasi, V. Barone, M. Cossi, R. Cammi, B. Mennucci, C. Pomelli, C. Adamo, S. Clifford, J. Ochterski, G. A. Petersson, P. Y. Ayala, Q. Cui, K. Morokuma, D. K. Malick, A. D. Rabuck, K. Raghavachari, J. B. Foresman, J. Cioslowski, J.

V. Ortiz, B. B. Stefanov, G. Liu, A. Liashenko, P. Piskorz, I. Komaromi, R. Gomperts, R. L. Martin, D. J. Fox, T. Keith, M. A. Al-Laham, C. Y. Peng, A. Nanayakkara, C. Gonzalez, M. Challacombe, P. M. W. Gill, B. Johnson, W. Chen, M. W. Wong, J. L. Andres, C. Gonzalez, M. Head-Gordon, E. S. Replogle, and J. A. Pople, (Gaussian Inc., Pittsburgh PA, 1998).

18 H.-J. Werner and P. J. Knowles, *J. Chem. Phys.* **89,** 5803 (1988).

19 R. A. Kendall, T. H. Dunning Jr, and R. J. Harrison, *J. Chem. Phys.* **96,** 6796 (1992).

20 P. J. Knowles and H.-J. Werner, *Chem. Phys. Lett.* **145,** 514 (1988).

21 H.-J. Werner and P. J. Knowles, *J. Chem. Phys.* **82,** 5053 (1985).

22 P. J. Knowles and H.-J. Werner, *Chem. Phys. Lett.* **115,** 259 (1985).

23 E. Haller, H. Koppel, L. S. Cederbaum, W. Vonniessen, and G. Bieri, *J. Chem. Phys.* **78,** 1359-1370 (1983).

24 S. G. Lias, J. E. Bartmess, J. F. Liebman, J. L. Holmes, R. D. Levin, and W. G. Mallard, *J. Phys. Chem. Ref. Data* **17 S1,** 1-861 (1988).

25 K. A. Newson, N. Tafadar, and S. D. Price, *J. Chem. Soc. Faraday Trans.* **94,** 2735-2740 (1998).

Chapter 6

Intramolecular isotope effects in the reactions of CO_2^{2+} and CF_3^{2+} with HD

6.1 Introduction

The most prolific type of reactivity between dications and neutral molecules is electron transfer.[1-5] However, such dication-neutral collision systems display other types of reactivity, such as collision-induced charge-separation[6] (dissociation) and collision-induced neutral-loss.[7] More recent experiments, involving collisions between dications and molecular targets, have revealed that molecular dications can undergo true "chemical" reactions involving the formation of new bonds.[8,9]

Experimental investigations of the bond-forming reactions of molecular dications have been principally restricted to the simple mass spectrometric detection of the product ions. Of the known bond-forming reactions, the reaction of CF_2^{2+} with D_2 to give DCF_2^+ and D^+ has received the most detailed attention.[8-10] A crossed beam scattering study has indicated that the mechanism of this reaction is predominantly 'direct', with forward scattering of the DCF_2^+ product dominating the dynamics.[11] This conclusion is consistent with recent experimental observation that the ion yields for the bond forming reaction in collisions with both H_2 and D_2 are identical, within the experimental uncertainty. These latter experiments also indicate that there is no energy barrier to this reaction. Furthermore, earlier work investigated the competition between the two potential bond-forming pathways in the reaction of CF_2^{2+}/HD as a function of the centre of mass collision energy.

$$CF_2^{2+} + HD \rightarrow HCF_2^+ + D^+ \qquad 6.11$$

$$CF_2^{2+} + HD \rightarrow DCF_2^+ + H^+ \qquad 6.12$$

These experiments show a strong intramolecular isotope effect, at low collision energies, favouring the formation of DCF_2^+. This preference was interpreted in terms of an orientational effect, where initial electron transfer between the reactants results in a pair of singly charged ions formed in close proximity. This orientation model will be discussed in more detail in this Chapter (section 6.2.2). As will be shown, the explanation for the CF_2^{2+}/HD intramolecular isotope effects is purely electrostatic in origin and as such should be present in any chemical reaction of a molecular dication and HD.

This Chapter presents an investigation of the product ions formed following collisions of CF_3^{2+} with HD and collisions of CO_2^{2+} with HD. Other groups have investigated similar systems such as CF_2^{2+}/HD in crossed beam scattering experiments and have studied in detail the dynamics of charge transfer products, dissociative products and also the dynamics of the formation of chemical rearrangement products.[11,12] Where appropriate comparisons between such data and the work carried out in our experimental investigation will be made.

6.2 Isotope Effects

The primary reason for studying isotope effects is that such effects provide the experimentalist with a powerful probe that can reveal information about the reaction mechanism of collision systems.[10,13-22] Isotope effects may be divided into two main types, the first being the intermolecular isotope effect and the second being the intramolecular isotope effect. Intramolecular isotope effects will be discussed below and intermolecular isotope effects will be discussed in Chapter 7 where they are relevant.

6.2.1 Intramolecular isotope effect

The intramolecular isotope effect [20,21,23-25] is encountered in situations where a reactant molecule is, either partly or wholly, composed of a combination of different isotopic atoms. For example, the most commonly used reactant of this type is deuterium hydride (HD), which is used in place of both H_2 and D_2. Other examples include NDH_2, CDH_3 and other partly deuterated hydrocarbons. The use of a reactant like HD in place of H_2 or D_2 provides an added dimension for the reaction process. That is, reactants like HD necessarily place two isotopic reactant atoms at the reaction site, thereby offering a choice of reaction outcomes, providing an intimate probe of the reaction process.

Intramolecular isotope effects in monocation reactions with HD have been the subject of a comprehensive series of experimental and theoretical investigations, which have been reviewed in detail.[10,13-22] For exothermic reactions, such as our dication reactions, and in collision energy regimes comparable to our experimental energies, the observed intramolecular isotope effects in monocation reactions usually favour the production of the hydrogenated product. These observations are in contrast to the intramolecular isotope effect observed in this work as will be shown later.

6.2.2 Orientation effect

As mentioned above HD is an excellent choice of reactant to study intramolecular isotope effects. HD is readily available commercially and, unlike other isotopic targets, HD can be prepared with relative ease in the laboratory.[26]

As discussed before intramolecular isotope effects between monocations with HD have been the subject of a comprehensive series of experimental and theoretical investigations. For exothermic reactions such as dication reactions the observed intramolecular isotope effects in monocation reactions, at comparable collision energies to which experiments have been performed in this thesis, usually favour the production of the hydrogenated product.

The greater probability for the formation of the hydrogenated product is usually explained as arising from an orientation effect.[21] The orientation of the HD molecule is explained by the fact that the attractive force between the monocation and HD molecule, coupled with the fact that the center of polarisability of HD does not lie at its center of mass results in a torque being exerted on the molecule as it approaches the reactant ion as shown in Figure 6.1

With a doubly charged ion, as in our experiments, one would expect such orientation effects to favour the hydrogenated product even more strongly, due to the larger torque on the HD molecule due to the higher charge on the reactant ion. In earlier work by Newson and Price, on the CF_2^{2+} and HD collision system,[27] it was observed that at low collision energies, the chemical reaction exhibited an intramolecular isotope effect favouring the formation of DCF_2^+. This isotope effect increased in strength with decreasing collision energy and at the lowest collision energies approximately twice as many DCF_2^+ as HCF_2^+ ions were detected. Thus, obviously other effects, with respect to monocation reactions, are clearly determining the dynamics of the ion-molecule reaction. In ion-molecule reactions, intramolecular isotope effects forming the

deuterated products can arise due to statistical (phase space) effects.[22] Where there are no additional complications, such as the effect of different endothermicities for forming the deuterated and hydrogenated products in endothermic reactions,[28,29] such statistical effects are usually small. Such statistical control can, of course, only affect the product-ion distribution if the ion-neutral encounter lasts for a sufficient time for energy randomisation to occur. Newson and Price thought such statistical effects to be unimportant.

Newson and Price provided a qualitative rationalisation of the isotope effect observed for the CF_2^{2+}/HD system by considering the possibility that electron transfer precedes the chemical reaction.[27] As has been discussed before, electron transfer is a major reaction channel in dication neutral collision systems. In order to rationalize the formation of the deuterated product in these dication/neutral collision systems, if electron transfer is considered to occur as the dication approaches the neutral, the

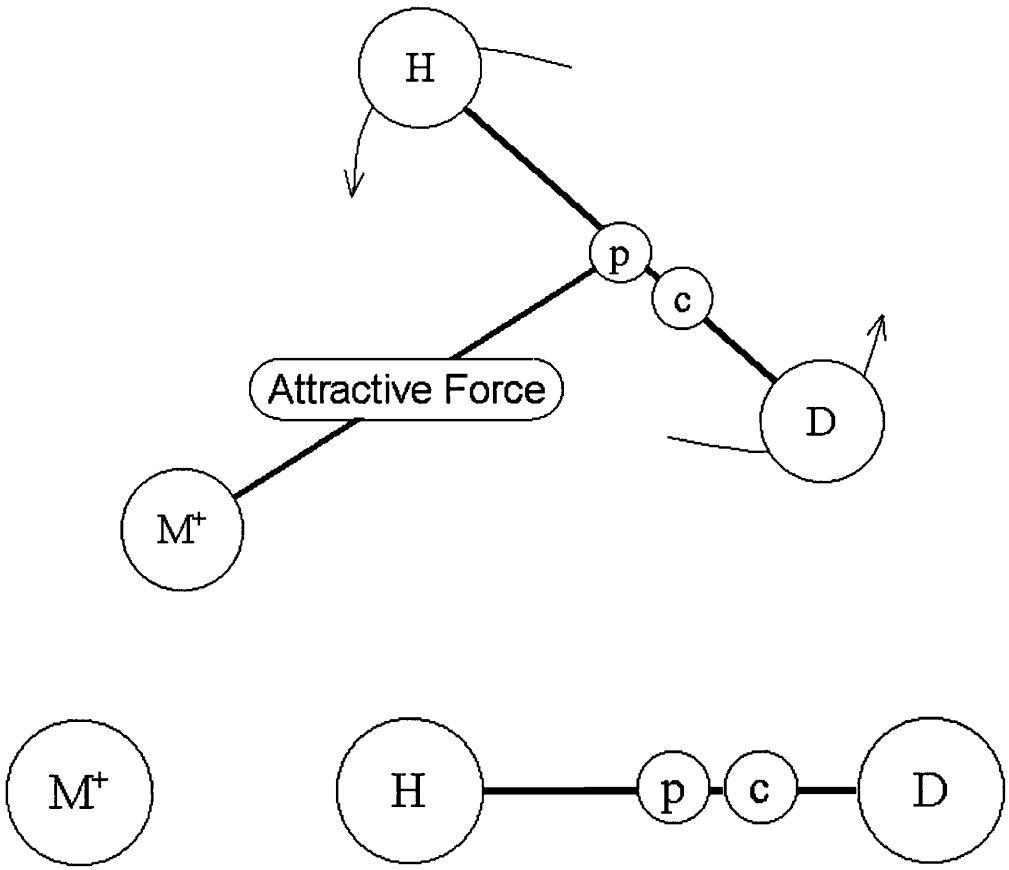

Figure 6.1 Schematic of the repulsive torque exerted during the encounter between a monocation and HD. As described in the above this torque will favour the [M-H-D] configuration.

resulting repulsive torque on the HD^+ ion will try to orient the ion so that at the point of closest approach the species are preferentially in the $[M\text{-}D\text{-}H]^+$ orientation as illustrated in Figures 6.2 and 6.3 below.

The above hypothesis assumes that electron transfer occurs at interspecies separations where the resulting singly charged ions can still, by virtue of their kinetic energy, approach each other to within separations that permit chemical reactivity to occur. Therefore, the above model, in which chemical (bond-forming) reactivity is preceded by electron transfer, requires that electron transfer occurs at small interspecies separations. A series of simple classical trajectory simulations were carried out by Newson and Price, where the approach of an HD molecule to a point doubly charged ion was modeled.[27]

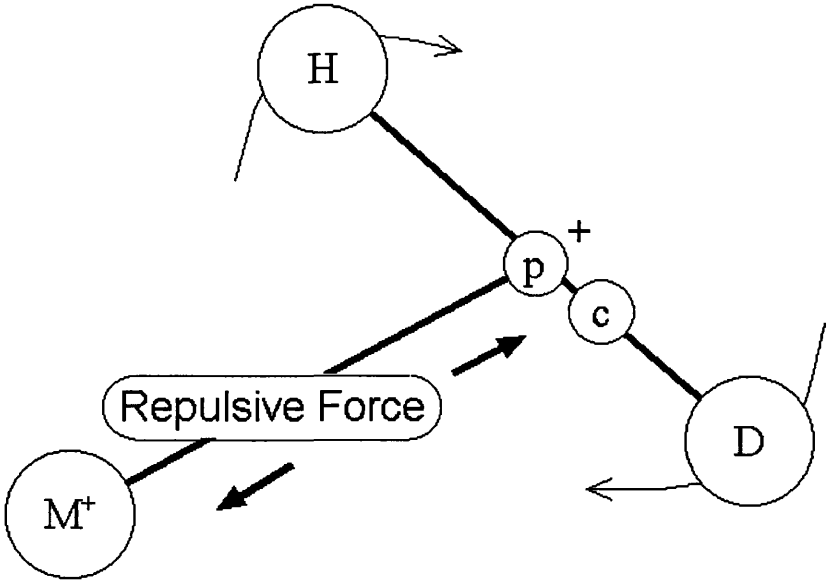

Figure 6.2 An electron transfer at some interspecies separation results in the formation of M^+ and HD^+ intermediates. The intermolecular potential produces a force that acts at the centre of polarisability, generating a torque on the HD bond, acting about the centre of mass, which tends to turn the HD bond so that the D end is directed towards the reactant ion.

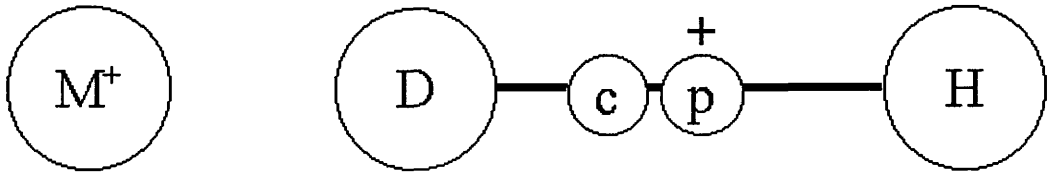

Figure 6.3 With the intermediates now in the [M-D-H] configuration, the bond forming reaction takes place. Thus the orientation of the reactants favors the preferential formation of the deuterated product ion.

At interspecies separation of 3Å, an electron is transferred to form a pair of singly charged ions and the orientation of the HD^+ ion at the point of closest approach of the

resulting monocations was monitored. Despite the approximations in the methodology of the simulation, for example, no allowance is made for the bonding interactions which may be present, the simulation showed a marked increase in the relative proportion of closest approaches in the $[M\text{-}D\text{-}H]^+$ orientation compared with a monocation/neutral reaction. If the chemical reaction between dications and HD does indeed proceed via initial electron transfer, which is a reasonably efficient process, it may explain why these reactions have a significantly larger cross section than the bond forming reactions between dications and other neutral molecules. If other systems react via alternative mechanisms, for example the formation of an intermediate complex, the cross section for these alternative pathways are likely to be much smaller.

6.2.3 Statistical behaviour

As mentioned above, monocation collisions with HD have been investigated extensively. In these systems, in order to explain the cross sections for the formation of the hydrogenated and deuterated products, statistical arguments have been used. This is usually done by examining the density of states of the products. A good example of this type of behaviour is provided by Si^+ and HD.[22] In systems such as this, where these statistical effects come into play, the typical statistical outcome is about 1:1 formation of SiH^+ and SiD^+.

6.2.4 Direct Behaviour

An explanation of the intramolecular isotope effect e.g. for the reactions of Ca^+ (^2S) with HD [22] is provided by a direct behaviour model. In this system, the hydrogenated product CaH^+ is favoured. The analysis of statistical behaviour shows that the internal density of states favours the formation of the deuterated product. Thus, instead of assuming that the internal and translational degrees of freedom equilibrate fully, it is assumed that the reaction is no longer sensitive to the density of internal energy states. According to this analysis, the translational density of states favours the production of the hydrogenated product ion.

6.2.5 Impulsive Behaviour

This type of intramolecular isotope effect is illustrated by the reaction of Xe^+ ($^2P_{3/2}$) and HD [22]. In this model, in the limit of a hard-sphere type of reaction, the collision will be a 'pairwise' one between A^+ and closest atom of HD. Thus, the energy relevant to the

reaction is not the centre of mass energy (relevant when the interaction is between A^+ and the entire molecule) but a pairwise interaction energy. In the CM system the energy available to cause chemical change is the relative kinetic energy between the incoming atom and the reactant molecule. In a pairwise interaction, A is sensitive to only the potential between A and the atom B that is transferred. The pairwise energy is always less than the energy available in the CM frame. The pairwise energy frame may also be familiar as the spectator-stripping model (SSM). The difference is that the SSM assumes there is no momentum transfer to the product atom, while the more general model allows for such transfer. As a consequence, the SSM makes very specific predictions about the velocity and the internal energy of the products, while the pairwise model allows for distribution of these quantities.

This Chapter presents and discusses the results of an investigation of the intramolecular isotope effects in the bond-forming channels following collisions of CO_2^{2+} and CF_3^{2+} with HD. The data shows strong intramolecular isotope effects are apparent in the major bond forming processes, similar to those observed in the CF_2^{2+}/HD system. The investigation also identifies a new reactive channel forming HF^+ and DF^+ following collisions of CF_3^{2+} with HD, which in contrast to the major chemical channel forming HCF_2^+ and DCF_2^+, does not appear to exhibit an intramolecular isotope effect. The implications of these observations are discussed.

6.3 Experimental

A wide variety of experimental techniques are available to study the consequences of ionic collisions with atoms and molecules, a summary of these have been presented in Chapter One. The apparatus used in these investigations has been described in detail in Chapter Two. Briefly the molecular dication of interest is mass selected using a velocity filter, from the positive ions produced by an electron impact ionization source. To produce the CF_3^{2+} and CO_2^{2+} dication we utilize the dissociative double ionization of CF_4 and non-dissociative double ionisation of CO_2 by ~150 eV electrons in a low-pressure electron-impact source. Electrostatic optics are employed to extract the ions from the source and transport them to a velocity filter where mass selection of the dications to form an ion beam is achieved. The experiments carried out in this work were performed at low collision energies to maximize the yield of the bond forming reaction. Hence, as mentioned before in the preceding Chapters, after traversing the

velocity filter at 400 eV in the laboratory-frame, the kinetic energy of the dications must be substantially reduced before they encounter the neutral molecules. Deceleration of the dication beam is achieved using further ion optics with subsequent refocusing. On leaving the decelerator, the dication beam intersects an effusive beam of the neutral collision partner in a collision region, which doubles as the source region of the TOFMS. Product ions formed following the interaction of the molecular dication with the neutral target, in addition to unreacted dications are periodically (50 kHz) extracted from the interaction region by pulsing the repeller plate of the TOFMS. The TOFMS is of the standard Wiley-McLaren design and ions reaching the end of the drift tube are accelerated to hit a multichannel plate detector. The pressure of the neutral collision partner is carefully controlled to ensure single collision conditions exist in the interaction region. This is confirmed by the linear dependence of the product-ion yield on the number density of the neutral target, as shown in Chapter 2. The procedure for data collection has been described in detail in Chapter 3. The data is corrected for background and impurity ions and any mass discrimination effects. The procedure is repeated at least three times to give an average product ion yield with an associated standard deviation. Sections of typical mass spectra of the data collected are shown in Figures 6.4 and 6.5

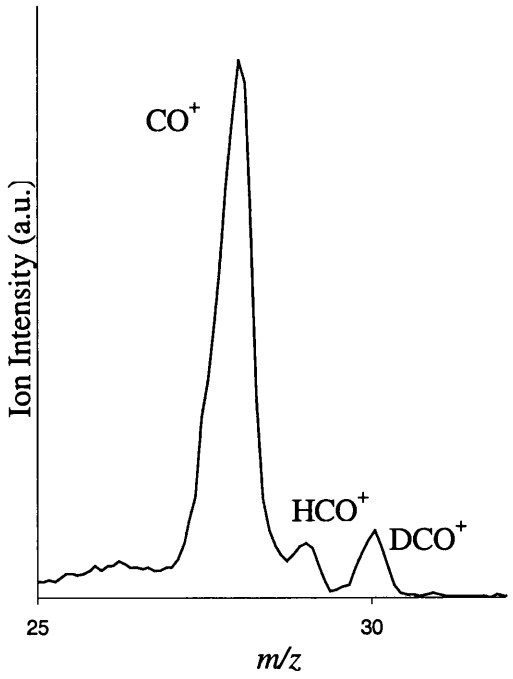

Figure 6.4 Section of representative mass spectrum showing the formation of HCO^+ and DCO^+ following collisions of CO_2^{2+} with HD at 0.32 eV centre of mass collision energy

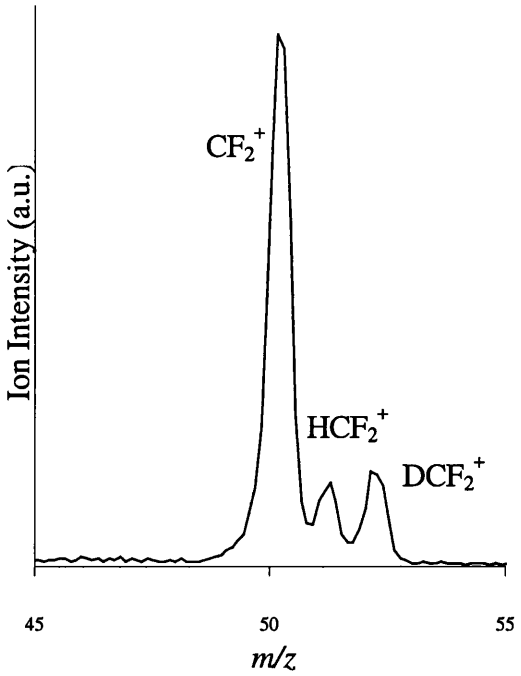

Figure 6.5 Section of representative mass spectrum showing the formation of HCF_2^+ and DCF_2^+ following collisions of CF_3^{2+} with HD at 0.29 eV at centre of mass collision energy.

The signals of interest in these product-ion mass spectra are those that result from the bimolecular encounters. As illustrated in Figure. 6.4 and 6.5, for both the CF_3^{2+}/HD and CO_2^{2+}/HD systems, the mass resolution of our apparatus allows us to clearly distinguish the product-ion signals resulting from bond-forming reactions. However, since these signals are not resolved at the baseline level, a peak fitting procedure was employed to determine accurately their relative intensities. This peak fitting procedure was performed in Excel, using a Gaussian function to fit the product ion curves. This was done after subtracting a constant background. In the peak fitting procedure we change the height and width of the Gaussian curves which are independently modeled, in the case of the CO_2^{2+}/HD system, onto the CO_2^+, HCO^+ and DCO^+ peaks, which then enable the area under these peaks to be determined.

In this work the bond forming products following collisions between CF_3^{2+} and HD and collisions between CO_2^{2+} and HD were monitored at centre of mass collision energies from 0.17 to 0.5 eV and 0.19 to 0.77 eV respectively. The centre of mass collision energy is calculated using the initial dication velocity, which is known from the beam potential, and assuming that the velocity of the neutral molecule is negligible with respect to the velocity of the dication. Given that the neutrals are admitted as an effusive beam and that the dication beams have energies between 3 and 12 eV in the laboratory frame, this approach is perfectly satisfactory.

6.4 Results and data analysis

This Chapter focuses on the intramolecular isotope effects we observe in the bond-forming reactions which form XCO^+ and XCF_2^+ (X = H, D). As with all the work carried out in this thesis, it is necessary to consider the ion detection efficiency, thereby allowing the extraction of the true relative ion yields from the mass spectra.[10,13] This methodology has been discussed in detail in Chapter 3. Using the described methodology, the values listed in Tables 6.1 and 6.2 are derived.

Calculating α (Table 6.1) for the CO_2^{2+}/HD collision system it can be seen that the detection efficiency varies very slightly (~0.9%) over the collision energies employed in this work and the HCO^+ ion is always very slightly discriminated against. Calculating α (Table 6.2) for the CF_3^{2+}/HD collision system, it can be seen that the detection efficiency again varies only slightly (~2%) over the collision energies employed. In our calculations we assume that we form dissociative states of HCF_3^+ and HCO_2^+ which give our product ions HCF_2^+ and HCO^+ respectively. Correcting our background corrected ion intensities using the values of α (Tables 6.1 and 6.2) yields the relative intensities which are also listed in Tables 6.1and 6.2. The corrected and the uncorrected relative signal intensities are plotted in Figures 6.6 and 6.7.

Table 6.1 Correction factors α calculated by using Equation (3.18) for the relative detection efficiency of HCO^+ and DCO^+ and the resulting relative ion intensities $R(HCO^+)/R(DCO^+)$ derived from the background corrected experimental data.

E_{COM} / (eV)	$I(HCO^+)/I(DCO^+)$	α	$R(HCO^+)/R(DCO^+)$
0.19	0.669	1.127	0.754
0.25	0.731	1.120	0.819
0.31	0.753	1.115	0.840
0.38	0.787	1.113	0.876
0.44	0.797	1.112	0.886
0.51	0.808	1.112	0.899
0.57	0.885	1.112	0.984
0.63	0.920	1.114	1.025
0.70	0.958	1.116	1.069
0.76	0.897	1.119	1.003

Table 6.2 Correction factors α calculated by using Equation (3.18) for the relative detection efficiency of HCF_2^+ and DCF_2^+ and the resulting relative ion intensities R (HCF_2^+)/R (DCF_2^+) derived from the background corrected experimental data

E_{COM} / (eV)	$I(HCF_2^+)/I(DCF_2^+)$	α	$R(HCF_2^+)/R(DCF_2^+)$
0.17	0.692	1.104	0.764
0.21	0.740	1.102	0.815
0.25	0.776	1.101	0.855
0.29	0.806	1.101	0.888
0.33	0.818	1.103	0.902
0.38	0.870	1.106	0.962
0.42	0.915	1.110	1.015
0.46	0.874	1.115	0.975
0.50	0.904	1.122	1.014

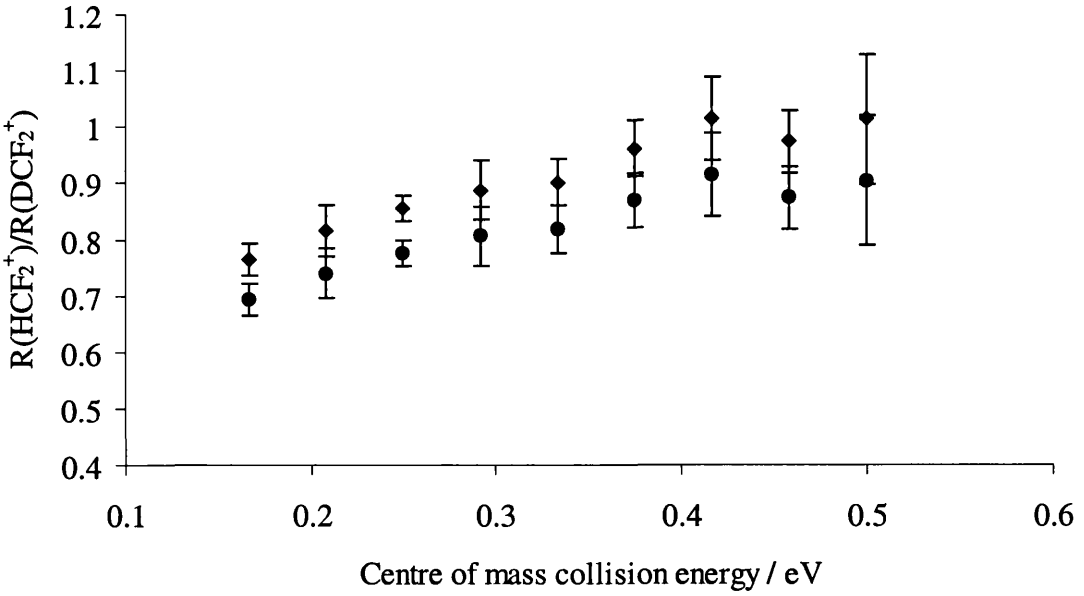

Figure 6.6 Variation of the corrected relative ion intensities (♦) and the uncorrected relative ion intensities (•) of the HCF_2^+ and DCF_2^+ product ions, as a function of collision energy, following collisions of CF_3^{2+} with HD.

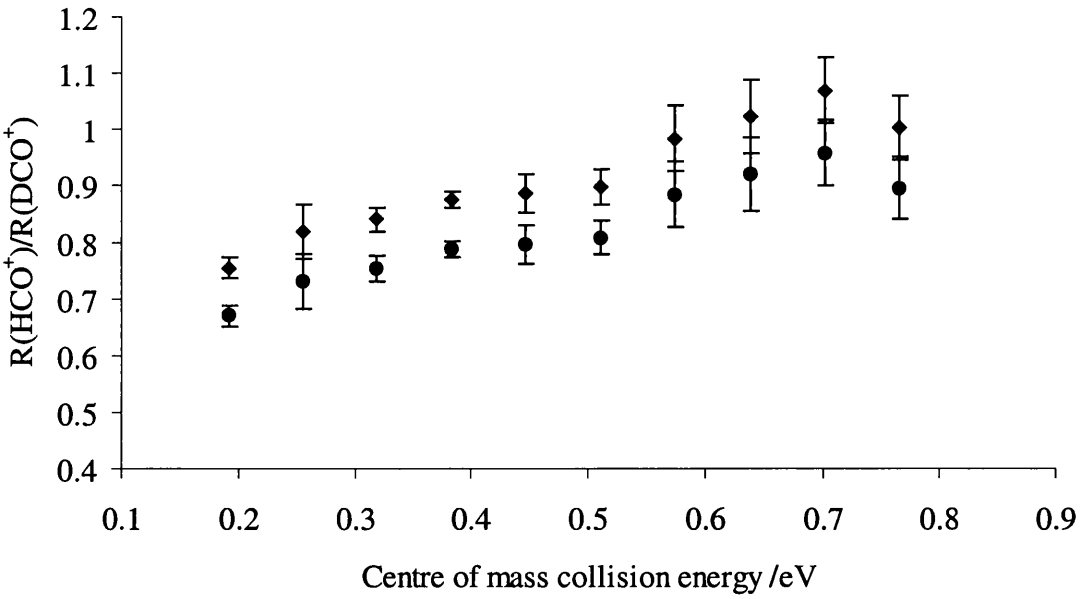

Figure 6.7 Variation of the corrected relative ion intensities (♦) and the uncorrected relative ion intensities (•) of the HCO^+ and DCO^+ product ions, as a function of collision energy, following collisions of CO_2^{2+} with HD.

Figures 6.6 and 6.7 show the corrected and uncorrected relative signal intensities of HCF_2^+ and DCF_2^+ from the CF_3^{2+}/HD reaction and HCO^+ and DCO^+ from the CO_2^{2+}/HD reaction as a function of the centre of mass collision energy. As mentioned before, each data point is an average of 3 or more determinations with an associated standard deviation. This ratio is a powerful probe of the intramolecular reactivity in the collision system, as it is independent of both the incident dication current and the collision gas density. It can be seen clearly from both Figures 6.6 and 6.7 for both collision experiments that we detect a higher yield of the deuterated product, an isotope effect which becomes more pronounced with decreasing collision energy.

The ionic products generated following collisions of CO_2^{2+} and CF_3^{2+} with H_2 or D_2, have been described before in the literature. In the previous investigations, XF^+ was not observed as a product ion from the $CF_3^{2+}/H_2/D_2$ collision system. However, in our investigation of the CF_3^{2+}/HD collision system, we do observe the formation of the XF^+ product ion.[11,12] Due to the low intensity of these signals, extensive tests have been carried out to see if they arise from some source other than the dication/neutral collision, such as reactions of impurity ions in the dication beam or reactions in the ion source. However, we are unable to find such a source which can account for the formation of these (XF^+) product ions other than the dication/neutral collision. We therefore conclude that they are real product ions from the CF_3^{2+} collisions with HD

and indeed in the $CF_3^{2+}/H_2/D_2$ collision system discussed in the next Chapter, we also observe the formation of this product ion.

For the reaction forming XF^+, only background corrected ion intensities are presented. Since the mechanism of formation of XF^+ is uncertain, assumptions about its scattering and energy distribution are speculative at best. However, given the above analysis it is likely that the relative discrimination between HF^+ and DF^+ in our experiment is small and perhaps slightly favours the detection of the DF^+ product ion. These data are presented and discussed in section 6.5.

Another minor bond forming channel following collisions of CO_2^{2+} with X_2 which forms XCO_2^+ has been seen in earlier experiments by Mrázek and Manning.[12] However, although in our mass spectra these weak signals are observable they are significantly masked by CO_2^+ and $^{13}CO_2^+$ signals. Hence it was not possible to extract meaningful relative intensities of the XCO_2^+ product ions from these masked signals and this reaction product is not considered any further.

6.5 Discussion.

Newson and Price[27] provided a qualitative rationalization of the observed intramolecular isotope effect in the CF_2^{2+}/HD reaction, a preference for the formation of DCF_2^+, was explained by the possibility that electron transfer preceded the chemical reaction and the hypothesis was tested by carrying out a series of simple classical trajectory simulations, where the approach of an HD molecule to a point doubly charged ion was monitored.[27] The orientation of the HD^+ ion formed following electron transfer was monitored at the point of closest approach. Despite the severe approximations in the methodology of the simulation, a marked increase in the relative proportion of closest approaches in the $[M\text{-}D\text{-}H]^{2+}$ orientation compared with a monocation/neutral reaction, was supported by this analysis. The time for this alignment is reduced at higher collision energies, accounting for the increasing preference for the formation of the deuterated product as the collision energy decreases. In this "orientation" model, the dynamically determining step is the approach of the reactants. In this simple model, the details of the reaction are not important and one would predict that all dication reactions should exhibit such intramolecular isotope effects if electron transfer precedes chemical reaction. The results produced in this investigation do not disagree with the prediction made by this model that deuterated products should be favoured generally.

However, although the orientation model has been used to explain the preferential formation of the deuterated product rather than the hydrogenated product in dication/HD systems, our data, presented in Figure 6.8 below, shows the ratio of HF^+ product ions to DF^+ product ions to be the same within our experimental uncertainty. As mentioned before, we have only presented background corrected ion intensities since from the calculations shown in section 6.3, the correction factors that we derive are not a strong function of the kinetic energy release and are close to unity. The observation of the absence of any isotope effect in the formation of the XF^+ product ion, perhaps casts doubt on the idea that orientational isotope effects are determining the product ion distribution in dication reactions with HD. Of course, one could postulate that for the formation of XF^+ that the orientation of closest approach is not significant in determining whether the H or D atom is transferred to the dication thus

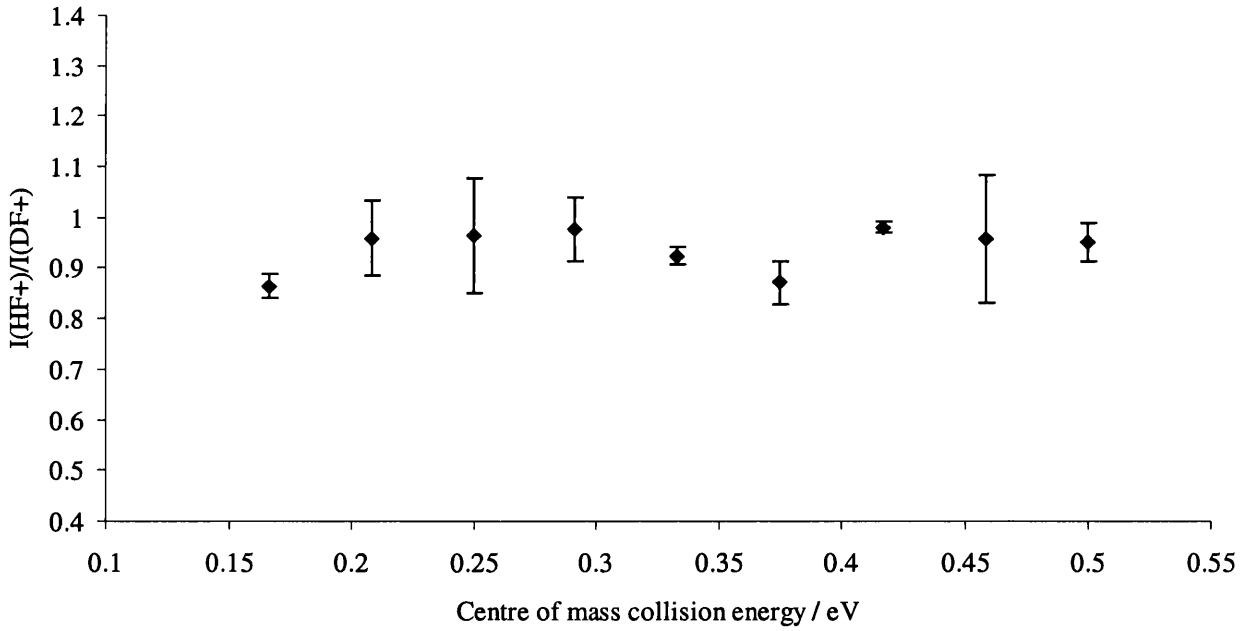

Figure 6.8 Variation of the uncorrected relative ion intensities of the HF^+ and DF^+ product ions, as a function of collision energy, following collisions of CF_3^{2+} with HD

the orientation model being inapplicable. However, further recent work also brings into question the applicability of orientational effects to explain dication intramolecular isotope effects. Specifically, the recent *ab initio* calculations of key points on the potential energy surface of the CO_2^{2+}/D_2 system by Mrázek *et al.* support an earlier qualitative model where competition between electron transfer and bond forming reactivity occurs early in the entrance channel on the bond-forming pathway.[12] Hence,

if electron transfer occurs this precludes access to the bond-forming channel and thus the repulsive torque following electron transfer, critical in the "orientational" model, does not influence the bond-forming channel. Furthermore, the calculations of Mrázek *et al.* [12] show that, despite having no barrier, as had been concluded experimentally, the $[CO_2\text{-}D_2]^{2+}$ potential energy surface possess several deep minima. Such minima, despite the considerable exoergicity of the reaction, explain why there is considerable evidence for "sticky collisions" in this system. Indeed, experiments estimate a lifetime of 0.8 ps for the collision complex in this system. The long-lived nature of a significant proportion of collisions again calls into question the importance of the initial orientation of the HD as it approaches the dication.

Although Newson and Price [27] in earlier work did not consider statistical effects to play an important role in intramolecular isotope effects, given this new information on the potential energy surface of $[CO_2\text{-}D_2]^{2+}$, and the inability of the orientational model to explain the formation of the XF^+ product ion, we have considered the fact that perhaps statistical effects are indeed responsible for the intramolecular isotope effects that we observe. A mechanism has been developed and proposed in the literature for the CO_2^{2+}/H_2 collision system.[12]

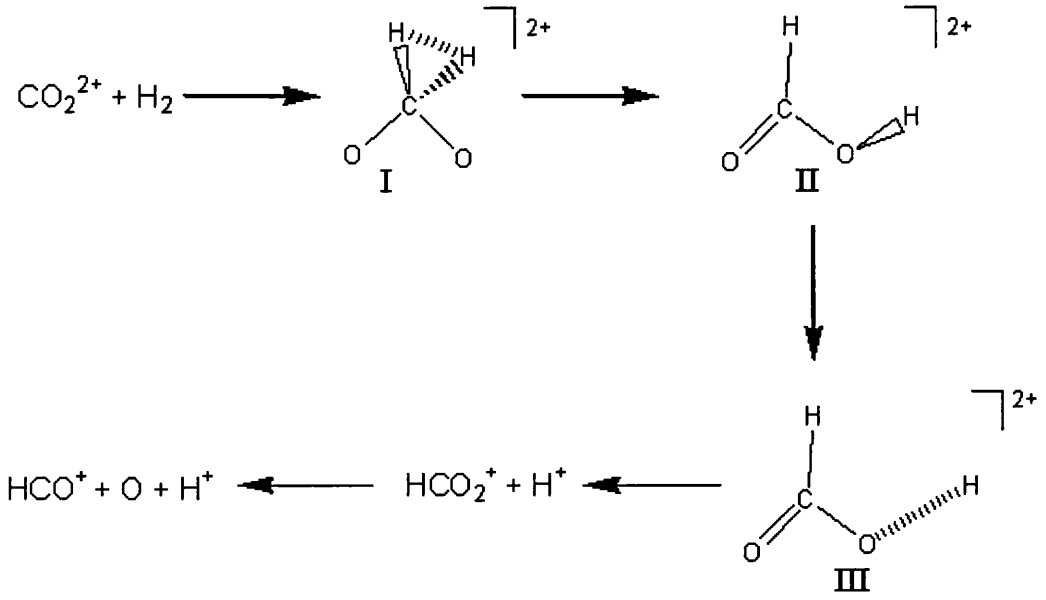

Figure 6.9 Proposed mechanism for the CO_2^{2+}/H_2 collision system.[12]

This proposed mechanism, shown in Figure 6.9, involves initial barrierless co-ordination of H_2 to CO_2^{2+} to form structure I. This is followed by the migration of one of the H atoms to an oxygen atom to form structure II. The cleaving of the O-X bond then proceeds over a barrier of 1.8 eV via a transition state, structure III, to form XCO_2^+ and X^+, with the XCO_2^+ subsequently dissociating to form XCO^+. If we assume the cleavage of the O-X bond of intermediate II is the rate determining step from the above mechanism one can see how statistical effects may be important in determining the intramolecular isotope effects we observe in the reaction with HD. For the reaction between CO_2^{2+} and HD there will be the two competitive pathways as shown below. From statistical rate theory,[30,31] the rate of reaction is expected to be proportional to the number of accessible states at the transition state. The number of accessible vibrational levels at the transition geometry will be greater for the decay of the pathway breaking an O-H bond, denoted VI in Figure 6.10, than the pathway for breaking an O-D bond, denoted VII in Figure 6.10. This difference in the accessible number of states arises because the omission from the transition state partition function of the reactive vibration results in more modes involving the motion of a D atom, as opposed to an H

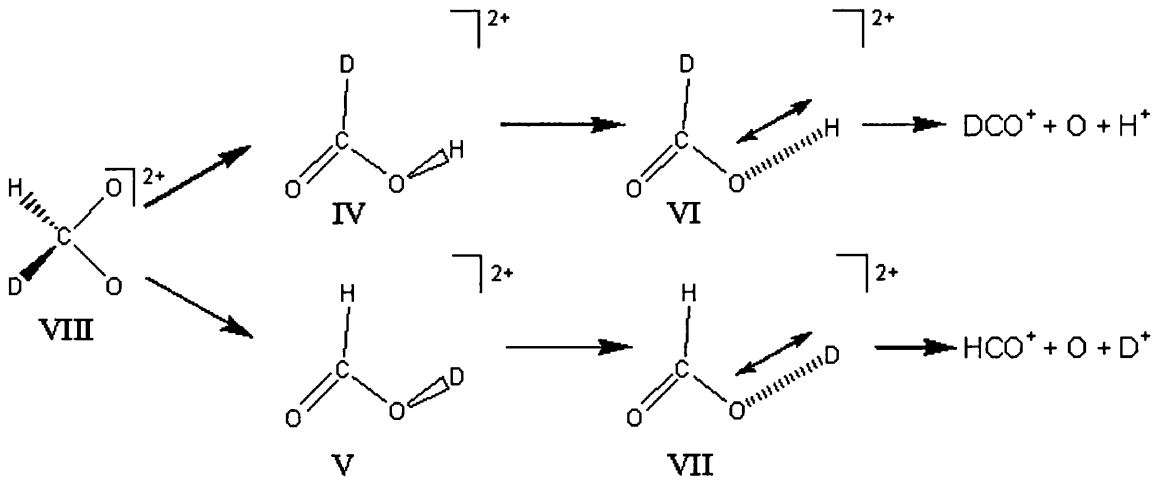

Figure 6.10 Proposed mechanism for the CO_2^{2+}/HD collision system.[12]

atom, being included in the sum of accessible states at the transition state for O-H cleavage than for O-D cleavage. The motion of the D atoms will have lower frequencies than the corresponding motion of H atoms and, hence, at a given reaction energy more vibrational states will be accessible for transition state VI than for transition state VII. So, qualitatively, the pathway via O-H cleavage to form $O(CD)O^+$

should be more rapid than the pathway via O-D cleavage to form $O(CH)O^+$, as we observe.

Simple vibrational RRKM calculations using Beyer and Swinehert state counting, supports this qualitative conclusion. Such calculations, using both *ab initio* structures for intermediates IV and V and also approximating the structures of these intermediates as the relevant isotopomer of formic acid, always indicate that the decay of transition state VII will occur at 70%-80% of the rate of transition state VI. This differential rate is not a strong function of the collision energy.

Figure 6.7 shows that at low collision energies we see a HCO^+ to DCO^+ ratio of 0.75 rising to approximately unity at the highest collision energy of 0.77 eV in the centre of mass frame. This variation of the HCO^+ to DCO^+ ratio may be explained as a result of a direct, stripping-style reaction mechanism which dominates at the higher collision energies, where the reactant dication abstracts either of the two atoms from HD to form XCO_2^+ without discrimination and a complexation mechanism may dominate at low collision energies where the complex lives long enough for the statistical process described above to take place.

However, the recent angular scattering experiments of Mrázek *et al.*[12] indicate that complexation is the major reactive pathway at collision energies of 2.5 eV and 0.78 eV, with the $[D_2\text{-}CO_2]^{2+}$ intermediates estimated to live several picoseconds at the lower energy and a few fractions of a picosecond at the higher energy. Thus, it is inconsistent with their results to propose a direct mechanism dominating the reactivity at our "higher" collision energies of around 0.77 eV. However, it is perfectly possible that the variation in the intramolecular isotope effect we observe reflects the lifetime of the intermediate complex, with the complex living long enough at low collision energies for true competition between the reactive channels to occur and the statistical effects to take place. Whilst at the higher collision energies the complex is not sufficiently long-lived for competition between the two channels to be effective and, hence, equal facility of O-H and O-D cleavage is observed, presumably reflecting an equal likelihood of H or D atom migration from the initial adduct $[HD\text{-}CO_2]^{2+}$ to the oxygen atom.

Following *ab initio* calculation of various minima on the reactive potential energy surface has, Hrusak has proposed a very similar mechanism to that discussed above for the bond-forming reaction of CO_2^{2+} with H_2 for the bond-forming reaction of CF_2^{2+} with H_2. [32]In this suggested mechanism initial co-ordination of H_2 to form $[H_2\text{-}CF_2]^{2+}$ is

followed by H atom migration to form $[F\text{-}CH\text{-}F\text{-}H]^{2+}$ and subsequent cleavage of the F-H bond yields the observed products. Hence, in the reaction of CF_2^{2+} with HD competitive decay of $[F(CH)F\text{-}D]^{2+}$ and $[F(CD)F\text{-}H]^{2+}$ intermediates is expected and, analogously to the arguments above, statistical effects may account for the observed intramolecular isotope effect in this system.

Unfortunately, there are no calculations of the potential energy surface available for the reaction of CF_3^{2+} with HD to give XCF_2^+. However, if we were to make an analogy with the mechanisms proposed above for the reaction of CO_2^{2+} and CF_2^{2+} with HD we would expect initial co-ordination followed by atom migration to an F atom to give an intermediate of the form $[F_2(CX)F\text{-}X]^{2+}$. Again, in the subsequent cleavage of the F-X bond the density of states arguments presented above will apply and we would predict the reaction of $[F_2(CD)F\text{-}H]^{2+}$ to give DCF_3^+ and H^+ to be faster than the reaction of $[F_2(CH)F\text{-}D]^{2+}$ to give HCF_3^+ and D^+. With the XCF_3^+ subsequently dissociating to XCF_2^+ this accounts for the preference for the formation of DCF_2^+ at low collision energies. Although this analogous mechanism for the CF_3^{2+}/HD system is speculative, the similarity of the intramolecular isotope effect in the bond forming reactions of CF_3^{2+}, CO_2^{2+} and CF_2^{2+} indicate that similar mechanisms operate in each case. This conclusion is supported by the theoretical work of Mrázek *et al* and Hrusak for the reactions of the last two dications.

Our observation of the absence of any isotope effect in the reaction of CF_3^{2+} with HD to form XF^+ indicates that this reaction occurs via a markedly different pathway to the formation of XCF_2^+. However, it is difficult to say more about the precise mechanism from our limited experimental evidence. Complexation appears to be involved, at least to some extent, in all of the bond-forming reactions observed to date in dication neutral/collision systems. Therefore it seems reasonable to assume that the formation of the XF^+ product ion proceeds via the same initial pathway. If the key complex is $[F_2(CX)F\text{-}X]^{2+}$, as suggested above, then an alternative decay channel via C-F cleavage would form XCF_2^+ and XF^+. For this bond cleavage the reactive mode would be a C-F motion and would not be influenced by the statistical effects described above that affect F-X cleavage. Hence, if this is the case then the formation of HF^+ and DF^+ would be equally probable, as is observed in our work.

6.6 Conclusion

Newson and Price had provided a qualitative rationalisation of the observed intramolecular isotope effect in the CF_2^{2+}/HD collision system, to explain the preferential formation of the deuterated product rather than the hydrogenated product. However, in this investigation our data shows the HF^+ and the DF^+ product ion from the CF_3^{2+}/HD collision system, to be the same within our experimental uncertainty. The data from this investigation and recent work by Mrázek *et al* on the potential energy surface of $[CO_2\text{-}D_2]^{2+}$ casts doubt on the applicability of the orientation model. Statistical effects have been suggested for being responsible for the intramolecular isotope effects that we observe and mechanisms have been proposed for the systems investigated.

References:

1 S. D. Price, S. A. Rogers, and S. R. Leone, *J. Chem. Phys.* **98,** 9455-9465 (1993).

2 S. A. Rogers, S. D. Price, and S. R. Leone, *J. Chem. Phys.* **98,** 280-289 (1993).

3 M. Manning, S. D. Price, and S. R. Leone, *J. Chem. Phys.* **99,** 8695-8704 (1993).

4 C. E. Melton and G. F. Wells, *J. Chem. Phys.* **27,** 1152 (1957).

5 Z. Herman, P. Johnathon, A. G. Brenton, and J. H. Beynon, *Chem. Phys. Lett.* **41,** 433 (1989).

6 S. E. Kupryanov, *Soviet J. Phys. Tech. Phys.* **9,** 659 (1964).

7 S. D. Price, M. Manning, and S. R. Leone, *Chem. Phys. Lett.* **214,** 553-558 (1993).

8 S. D. Price, M. Manning, and S. R. Leone, *J. Am. Chem. Soc.* **116,** 8673-8680 (1994).

9 Z. Dolejsek, M. Farnik, and Z. Herman, *Chem. Phys. Lett.* **235,** 99-104 (1995).

10 K. A. Newson and S. D. Price, *Chem. Phys. Lett.* **269,** 93-98 (1997).

11 Z. Herman, J. Zabka, Z. Dolejsek, and M. Farnik, *Int. J. Mass Spectrom.* **192,** 191-203 (1999).

12 L. Mrázek, J. Zabka, Z. Dolejsek, J. Hrusak, and Z. Herman, *Journal of Physical and Chemical A* **104,** 7294-7303 (2000).

13 S. D. Price, *J. Chem. Soc. Faraday Trans.* **93,** 2451-2460 (1997).

14 R. H. Schultz and P. B. Armentrout, *J. Chem. Phys.* **96,** 1036-1045 (1992).

15 K. M. Ervin and P. B. Armentrout, *J. Chem. Phys.* **85,** 6380-6395 (1986).

16 E. A. Gislason, B. H. Mahan, C. W. Tsao, and A. S. Werner, *J. Chem. Phys.* **50,** 5418 (1969).

17 K. Tanaka, T. Kato, P. M. Guyon, and I. Koyano, *J. Chem. Phys.* **79,** 4302-4305 (1983).

18 K. A. Newson, N. Tafadar, and S. D. Price, *J. Chem. Soc. Faraday Trans.* **94,** 2735-2740 (1998).

19 R. A. Dressler, R. H. Salter, and E. Murad, *J. Chem. Phys.* **99,** 1159-1171 (1993).

20 C. E. Dateo and D. C. Clary, *J. Chem. Soc. Faraday Trans.* **85,** 1685-1696 (1989).

21 P. M. Hierl, *J. Chem. Phys.* **67,** 4665-71 (1977).

22 P. B. Armentrout, *ACS Symposium Series* **502,** 194-209 (1992).

23 P. Tosi, O. Dmitrijev, Y. Soldo, D. Bassi, D. Cappelletti, F. Pirani, and V. Aquilanti, *J. Chem. Phys.* **99,** 985 (1993).

24 F. S. Klein and I. Friedman, *J.Chem. Phys.* **41,** 1789 (1964).

25 T. F. Moran and I. Friedman, *J. Chem. Phys.* **42,** 2391 (1965).

26 I. Wender, R. A. Friedel, and M. Orchin, *J. M. Chem. Soc.* **71,** 1140 (1949).

27 K. A. Newson and S. D. Price, *Chem. Phys. Lett.* **294,** 223-228 (1998).

28 K. M. Ervin and P. B. Armentrout, *J. Chem. Phys.* **84,** 6750-6760 (1986).

29 K. M. Ervin and P. B. Armentrout, *J. Chem. Phys.* **84,** 6738-6749 (1986).

30 T. Beyer and D. F. Swinehart, *Communication of the ACM* **16,** 379 (1973).

31 T. Baer and P. M. Mayer, *J. Am. Soc. Mass Spectrom.* **8,** 103-115 (1996).

32 J. Hrusak, *Chem. Phys. Lett.* **338,** 189-194 (2001).

Chapter 7

Electron-transfer and bond-forming reactivity between CF_3^{2+} and H_2/D_2

7.1 Introduction

Isotope effects offer a powerful probe of the dynamics and mechanism of a chemical reaction. Hence, substituting H_2 in place of D_2 as the neutral collision partner in reactions of dications should provide an insight into the associated reaction mechanisms,[1-5] by allowing the relative cross-sections of the electron-transfer and bond-forming reaction channels for the two collision systems to be compared. In this investigation, the relative reactivity of the two collision systems may be assessed using mass spectrometric techniques rather than measurements of the product ion scattering angle distributions.

This Chapter presents an investigation of the resulting product yield of ions formed following collisions of CF_3^{2+} with H_2 and D_2 and their variation with collision energy.

7.2 Intermolecular isotope effects

Isotope effects have proven to be a powerful probe of the dynamics of chemical reactions.[6-19] If an atom in a reactant molecule is replaced by one of its isotopes, both the equilibrium constant and the rate constants are altered. Isotope effects are greatest when there is a large relative change in the masses. The effects are usually large when an ordinary hydrogen atom (H) is replaced by deuterium (D) or Tritium (T). When an atom is replaced by an isotope, there is no change in the classical potential-energy surface, but there are changes in vibrational frequencies and therefore in zero-point energies. Under most circumstances the predominant factor in an isotope effect is the zero-point energy, which is affected strongly by atomic masses. For example the ZPE of H_2 molecules is 26.1 $kJmol^{-1}$ which is 7.6 $KJmol^{-1}$ more than the ZPE of D_2 molecules. Since these standard kinetic experiments are performed at room temperature or below, most H_2 and D_2 molecules would be in their ZPE levels. Therefore, as the H_2 molecules have more ZPE than D_2 molecules, reactions involving H_2 are more rapid than D_2 reactions due to a lower activation energy barrier and are therefore characterized by larger cross-sections.

Intermolecular isotope effects, or their absence, can provide much information regarding the mechanism of a reaction process. For example, consider the general reactions 7.11 and 7.12, having cross-sections σ (H_2) and σ (D_2) respectively.

$$A^+ + H_2 \rightarrow AH^+ + H \qquad 7.11$$

$$A^+ + D_2 \rightarrow AD^+ + D \qquad 7.12$$

If the values of σ (H_2) and σ (D_2) were plotted as a function of the centre of mass collision energy and found to be the same then this absence of isotope effect is consistent with the operation of a direct reaction mechanism.[12] Additionally, the absence of an isotope effect in reactions 7.11 and 7.12, may point to the lack of an energy barrier to the transfer of $H^-(D^-)$. Isotope effects in the $H^-(D^-)$ transfer reactions in dications are expected if a Landau-Zener style mechanism [20,21] operates. The reason for this is that one would predict an energy barrier to $H^-(D^-)$ transfer, hence the lighter H^- ion tunnels through the barrier with greater efficiency than the relatively heavy D^- ion. Hence, the presence of an isotope effect provides a means of determining the applicability of the Landau-Zener theory to $H^-(D^-)$ transfer in dication reactions, which will be discussed further in section 7.7.

7.3 Experimental

The apparatus used in this investigation has been discussed in detail in the preceding Chapters. In this work the product ions formed following collisions between CF_3^{2+} with H_2/D_2 were monitored at the centre of mass collision energies from 0.17 to 0.5 eV and 0.19 to 0.77 eV respectively. As in the previous investigations reported in this thesis, the centre of mass collision energy is calculated using the initial dication velocity, which is known from the beam potential, and assuming that the velocity of the neutral molecule is negligible with respect to the velocity of the dication.

7.4 Results and Analysis

Time of flight mass spectra were recorded following collisions between the dication and the neutral reactant at laboratory frame collision energies in the range 3 to 12 eV. Sections of representative time-of-flight mass spectra are shown in Figures 7.1 and 7.2 below.

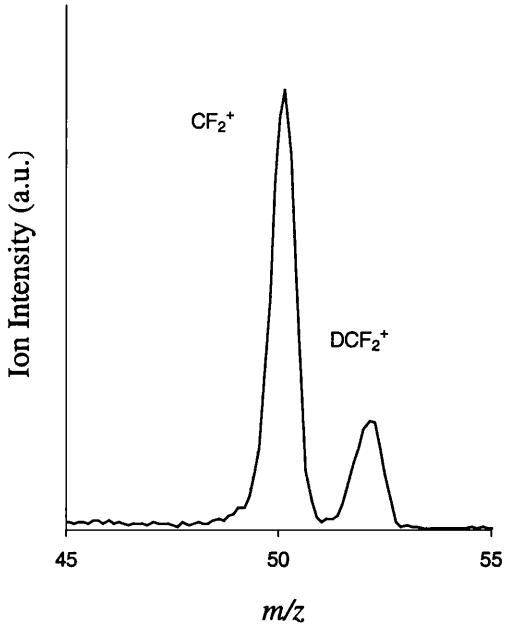

Figure 7.1 Section of a representative mass spectrum showing the formation of CF_2^+ and DCF_2^+ following collisions of CF_3^{2+} with D_2 at 0.49 eV centre of mass collision energy.

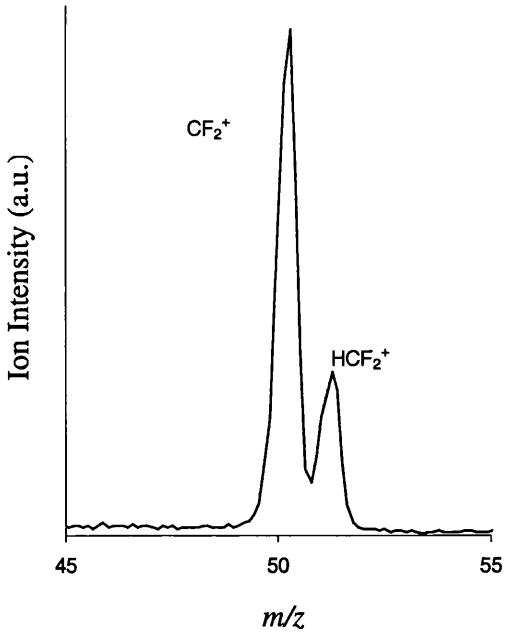

Figure 7.2 Section of a representative mass spectrum showing the formation of CF_2^+ and HCF_2^+ following collisions of CF_3^{2+} with H_2 at 0.25 eV centre of mass collision energy.

From these spectra collected following collisions of CF_3^{2+} with the neutral target gas X_2, (X = H, D), we observe that X_2^+, X^+, CF_2^{2+}, CF_2^+, CF^+, XCF_2^+ and XF^+ product ions are formed.

7.5 Assignment of product ions

The ionic products generated following collisions of CF_3^{2+} with H_2 and D_2 have been described before in the literature before. In this work as mentioned above, the TOF mass spectra indicates the presence of X^+, X_2^+, CF_2^{2+}, CF_2^+, CF^+, $XCF_2^+$and XF^+ product ions. Previous work carried out by Manning *et al* in studies of CF_3^{2+} and D_2 collisions, did not reveal the formation of the XF^+ product ion.[3] However, in our investigation of the CF_3^{2+}/HD/H_2/D_2 collision systems we observe the formation of the XF^+ product ion. As in the previous Chapter, tests were carried out to identify alternate sources other than the dication/neutral collision by slightly varying the electric field in the velocity filter to look at higher and lower masses. The XF^+ signal intensity was found to be directly proportional to the dication current and insensitive to impurities. We thus conclude that there is no such alternate source and that the XF^+ product ions arise from the dication/neutral collision. Manning *et al* do observe all the other product ions listed in Table 7.1. Representative values of the background-corrected product ion intensities, recorded following collisions between CF_3^{2+} and H_2, at a centre of mass collision energy 0.197 eV are given in Table 7.1. A number of mass spectra were recorded at various collision energies to determine, qualitatively, the presence of these ions. The TOF mass spectra also indicate the presence of a weak F^+ signal. However, when corrected for background ions this F^+ signal is not found to be a 'true' product ion, and is concluded to be an impurity present in the dication beam or due to unimolecular decay.

Table 7.1: Background corrected intensities (arbitrary units) of ions formed in collisions between CF_3^{2+} and H_2 at a centre of mass collision energy of 0.197 eV

CF_2^{2+}	CF_2^+	CF^+	HF^+	HCF_2^+	CF_3^+
3156	14717	623	289	5590	3964

The product ion intensities, such as those listed in Table 7.1, indicate that three types of reactivity are observed. Firstly, the CF_3^+ ions that we detect are clearly formed via non-dissociative electron transfer

$$CF_3^{2+} + X_2 \rightarrow CF_3^+ + X_2^+ \qquad 7.13$$

the CF_2^+ product ion that we detect can be formed by either dissociative electron-transfer

$$CF_3^{2+} + X_2 \rightarrow CF_3^{+*} + X_2^+ \rightarrow CF_2^+ + F + X_2^+ \qquad 7.14$$

or collision induced charge-separation:

$$CF_3^{2+} + X_2 \rightarrow CF_2^+ + F^+ + X_2 \qquad 7.15$$

or via the following reaction

$$CF_3^{2+} + X_2 \rightarrow CF_2^+ + XF^+ + X \qquad 7.16$$

However, the absence of any bimolecular F^+ signal in our mass spectra eliminates the possibility of collision-induced charge separation as the source of CF_2^+ product ions. As can be seen from Table 7.1, the intensity for the formation of the CF_2^+ product ion is significantly larger than the intensity for formation of the XF^+ product ion. This leads us to conclude that the reaction shown in Equation 7.16 is not the major reaction channel. Thus it would be reasonable to conclude that the major reaction channel for the formation of the CF_2^+ product ion is via dissociative electron transfer as shown in Equation 7.14. However, we are unable to assign branching ratios for reaction channels 7.14 and 7.16 from our simple mass spectrometric data.

CF^+ can be produced via dissociative electron transfer

$$CF_3^{2+} + X_2 \rightarrow CF^+ + X_2^+ + F_2 \qquad 7.17$$

or via

$$CF_3^{2+} + X_2 \rightarrow XF^+ + CF^+ + F + X \qquad 7.18$$

Again, as before we are unable to assign branching ratios for the reaction channels 7.17 and 7.18, for formation of the CF^+ product ion from the data available. However, we do not expect the reaction channel shown in Equation 7.18 to be the major reaction channel. As mentioned above, Table 7.1 shows that we clearly do not form comparable

XF^+ product ions to CF^+ or CF_2^+ product ions, indicating that Equation 7.18 and 7.16 are not major reaction channels. Hence, we identify dissociative electron transfer (Equation 7.17) to be the major reaction channel for the formation of CF^+. Clearly more sophisticated experimental work needs to be carried out, such as coincidence experiments, to assign branching ratios to the reaction channels of these product ions. The formation of the XF^+ product ion will be discussed further below.

A second type of reactive process that also leads to the formation of new chemical bonds is observed. This bond-forming reaction results in the generation of the XCF_2^+ product ion. The observation of an X^+ signal, together with the absence of any real F^+ signal allows the formation of the XCF_2^+ product ion to be unambiguously assigned to the reaction given in Equation 7.19

$$CF_3^{2+} + X_2 \quad \rightarrow \quad XCF_2^+ + X^+ + F \qquad 7.19$$

Finally we observe the doubly charged product ion CF_2^{2+} which occurs as a result of collision induced neutral loss (CINL) reactivity from the collision of CF_3^{2+} with X_2 (X=H, D). The structure of CF_3^{2+} has previously been investigated via collisions of CF_3^{2+} and Ar.[22] The C_{2v} geometry of CF_3^{2+} has been ascribed to a second-order Jahn-Teller distortion. This distortion results in the lowering of the symmetry of the ground state with a lengthening, and consequent weakening, of one of the C-F bonds. The neutral loss reactivity exhibited in the collisional reactions of CF_3^{2+} is not an isolated phenomenon. In fact neutral-loss reactivity contributes significantly to the product ion yields following bimolecular collisions of a wide variety of perfluorinated dications.[23,24]

7.6 Product ion intensities

Having assigned the product ions to their respective reaction pathways, we now consider their relative intensities, and the collision energy dependence of the chemical reaction. As stated before, the collision energy dependence is a powerful probe of the reaction mechanism. In common with all the results of collision experiments reported in this thesis, the relative cross-sections of the competing electron-transfer and chemical (bond-forming) reaction channels are obtained from suitably background-corrected measurements of the detected intensities of the product ion.[6,7]

For the reactions of CF_3^{2+} and Ar as described in a preceding Chapter, the relative intensities of the products of the electron-transfer reactions were corrected for differences in the detection efficiency of the fluxes of the respective product ions. As stated in Chapter 3, the detection efficiency variability is caused by the differences in the amount and distribution of the kinetic energy released in a given reaction process. The kinetic energy release (KER) changes the ion's laboratory frame transverse velocity component, which, in turn, affects the ion detection efficiency. Therefore, because different reaction processes may have different kinetic energy releases, ions formed in different reaction processes may be detected with differing efficiencies. Hence, to overcome the problems caused by these differences in detection efficiencies, the analysis procedure incorporates a correction process which makes allowance for such differences in the ion detection efficiencies. The detailed description of the methodology behind this correction is presented in Chapter 3.

The calculation of the correction factor α (Equation 3.18) requires the kinetic energy released upon reaction of the dication and neutral. In the case of CF_3^{2+} and H_2/D_2 no such data was available in the literature. However despite the lack of appropriate data the correction procedure can be still carried out using the KER value for the CF_2^{2+} and H_2/D_2 system. We do not feel that this is a major approximation since both systems will be dominated by Coulombic repulsion between the singly charged product ions. Values of the correction factors α for the CF_3^{2+}/H_2 and CF_3^{2+}/D_2 systems are given below in Table 7.2 and table 7.3 respectively. The Tables also lists the intensity of the bond-forming product ion XCF_2^+ relative to the CF_2^+ electron transfer product. Figures 7.3 and 7.4 show a plot of both the uncorrected and corrected relative ion intensities.

It can be seen from the Tables below that the values of the correction factor, α, are close to unity and as a result there is little change in the corrected relative product ion intensity from the uncorrected product ion intensity ratios. In view of the relative values of the correction factors, which do not significantly change the values of the product ion ratios, we are confident that the observed product ion yield provides a reliable estimate of the relative cross-sections of the bond forming process.

Table 7.2 Relative detection efficiency correction factors (α) for the bond-forming reaction giving HCF_2^+/CF_2^+ in collisions between CF_3^{2+} with H_2 at centre of mass collision energies. The KER value used to calculate these correction factors is 7 eV. The experimental product ion intensity together with the corrected intensities $R(HCF_2^+)/R(CF_2^+)$ are also listed.

Ecom	$I(HCF_2^+)/I(CF_2^+)$	α(H)	$R(HCF_2^+)/R(CF_2^+)$
0.11	0.37335	0.9059	0.338215
0.14	0.37282	0.9077	0.338422
0.17	0.352421	0.9082	0.320081
0.20	0.355657	0.9077	0.322826
0.23	0.332195	0.9062	0.301048
0.25	0.340871	0.9039	0.308117
0.28	0.311112	0.9007	0.280205
0.31	0.317183	0.8964	0.284312
0.34	0.335408	0.8908	0.298792

Table 7.3 Relative detection efficiency correction factors (α) for the bond-forming reaction giving DCF_2^+/CF_2^+ in collisions between CF_3^{2+} with D_2 at centre of mass collision energies. The KER value used to calculate these correction factors is 7 eV. The experimental product ion intensity together with the corrected intensities $R(DCF_2^+)/R(CF_2^+)$ are also listed.

Ecom	$I(DCF_2^+)/I(CF_2^+)$	α(D)	$R(DCF_2^+)/R(CF_2^+)$
0.22	0.324849	0.8747	0.284138
0.27	0.348489	0.8773	0.305719
0.33	0.322205	0.8783	0.282978
0.38	0.308159	0.8780	0.270558
0.44	0.307246	0.8766	0.269334
0.49	0.280335	0.8742	0.245061
0.55	0.278578	0.8706	0.242533
0.60	0.256665	0.8658	0.222216
0.66	0.265448	0.8594	0.228134

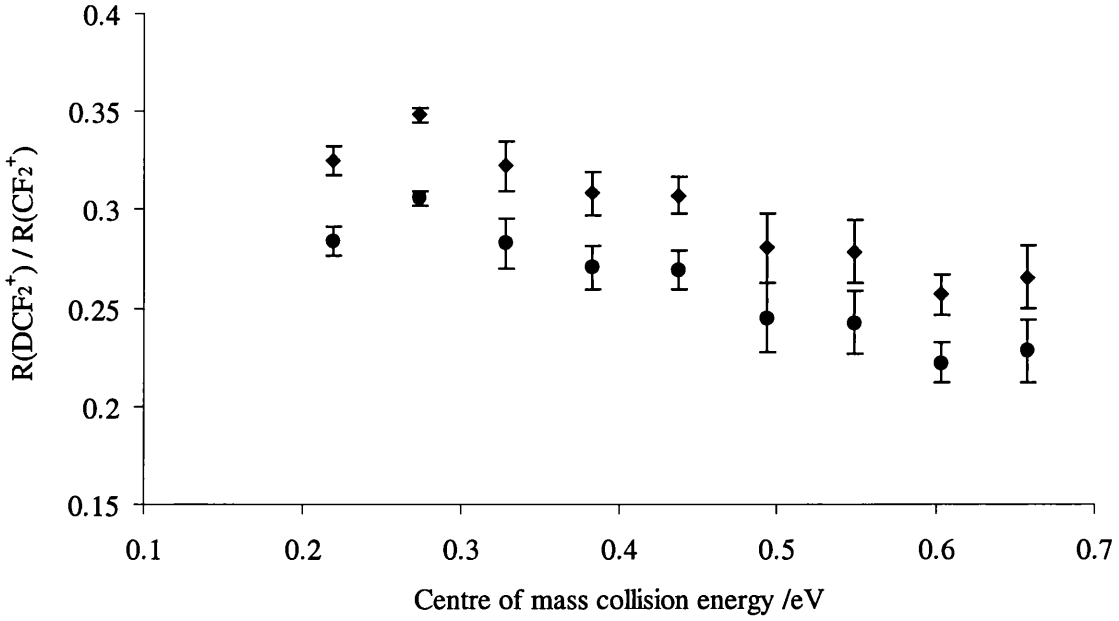

Figure 7.3 The relative product ion intensities and the corrected product ion intensities of the DCF_2^+ and CF_2^+ product ions as a function of the centre of mass collision energy. (♦) represent the uncorrected relative ion intensities and (•) represent the corrected product ion intensities.

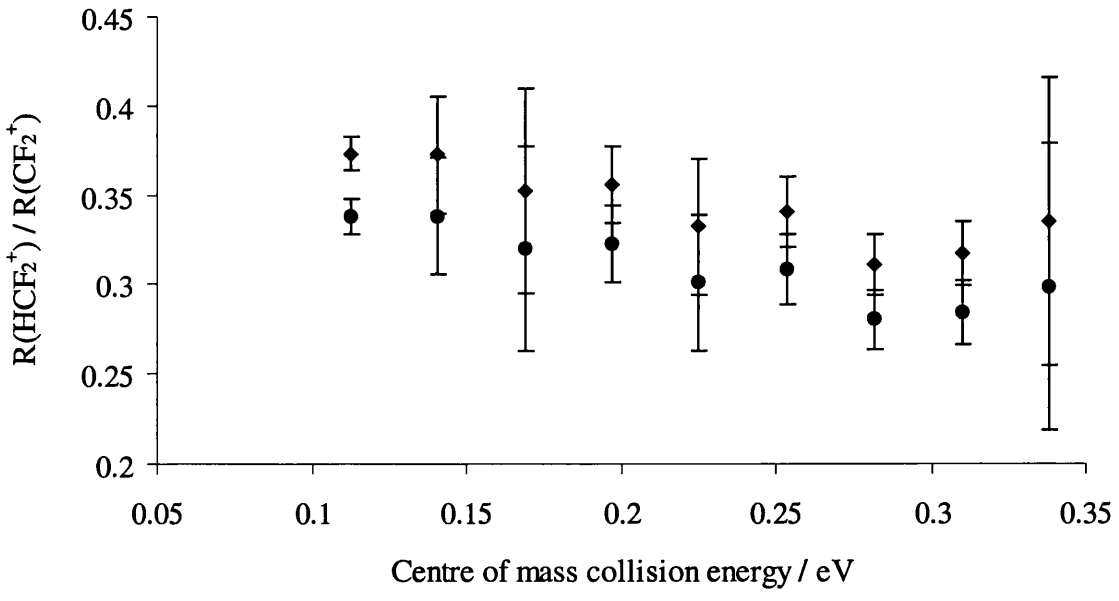

Figure 7.4 The relative product ion intensities and the corrected product ion intensities of the HCF_2^+ and CF_2^+ product ions as a function of the centre of mass collision energy. (♦) represent the uncorrected relative ion intensities and (•) represent the corrected product ion intensities

7.7 Discussion

Figure 7.5 shows the variation of the corrected relative ion intensities of XCF_2^+ with respect to the CF_2^+ from the series of experiments as a function of centre-of-mass collision energy. This ratio is a powerful probe of the intrinsic reactivity in the collision system, as it is independent of both the incident dication current and the collision gas density. As mentioned before this ratio should reveal any isotope effects in the reactive scattering as the electron transfer cross-section, and hence the CF_2^+ yield, should be similar for both D_2 and H_2 as a function of centre of mass collision energy. The data presented below in Figure 7.5 shows that at a given collision energy, it is equally probable to form DCF_2^+ from collisions of CF_3^{2+} with D_2 or HCF_2^+ from collisions of CF_3^{2+} with H_2. The data show a gradual increase of the corrected relative ion intensities. Work previously carried out on the $CF_2^{2+}/H_2/D_2$ system by Newson & Price and Z. Herman *et al*, shows this same trend; that at a given collision energy it is equally probable to form DCF_2^+ from CF_2^{2+} and D_2 and HCF_2^+ from CF_2^{2+} and H_2.

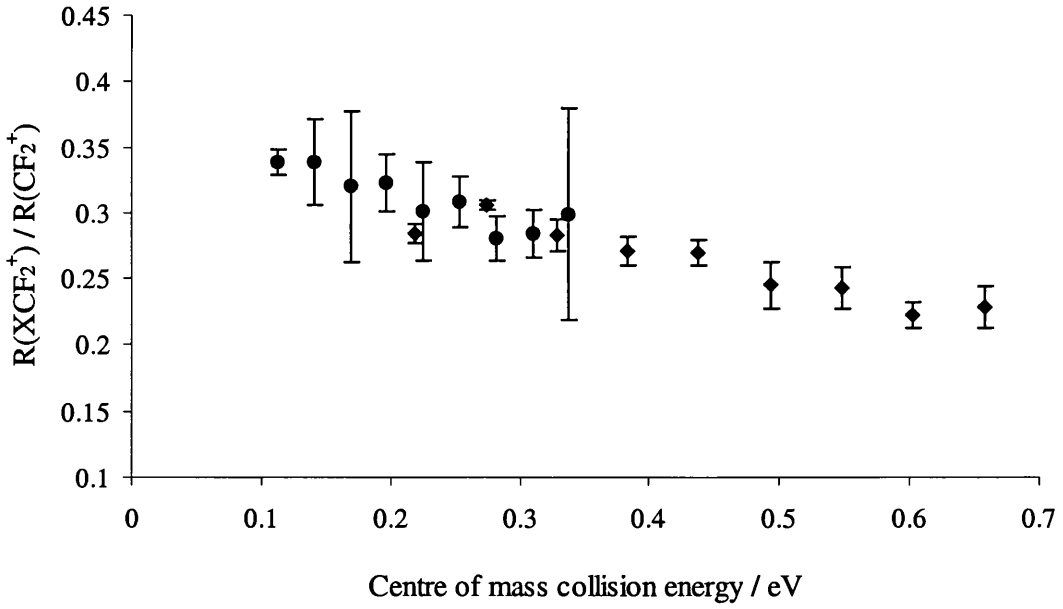

Figure 7.5 Variation of the corrected relative ion intensities of XCF_2^+ following collisions between CF_3^{2+} and D_2 represented by (♦) and of the collisions between CF_3^{2+} and H_2 represented by (•) as a function of the centre of mass collision energy.

As mentioned, the relative intensities of the products of bond-forming and electron transfer reactions of CF_3^{2+} with both H_2 and D_2 neutral targets are within experimental uncertainties, the same, for a given collision energy (Figure 7.5).

Similar hydride transfer reactions have been seen before in other dication bond forming reactions with D_2 which posses significant cross-sections. Crudely all of these bond-forming reactions appear to involve effective D^- transfer from the neutral molecule to the molecular dication.

$$M_2^+ + D_2 \rightarrow DM^+ + D^+ \qquad 7.20$$

Similar reactivity has been observed for atomic dications of the transition metals, which are observed to abstract H^- from organic molecules and with C_{60}^{2+} which abstracts OH^- from alcohols. The transfer of a hydride ion from an organic molecule to a dication has been modeled in an identical way to the electron-transfer reactions discussed in Chapter 4.

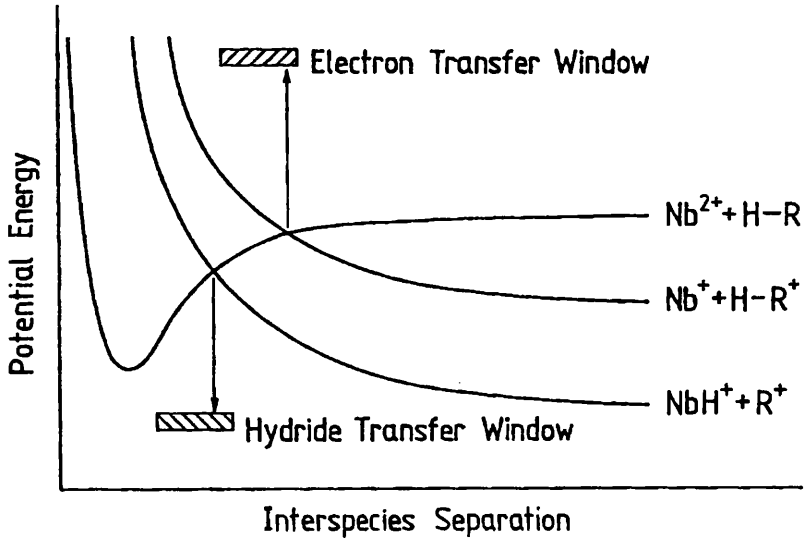

Figure 7.6 Schematic potential-energy curves to illustrate the competition between electron and H^- (D^-) transfer reactivity for atomic dications.

In this model the hydride ion is considered as simply a 'heavy electron' and its transfer is pictured (shown in Figure 7.6) as occurring at a curve crossing between an attractive reactant potential ($Nb^{2+} + C_2H_6$) and a repulsive product potential ($NbH^+ + C_2H_5^+$).[25-27] The applicability of this model had been supported by the fact that the transition-metal systems for which H^- transfer has been observed all possess curve crossings in a 'reaction window' at 3-7 Å. Systems which do not possess curve crossings in the window do not exhibit D^- transfer reactivity. In this curve-crossing model, the negative

ion must tunnel between the potential wells of the neutral molecule and the dication; hence the lighter hydride ion should exhibit a significantly larger bond-forming cross-section than the heavier deuteride ion. From the data presented in Figure 7.5 it is clear that as a function of the centre-of-mass collision energy, there is no dramatic difference between the relative ion yields for bond-forming reactivity when H_2 or D_2 is the collision partner. In the data presented in Figure 7.5 we assume that there is little or no variation of the CF_2^+ product ion. Mrazek *et al* support this approach in their investigation of the CO_2^{2+}/D_2 system, observing no significant variation of the charge transfer product CO_2^+. Indeed the absence of isotope effects has been seen before for other systems such as $CF_2^{2+}/H_2/D_2$ system. This absence of any isotope effect does not support the applicability of the simple curve-crossing model of the hydride transfer to molecular dication reaction. The absence of a strong isotope effect for the CF_3^{2+} and H_2/D_2 reaction is consistent with a direct reaction mechanism, which pictures the dication as flying past the neutral species and pulling off the negative ion. This direct reaction mechanism has previously been proposed for the $CF_2^{2+}/H_2/D_2$ collision system by Newson and Price, which is in accord with results from crossed beam scattering experiments which observed the DCF_2^+ product to be predominantly forward scattered; a characteristic signature of a direct mechanism.

The relative ion intensity for the bond-forming product, XCF_2^+, in the $CF_3^{2+}/H_2/D_2$ collision system share very similar collision energy dependencies. In both cases the cross-section for the bond-forming reactions rise steadily with decreasing collision energy. This collision energy dependence is indicative of a reactive pathway in which there is no energy barrier. The observed increase in bond forming reactivity with decreasing collision energy may be qualitatively explained as arising as a result of the increased time for interaction of the collision partner at lower collision energies and this apparent lack of an energy barrier casts doubt on the applicability of the simple Landau-Zener model of hydride transfer.

The above curve-crossing model for hydride transfer is a simple model and a more detailed model has been developed. In this new model (Herman model) three types of potential energy surfaces are involved as shown in the schematic diagram (Figure 7.7):

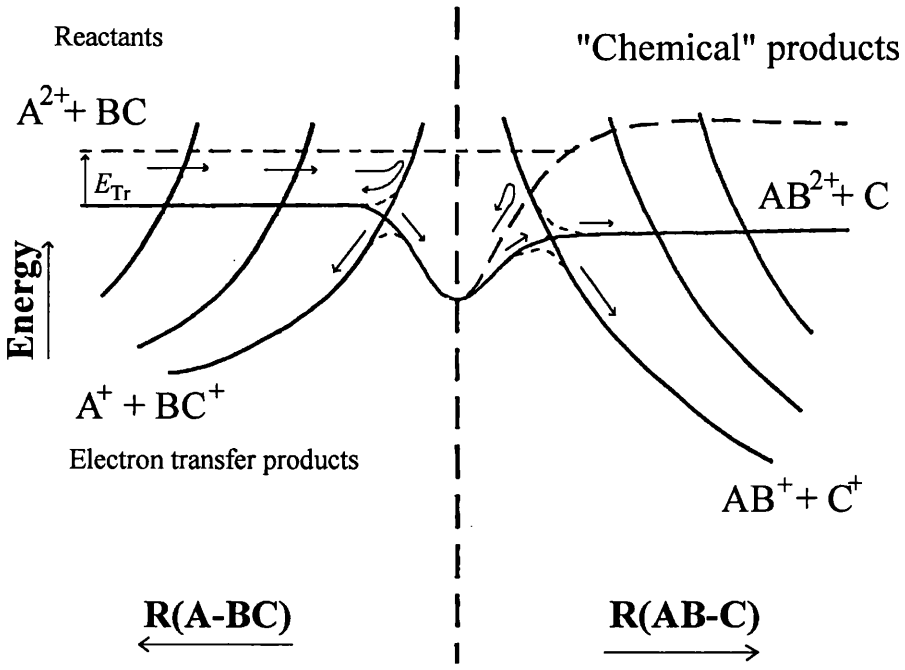

Figure 7.7 Schematics of the potential energy surfaces and their possible crossing for dication-neutral reactions

Firstly, the potential energy surface of the dication A_2^+ + BC which continues through the coordination region to the neutral transfer asymptote AB^{2+} + C. Secondly, the Coulomb repulsion surfaces in the reactant valley leading to charge transfer products A^+ + BC^+ and possibly to further dissociative charge transfer products, and finally, the Coulomb repulsive surfaces in the product valley leading to chemical rearrangement to form singly charged products AB^+ + C^+. In this model the existence or non-existence of crossings between the dication surface and Coulomb repulsive surfaces at different interparticle separation influences the outcome of a dication-neutral collision and represents an application of the 'reaction window' concept to chemically reactive systems. As shown in the diagram above the system approaches along the slightly attractive (ion-induced dipole) term marked A^{2+} + BC and in general, several possible cases of crossing between mutually interacting terms can occur. This model indicates why chemical reactions of dications tend to occur much less frequently than charge transfer processes by suggesting that the colliding reactants have to pass through the charge transfer crossings in the reactant valley to reach small interparticle separations in order to react chemically, and the number of systems that may succeed may be considerably reduced. Formation of the chemical rearrangement dication product AB^{2+} + C, is even more difficult, as the system has to pass through the possible crossings with coulomb repulsion surfaces in the product valley which leads to AB^+ + C^+. The behaviour of the system at small interparticle separations depends on the stability of the collision species ABC^{2+}. For relatively flat surfaces the system may be expected to go

in a single-passage type trajectory into the product valley. If however, ABC^{2+} is appreciably stable with respect to dissociation to both A^{2+} + BC and AB^{2+} + C and the surface exhibits a well, an intermediate complex may be formed with a mean lifetime of many rotations. Indeed the potential energy surface model described above has been applied to the CF_2^{2+}/D_2 system and the results further support this approach. As discussed in Chapter Six, calculations by Mrazek *et al*, for the CO_2/D_2 system show that the $[CO_2\text{-}D_2]^{2+}$ potential energy surface possesses several deep minima resulting in the collision complex having a lifetime of about a picosecond despite having no barrier, as had been concluded experimentally. Unfortunately at the moment there are no calculations of the $CF_3^{2+}/H_2/D_2$ potential surfaces.

As mentioned above, in our mass spectra we also observe the formation of the XF^+ product ion. Figure 7.8 below shows the ratio of the XF^+ product ion to the CF_2^+ product ion on the centre of mass scale. The graph shows markedly different behaviour to that observed for the bond-forming reaction of XCF_2^+ as shown in Figure 7.5 and leads us to tenuously conclude that perhaps the formation of this ion is via a different mechanism and there exists a barrier for the formation of the XF^+ product ion and we are observing isotope effects.

A plot of this data on the relative velocity of the reactants (Figure 7.9) shows both sets of data lying on top of each other. In this representation the data collapse, for both the H_2 and D_2 collisions, within the accuracy of the measurements, to a single line descending with decreasing relative velocity. As shown in previous work by Z. Herman *et al.* this type of behaviour suggests that our observation of the formation of the XF^+ product ion is connected with charge transfer processes which may be the rate-determining step. In the previous Chapter a speculative mechanism was suggested for XF^+ formation for the CF_3^{2+}/HD system. In a similar fashion we would expect initial co-ordination followed by X migration to an F atom and subsequent cleavage of the F-X bond.

In the $CF_3^{2+}/H_2/D_2$ system, as in the CF_3^{2+}/HD system it is difficult to give a precise mechanism for the formation of the XF^+ ion. However, if complexation appears to be involved as suggested for the CF_3^{2+}/HD system it seems reasonable to assume that the formation of this ion proceeds via the same initial pathway.

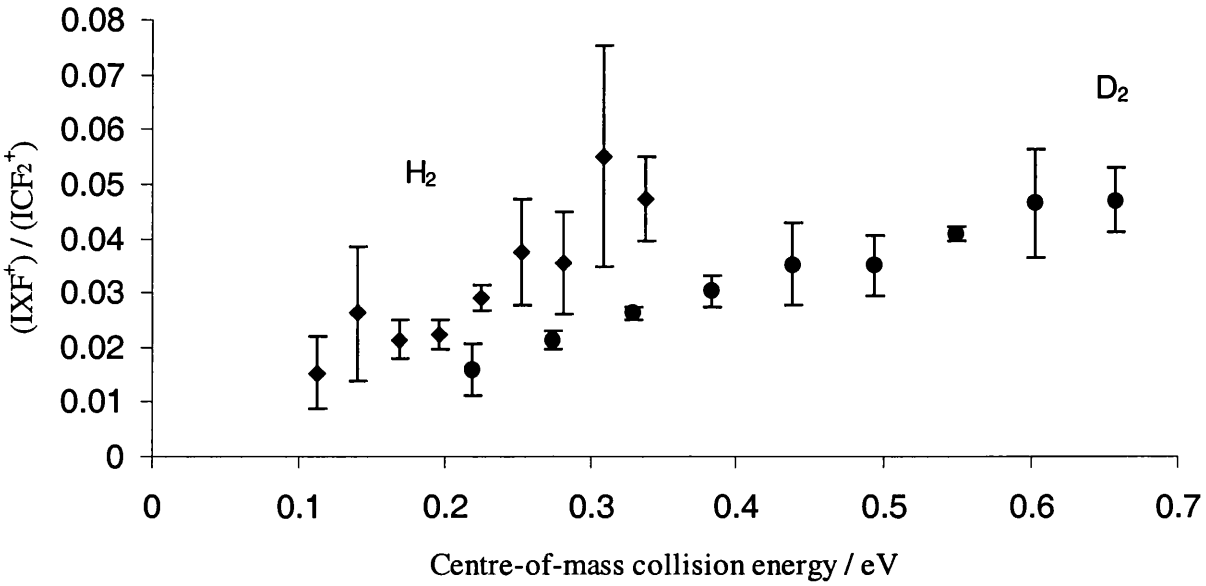

Figure 7.8 Relative intensities of the XF^+ and the CF_2^+ product ions as a function of the centre of mass collision energy, formed in collisions of CF_3^{2+} and H_2/D_2. Collisions with H_2 are represented by (♦) and collisions with D_2 are represented by (•)

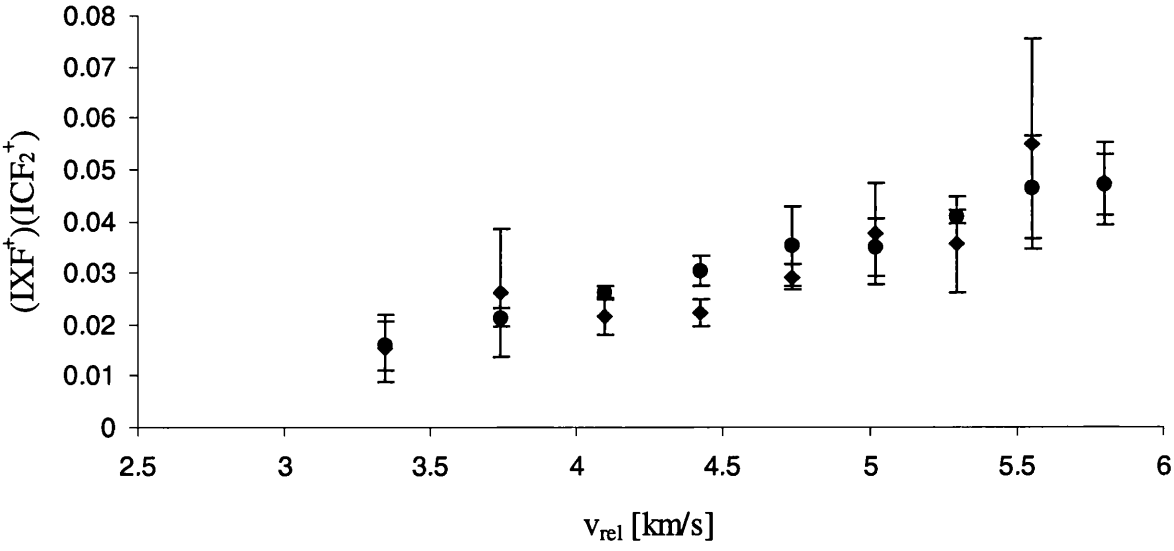

Figure 7.9 Relative intensities of the XF^+ and the CF_2^+ product ions as a function of the relative velocity of reactants, v_{rel}, formed in collisions of CF_3^{2+} and H_2/D_2. Collisions with H_2 are represented by (♦) and collisions with D_2 are represented by (•)

7.8 Conclusion

Relative yields of the electron-transfer and bond-forming product ions, following collisions between CF_3^{2+} and H_2/D_2 have been recorded as a function of the centre of mass collision energy. The ratios of the XCF_2^+ bond forming product ions indicate that no isotope effect is in operation when H_2 is used in place of the D_2 neutral reactant, that the probability of forming the XCF_2^+ product ion is independent of the choice of hydrogen isotope used as the neutral reactant at a given collision energy. In addition, the collision energy dependence of the bond forming reaction is indicative of a reactive pathway in which there is no energy barrier.

The similarities of both magnitude and collision energy dependence of the cross-sections of the XCF_2^+ bond forming reaction in $CF_3^{2+}/H_2/D_2$ and $CF_2^{2+}/H_2/D_2$ collision systems, are such that it is probable that both collision systems share the same reactive pathway of bond formation.

However, we observe the formation XF^+ product ions; a product ion not observed before in the $CF_2^{2+}/H_2/D_2$ system or indeed earlier experiments of collisions of CF_3^{2+} and D_2. From the data presented we tenuously conclude that perhaps we do observe isotope effects in the formation of this product ion and perhaps charge transfer reaction precedes the bond-forming reaction which may be the rate determining step in the formation of this product ion. Obviously further investigation is required to determine the reaction channel of XF^+, CF_2^+ and CF^+.

References:

1 S. D. Price, S. A. Rogers, and S. R. Leone, *J. Chem. Phys.* **98,** 9455-9465 (1993).

2 S. A. Rogers, S. D. Price, and S. R. Leone, *J. Chem. Phys.* **98,** 280-289 (1993).

3 M. Manning, S. D. Price, and S. R. Leone, *J. Chem. Phys.* **99,** 8695-8704 (1993).

4 C. E. Melton and G. F. Wells, *J. Chem. Phys.* **27,** 1152 (1957).

5 Z. Herman, P. Johnathon, A. G. Brenton, and J. H. Beynon, *Chem. Phys. Lett.* **41,** 433 (1989).

6 S. D. Price, *J. Chem. Soc. Faraday Trans.* **93,** 2451-2460 (1997).

7 K. A. Newson and S. D. Price, *Chem. Phys. Lett.* **269,** 93-98 (1997).

8 R. H. Schultz and P. B. Armentrout, *J. Chem. Phys.* **96,** 1036-1045 (1992).

9 K. M. Ervin and P. B. Armentrout, *J. Chem. Phys.* **85,** 6380-6395 (1986).

10 J. L. Elkind and P. B. Armentrout, *J. Chem. Phys.* **84,** 4862-4871 (1986).

11 E. A. Gislason, B. H. Mahan, C. W. Tsao, and A. S. Werner, *J. Chem. Phys.* **50,** 5418 (1969).

12 K. Tanaka, T. Kato, P. M. Guyon, and I. Koyano, *J. Chem. Phys.* **79,** 4302-4305 (1983).

13 R. A. Dressler, R. H. Salter, and E. Murad, *J. Chem. Phys.* **99,** 1159-1171 (1993).

14 P. Tosi, O. Dmitrijev, Y. Soldo, D. Bassi, D. Cappelletti, F. Pirani, and V. Aquilanti, *J. Chem. Phys.* **99,** 985 (1993).

15 F. S. Klein and I. Friedman, *J.Chem. Phys.* **41,** 1789 (1964).

16 T. F. Moran and I. Friedman, *J. Chem. Phys.* **42,** 2391 (1965).

17 C. E. Dateo and D. C. Clary, *J. Chem. Soc. Faraday Trans.* **85,** 1685-1696 (1989).

18 P. M. Hierl, *J. Chem. Phys.* **67,** 4665-4671 (1977).

19 P. B. Armentrout, *Acs Symposium Series* **502,** 194-209 (1992).

20 L. Landau, *Phys. Z. Sowjetunion* **2,** 26 (1932).

21 C. Zener, *Proc. Roy. Soc. Lond. Ser. A* **137,** 696 (1932).

22 N. Tafadar, N. Kaltsoyannis, and S. D. Price, *Int. J. Mass Spectrom.* **192,** 205-214 (1999).

23 Y. Y. Lee, S. R. Leone, P. H. Champkin, N. Kaltsoyannis, and S. D. Price, *J. Chem. Phys.* **106,** 7981-7994 (1997).

24 S. D. Price, M. Manning, and S. R. Leone, *Chem. Phys. Lett.* **214,** 553-558 (1993).

25 J. C. Weisshaar, *Accounts of Chemical Research* **26,** 213-219 (1993).

26 R. Tonkyn and J. C. Weisshaar, *J. Am. Chem. Soc.* **108,** 7128-7130 (1986).

27 L. M. Roth and B. S. Freiser, *Mass Spec. Rev.* **10,** 303-328 (1991).

Chapter 8

Reactions between CO_2^{2+} and H_2/D_2

8.1 Introduction

The earlier investigation of intermolecular isotope effects in the reaction between CF_3^{2+} and H_2/D_2, discussed in Chapter 7, and previous work on CF_2^{2+} with H_2/D_2, has provided a significant amount of data regarding the mechanism of the bond-forming reactions in these collision systems.[1,2] Since CF_3^{2+} and CO_2^{2+} are similar systems, in that they show significant reactivity with H_2 and D_2, it would be expected that they might share similar reactive characteristics, such as their reaction mechanism. Hence, in order to study the mechanism and collision energy-dependence of the bond forming reaction of CO_2^{2+} with H_2/D_2, studies of this collision system were performed under exactly the same conditions and collision energies as those performed in the $CF_3^{2+}/H_2/D_2$ system. As mentioned before, substituting H_2 in place of D_2 as the neutral collision partner in the reaction of dications should provide an insight into the reaction mechanism, by comparing the relative cross-sections of the electron-transfer and bond-forming reaction channels for the collision systems.[3-7]

This chapter presents an investigation of the product ions formed following collisions of CO_2^{2+} with H_2 and D_2 and their dependence on collision energy.

8.2 Experimental

The apparatus used in this investigation has been discussed in detail in the preceding chapters of this thesis. In this work the product ions formed following collisions between CO_2^{2+} with H_2/D_2 were monitored at the centre of mass collision energies from 0.17 to 0.52 eV and 0.33 to 1 eV respectively. The centre of mass collision energy is calculated using the initial dication velocity, which is known from the beam potential, and as before, assumes that the velocity of the neutral molecule to be negligible with respect to the velocity of the dication.

8.3 Results and Analysis

The apparatus used in these investigations has been described in detail in Chapter Two. Briefly the molecular dication of interest, in this case CO_2^{2+}, is mass selected using a velocity filter from the positive ions produced by an electron impact ionization source. To produce the CO_2^{2+} dication we utilize the non-dissociative double ionization of CO_2 with ~150 eV electrons in a low-pressure electron-impact source. As with previous work reported here, the experiments were performed at low collision energies in order to maximize the yield of the bond forming reaction. After traversing the velocity filter the kinetic energy of the dications is reduced before they encounter the neutral molecules. Product ions formed following the interaction of the molecular dication with the neutral target, in addition to unreacted dications, are periodically extracted from the interaction region by pulsing the repeller plate of the TOFMS. Ions reaching the end of the drift tube are accelerated to hit a multichannel plate detector. The pressure of the neutral collision partner is carefully controlled to ensure single collision conditions exist in the interaction region. Sections of typical mass spectra are shown in Figures 8.1 and 8.2.

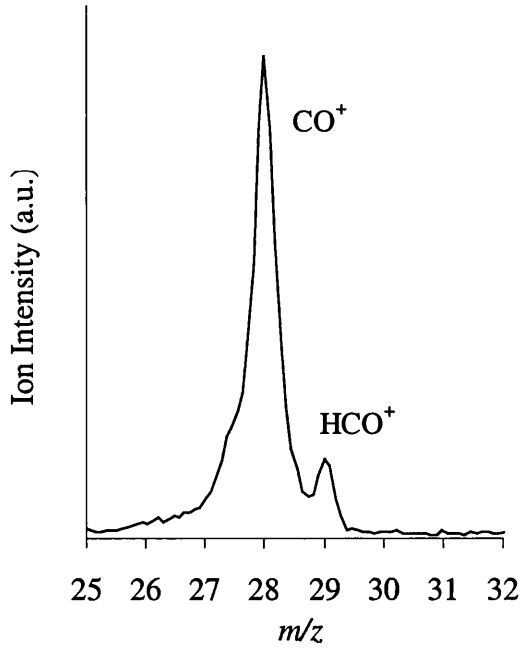

Figure 8.1 Sections of representative mass spectra showing the formation of HCO^+ following collisions of CO_2^{2+} with H_2 at 0.30 eV centre of mass energy.

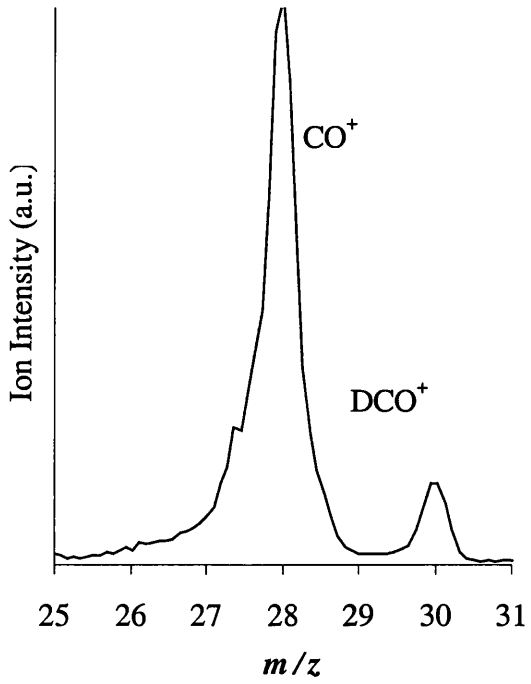

Figure 8.2 Sections of representative mass spectra showing the formation of DCO^+ following collisions of CO_2^{2+} with D_2 at 0.58 eV centre of mass collision energy.

From these spectra collected, following collisions of CO_2^{2+} with the neutral target gas (X = H, D) we observe that X^+, X_2^+, CO_2^+, CO_2^{2+}, CO^+, O^+, O_2^+, XCO^+ and XCO_2^+ are present in the spectrum. The variation of the relative signal intensities of XCO^+ with respect to the CO_2^+ product ion should prove to be a powerful probe of the intrinsic reactivity in the collision system, as it is independent of both the incident dication current and the collision gas density. As before this ratio should reveal any isotope effects in the reactive scattering as the electron transfer cross-section, and hence the CO_2^+ yield should be similar for both D_2 and H_2, which has been shown to be true for the $CF_2^{2+}/H_2/D_2$ collision system in the formation of CF_2^+ by Z. Herman *et al.*[1]

The signals of interest in these product-ion mass spectra are those which result from the bimolecular encounters. For example after traversing the velocity filter the metastable states of the dication (CO_2^{2+}) dissociate to give CO^+ and O^+. As before in the previous work in this thesis, to remove any contribution to the mass spectral signal from impurity ions present in the dication beam, background mass spectra of the ions present in the interaction region in the absence of the collision gas are also recorded. These background spectra are then used to correct the spectra recorded in the presence of the collision gas to

leave only the signals which are due to the bimolecular reactions. In general these corrections are small. However, as will be shown in section 8.5, for the $CO_2^{2+}/H_2/D_2$ collision system these correction factors are relatively large and the size of these correction factors is taken into consideration in the interpretation of the data.

As illustrated in Figures 8.1 and 8.2, for both the CO_2^{2+} and H_2/D_2 reaction the mass resolution of our apparatus allows us to clearly distinguish the product-ion signals resulting from the bond-forming reactions.

8.4 Assignment of product ions

As mentioned above, the TOF mass spectra indicate the presence of CO_2^+, CO_2^{2+}, CO^+, O^+, O_2^+, XCO^+ and XCO_2^+ product ions. The TOF mass spectra also indicate the presence of X^+ and X_2^+ ions. However due to these ions being formed in the interaction region well off the axis in the TOFMS and possessing negligible lab frame translational energy few enter the time of flight tube resulting in low detection efficiency for the species. Hence they have not been presented in the table below. A number of mass spectra were recorded at various collision energies to determine, qualitatively, the presence of these ions as shown below in table 8.1.

Table 8.1: Background corrected intensities of ions formed in collisions between CO_2^{2+} and D_2 at a centre of mass collision energy of 0.67 eV

CO^+	DCO^+	CO_2^+	DCO_2^+	O_2^+	O^+
5699	1950	6653	38	28	2066

Firstly the CO_2^+ product ion can be formed only via a non-dissociative electron transfer reaction

$$CO_2^{2+} + X_2 \rightarrow CO_2^+ + X_2^+ \qquad 8.11$$

The reaction product XCO^+ is obviously a product of a dissociative chemical reaction. It has been shown by Mrázek *et al.* in scattering experiments, that this product ion is formed via decomposition of XCO_2^+ and is formed in a high translational energy release channel to give $XCO^+ + O$ as shown in equation 8.12 below.[8]

$$CO_2^{2+} + X_2 \rightarrow XCO_2^+ + X^+ \rightarrow XCO^+ + X^+ + O \qquad 8.12$$

The presence of X^+ ions in our mass spectra further supports this conclusion.

CO^+ can be formed in several possible processes. Firstly, via dissociative electron transfer reaction as shown in Equation 8.13 below

$$CO_2^{2+} + X_2 \rightarrow CO_2^{+*} + X_2^+ \rightarrow CO^+ + O + X_2^+ \qquad 8.13$$

Or via collision induced dissociation as shown in equation 8.14 below

$$CO_2^{2+} + X_2 \rightarrow CO^+ + O^+ + X_2 \qquad 8.14$$

Table 8.1 shows that we do not form comparable intensities of O^+ to CO^+ ions indicating that collision induced dissociation (Equation 8.14) is not the only reaction channel for forming CO^+ and that CO^+ product ions must also be formed from dissociative electron transfer reactions as shown in Equation 8.13. However from the data we are unable to assign branching ratios for these reaction channels.

As mentioned above we also see formation of CO^+ and O^+ ions from the dissociation of metastable states of the dication which are background subtracted and are not considered further. As discussed in the previous chapter, it has been shown by studies by several groups that electron transfer dominates the product ion yield, thus we expect the product yield to be dominated by charge transfer reactions. This behaviour has also been observed following the collisions of these heavier rare gases with CO^{2+}, CO_2^{2+}, CS_2^{2+}, CF^{2+} and

CF_2^{2+}.[3-5,9] Mrázek *et al.* have also concluded from scattering experiments that the main channel of CO^+ formation is charge transfer to CO_2^+ and a subsequent decomposition of this predissociative state, as shown in Equation 8.13.[8] This is in agreement with what we have concluded above

We also observe XCO_2^+, however due its extremely low intensity, as shown in Table 8.1, and the fact that these ions are masked by the broad peaks of the energetic CO_2^+ ions, it is not possible to extract any meaningful data from our simple mass spectrometric data and will not be considered further. However, in scattering experiments Mrázek *et al.* also observe this product ion and their data shows that the cross section for the formation of XCO_2^+ is about two orders of magnitude smaller than for the formation of CO_2^+ and is a result in agreement with our data.

8.5 Product ion intensities

In common with all the results of collision experiments reported in this thesis, the relative cross sections of the competing electron-transfer and chemical (bond-forming) reaction channels are obtained from suitably background-corrected measurements of the detected intensities of the product ions. Furthermore when we wish to consider the relative intensities of the product ion signals we must also consider the possibility that mass discrimination effects may mean that these background corrected signals do not exactly represent the true ion yields. This methodology and the calculation of the correction factor α has been discussed and demonstrated in the preceding Chapters. Below, in tables 8.2 and 8.3, the raw intensities, the correction factors and the corrected ion intensities are presented.

By calculating α (Table 8.2) for the CO_2^{2+}/H_2 collision system it can be seen that the detection efficiency varies by ~29% and by calculating α (Table 8.3) for the CF_3^{2+}/D_2 collision system, it can be seen that the detection efficiency again varies by ~28% over the collision energies employed and is far from unity. The CO_2^+ ion is always discriminated against. This is due to the kinematics involved in the separation of the singly charged products, which result in the CO_2^+ product ion having a significantly higher transverse kinetic energy than the XCO^+ product ion, resulting in its lower detection efficiency. The

kinematics involved has been discussed in detail in Chapter 3. Correcting our background corrected ion intensities using the values of α (Tables 8.2 and 8.3) yields the relative intensities also listed in Tables 8.2 and 8.3 and plotted in Figures 8.3 and 8.4.

Table 8.2 Correction factors α calculated by using equation (3.18) for the relative detection efficiency of HCO^+ and DCO^+ and the resulting relative ion intensities $R(HCO^+)/R(DCO^+)$ derived from the background corrected experimental data.

E_{COM} / (eV)	$I(HCO^+)IR(CO_2^+)$	α	$R(HCO^+)/R(CO_2^+)$
0.17	0.190	0.695	0.132
0.22	0.229	0.661	0.152
0.26	0.275	0.623	0.171
0.30	0.219	0.581	0.127
0.34	0.252	0.534	0.135
0.39	0.274	0.481	0.132
0.43	0.263	0.422	0.111
0.48	0.257	0.355	0.091
0.52	0.256	0.278	0.071

Table 8.3 Correction factors α calculated by using equation (3.18) for the relative detection efficiency of DCO^+ and CO_2^+ and the resulting relative ion intensities $R(DCO^+)/R(CO_2^+)$ derived from the background corrected experimental data.

E_{COM} / (eV)	$I(DCO^+)/I(CO_2^+)$	α	$R(DCO^+)/R(CO_2^+)$
0.33	0.256	0.650	0.166
0.42	0.241	0.616	0.149
0.5	0.322	0.578	0.186
0.58	0.243	0.536	0.130
0.67	0.284	0.488	0.139
0.75	0.307	0.435	0.134
0.83	0.322	0.374	0.120
0.92	0.320	0.305	0.098
1.00	0.328	0.226	0.074

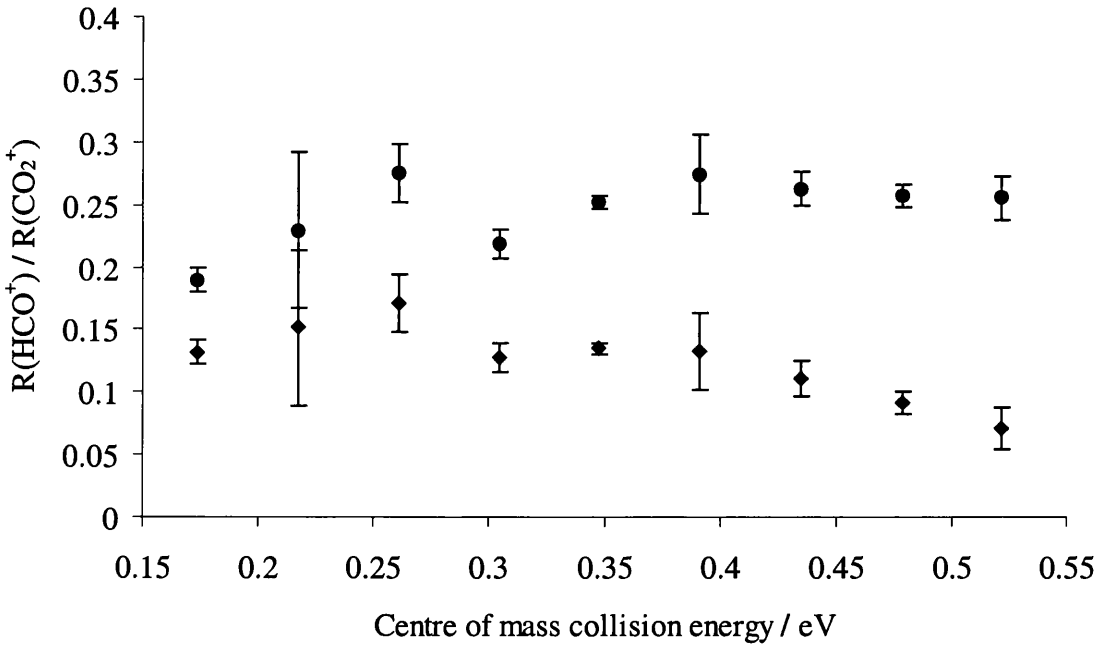

Figure 8.3 Variation of the corrected relative ion intensities (♦) and the uncorrected relative ion intensities (•) of the HCO^+ and CO_2^+ product ions, as a function of collision energy, following collisions of CO_2^{2+} with H_2

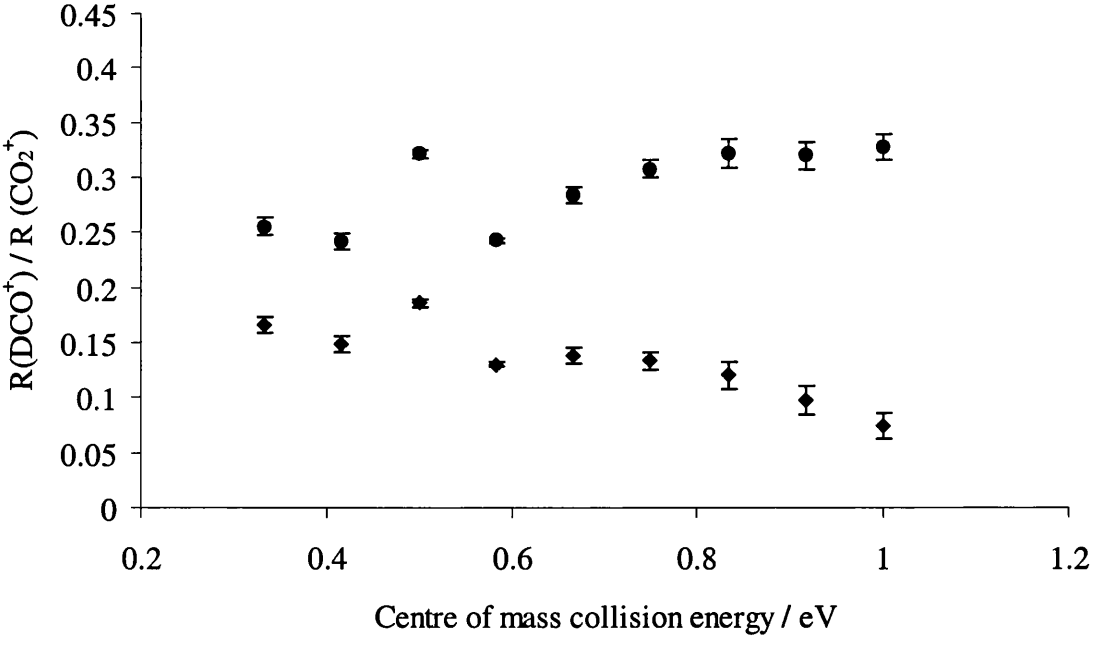

Figure. 8.4 Variation of the corrected relative ion intensities (♦) and the uncorrected relative ion intensities (•) of the DCO^+ and the CO_2^+ product ions, as a function of collision energy, following collisions of CO_2^{2+} with D_2

Tables 8.2 and 8.3 show that there is a large variation of the correction factors, unlike those calculated in previous Chapters, for example for the $CF_3^{2+}/H_2/D_2$ collision system. This additional uncertainty in the data will be considered in the discussion below

Figures 8.3 and 8.4 show the relative signal intensities of HCO^+ and DCO^+ from the $CO_2^{2+}/H_2/D_2$ reaction as a function of the centre of mass collision energy and both corrected and uncorrected relative ion intensities have been presented. Each data point is an average of 3 or more determinations. As mentioned before this ratio is a powerful probe of the intramolecular reactivity in the collision system, as it is independent of both the incident dication current and the collision gas density. It can be seen from both Figures 8.3 and 8.4, that there is only a slight variation of the relative product ion intensities with collision energy unlike the data shown in Chapter 7 for the $CF_3^{2+}/H_2/D_2$ collision system where there is a significant variation in the relative product ion intensities of the bond forming product, HCF_2^+ to the charge transfer product CF_2^+, between the collision energies that we have employed. For the data presented for the $CO_2^{2+}/H_2/D_2$ system, the corrected relative ion intensities do show a gradual increase with decreasing collision energy within our errors as one might expect. However, due to the large correction factors involved and the added uncertainty introduced we can only tenuously make this conclusion. As mentioned, the ionic products generated following collisions of CO_2^{2+} and CF_3^{2+} with H_2 and D_2 have been described in the literature before, and will be referred to as appropriate in the discussion.

8.6 Discussion

Figure 8.5 below shows the variation of the corrected relative ion intensities of XCO^+ with respect to CO_2^+ for collisions with both H_2 and D_2, from a series of experiments as a function of centre of mass collision energy. As mentioned before this ratio should reveal any isotope effects in the reactive scattering as the electron charge transfer cross section and hence the CO_2^+ yield should be similar for both D_2 and H_2 as a function of centre of mass collision energy. As mentioned above, it is necessary here to take into consideration the additional uncertainty introduced into the data from our calculated correction factors and the significant change to the nature of the data, unlike in previous Chapters. Figures

8.3 and 8.4 show that at higher collision energies there is an increasingly pronounced difference between the corrected and uncorrected relative ion intensities. Given this additional uncertainty, especially at higher collision energies, it seems reasonable, therefore, to conclude from the data presented in Figure 8.5, that within our experimental uncertainty we do not observe any isotope effect and that at a given collision energy it is equally probable to form DCO^+ from collisions of CO_2^{2+} with D_2 or HCO^+ from collisions of CO_2^{2+} with H_2.

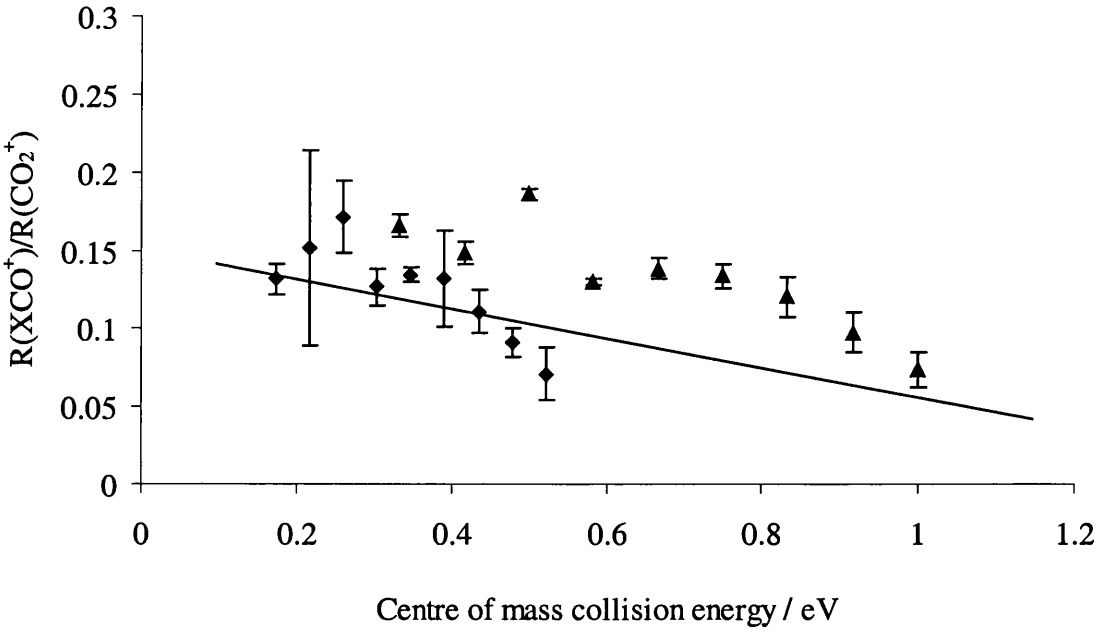

Figure 8.5 Dependence for the relative ion intensities of the XCO^+ and the CO_2^+product ions, as a function of centre of mass collision energy, following collisions of CO_2^{2+} with H_2 and D_2. Collisions with H_2 is represented by (♦) and (▲) for collisions with D_2. The line is used to guide the eye only and not a regression line.

From the data presented in Chapter 7, it can be seen that the relative intensities of the products of bond-forming and electron transfer reactions of CF_3^{2+} with both H_2 and D_2 neutral targets are, within experimental uncertainties, the same for a given collision energy (Figure 7.5). The similar lack of any isotope effect, for the analogous $CO_2^{2+}/H_2/D_2$ collision system matches the observed behaviour for the $CF_3^{2+}/H_2/D_2$ collision system. This observation leads us to conclude that perhaps the mechanism of the bond forming

reaction in the $CF_3^{2+}/H_2/D_2$ and the $CF_2^{2+}/H_2/D_2$ collision systems are intrinsically similar to the reaction mechanism of the $CO_2^{2+}/H_2/D_2$ collision system. As mentioned in Chapter 6, recent *ab initio* calculations by Mrázek *et al.* show that despite having no barrier the potential surface energy of $[CO_2\text{-}D_2]^{2+}$ possesses several deep minima, thus explaining why despite the considerable exoergicity of the reaction there is considerable evidence for sticky collisions in this system. A mechanism for the formation of the chemical bond has been proposed in the literature for the $CO_2^{2+}/H_2/D_2$ collision system. This proposed mechanism has been described in detail in Chapter 6 and for this mechanism we expect to see no isotope effect due to the lack of a barrier in the reaction pathway. The data presented in Figure 8.5 assumes that there is little or no variation of the CO_2^+ product ion yield with collision energy. Mrázek *et al.* have shown this to be true and support this approach, observing little or no significant variation of the charge transfer product CO_2^+ in their study.

As mentioned before Mrázek *et al.* have reported a cross-beam scattering study of the processes in the CO_2^{2+} $/H_2/D_2$ collision system. In order to compare the data from our investigation presented in this thesis with their data, it is necessary to convert our data to the relative velocity of the reactants, v_r, scale. Mrázek *et al.* have performed their work at high collision energies and present data between 4 and 16 km/s on the v_r scale. The experimental work that we have carried out is between 3.63 and 7.25 km/s on the, v_r scale. A comparison of our experimental data and those produced by Mrázek *et al.* is presented in Figures 8.6 and 8.7. As can be seen from Figures 8.6 and 8.7 the data produced from our investigation for the relative cross-section for formation of the XCO^+ and CO_2^+ ion, within this region is in good agreement with those produced from the experimental work carried out by Mrázek *et al.* The results from both our investigation and that reported by Mrázek and co-workers show the relative cross section for formation of the XCO^+ product ion to be approximately an order of magnitude smaller than the cross-section for the formation of the CO_2^+ product ion, which exhibits the largest cross section.

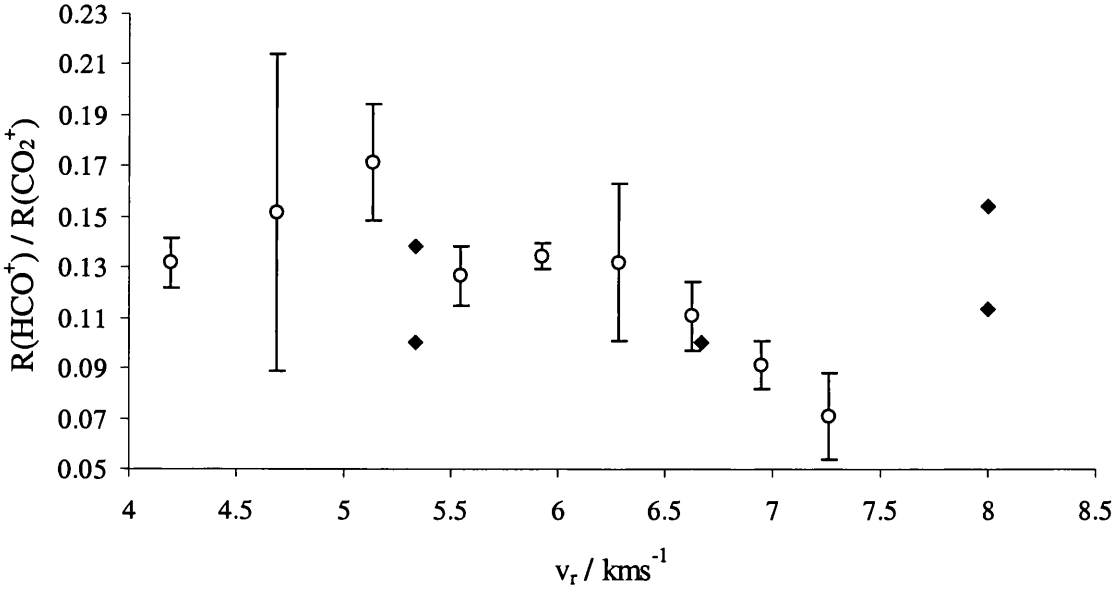

Figure 8.6 Dependence of the relative ion intensities of the HCO^+ and the CO_2^+ product ions, as a function of relative velocity of the reactants, following collisions of CO_2^{2+} with H_2. (♦) show data by Mrázek *et al.* and (○) represents the data from our experimental observations.

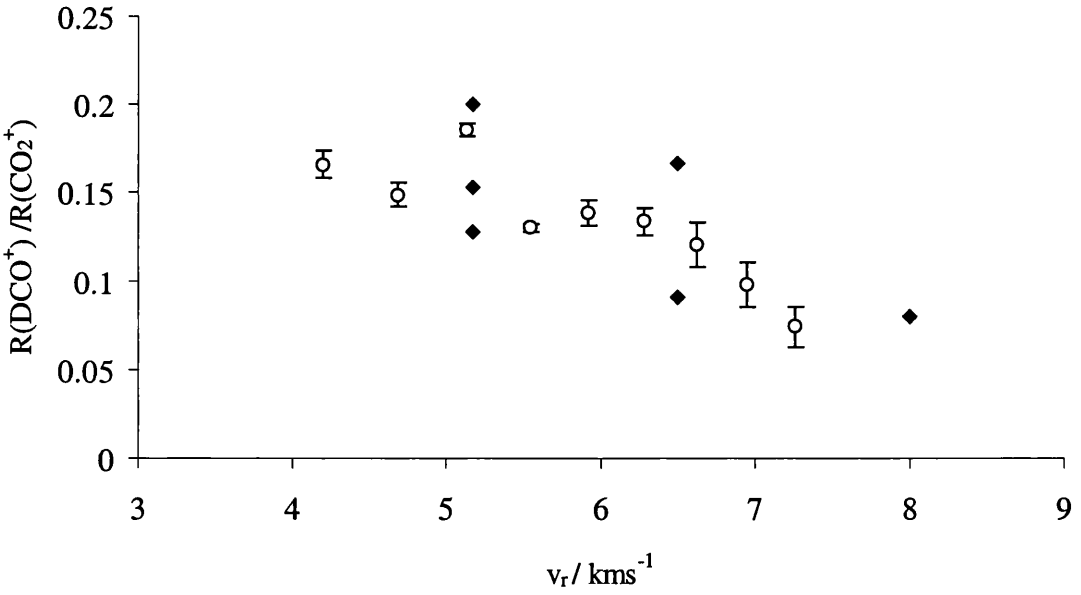

Figure 8.7 Dependence for the relative ion intensities of the DCO^+ and the CO_2^+ product ions, as a function of relative velocity of the reactants, following collisions of CO_2^{2+} with D_2. (♦) show data by Mrázek *et al.* and (○) represents the data from our experimental observations.

In order to compare our data to the absolute cross sections presented by Mrázek *et al.*, it is necessary to present the relative ratios of the bond forming and charge transfer reaction with respect to the dication. Although this ratio is pressure dependent, given that the experiments were performed under identical conditions, it is reasonable to conclude that these product to reactant ratios should be proportional and indicative of the absolute cross section. The data presented below in Figures 8.8 and 8.9 does clearly show that we do not observe any significant change in the absolute cross sections for the reactions of H_2 compared with those for the reactions with D_2 and the data produced by Mrázek *et al.* are in disagreement with our data. Although our relative ion intensities agree well with that produced by Mrázek *et al.*, our data does not agree with the absolute values of the cross section for the bond-forming product XCO^+ and the charge transfer product CO_2^+. Mrázek *et al* show that the cross-section for the formation of the CO_2^+ product ion to be approximately twice that for the reactions of CO_2^{2+} with H_2 compared to that produced in reactions with D_2.

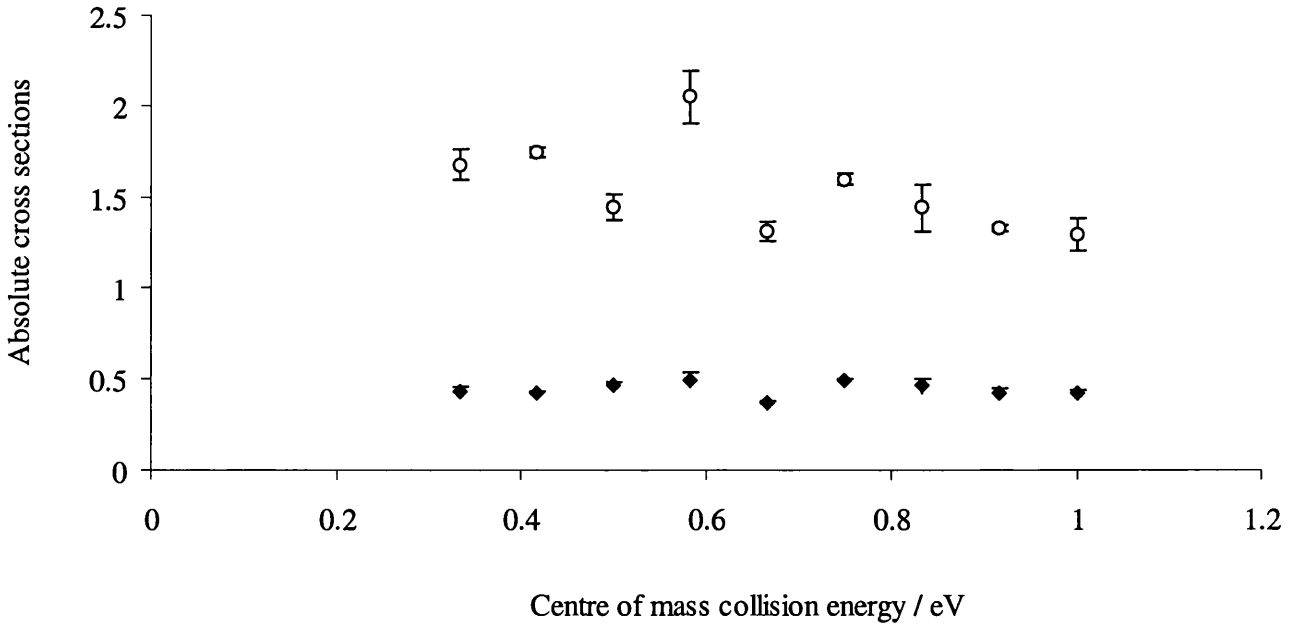

Figure 8.8 Product to reactant ratios for the CO_2^+ product ions is represented by (○) and DCO^+ is represented by (♦), as a function of centre of mass collision energy, following collisions of CO_2^{2+} with D_2

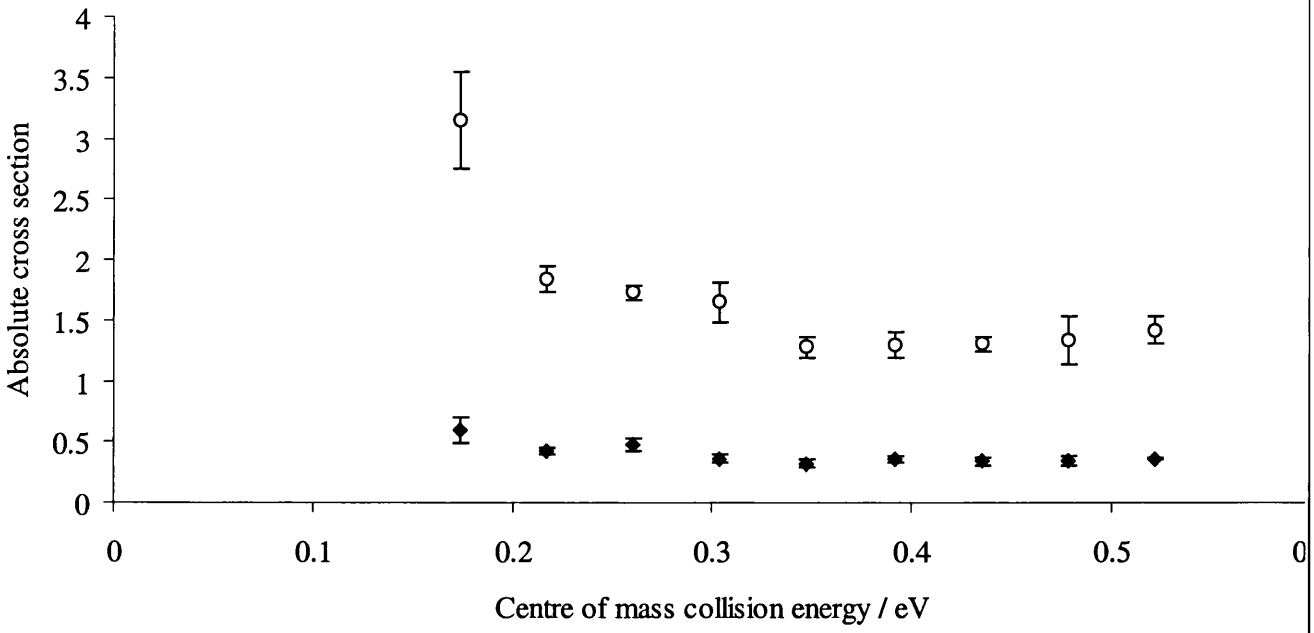

Figure 8.9 Product to reactant ratios for the CO_2^+product ions is represented by (○) and HCO^+ is represented by (♦), as a function of centre of mass collision energy, following collisions of CO_2^{2+} with H_2

Studies carried out by the same group on the $CF_2^{2+}/H_2/D_2$ collision system, show that the ratio of ion products of the bond forming reaction, (XCF_2^+) to the charge transfer reaction (CF_2^+) to be in good agreement with the data produced by Newson and Price for the same system and show an absence of any isotope effect. For the $CF_2^{2+}/H_2/D_2$ collision system Newson and Price and Z. Herman *et al.*, both observe a gradual increase in the bond forming product with decreasing collision energy and that at a given collision energy it is equally probable to form DCF_2^+ from CF_2^+ and D_2 and HCF_2^+ from CF_2^{2+} and H_2. Their data do not show the cross section for the charge transfer product to be significantly different from collisions with H_2 compared with D_2 unlike the data produced by Mrazek *et al.* for the charge transfer reaction in the $CO_2^{2+}/H_2/D_2$ collision system. The fact that Mrazek *et al.* show the cross-section for the formation of the CO_2^+ product ion to be approximately twice that for the reactions of CO_2^{2+} with H_2 compared to those for the reactions with D_2 is in conflict with our experimental data. We feel that this may be due to

a systematic error in the study conducted by Mrázek *et al.* and requires further investigation.

8.7 Conclusion

Relative yields of the electron transfer and bond forming product ions, following collisions between CF_3^{2+} and H_2/D_2 have been recorded as a function of centre of mass collision energy. The ratio of the bond forming product ions indicate that no isotope effect is in operation when H_2 is used in place of D_2 and the probability of forming XCO^+ is independent of the choice of hydrogen isotope. The collision energy dependence is indicative of a reactive pathway in which there is no energy barrier.

Our relative cross sections agree with those produced by Mrázek *et al.* however we are in disagreement with the absolute cross sections produced for the CO_2^+ product ion by Mrázek *et al.* which show the cross section for formation of this product ion to be approximately twice as large for those produced from collisions with H_2 compared with D_2 and need further work to resolve.

References:

1 Z. Herman, J. Zabka, Z. Dolejsek, and M. Farnik, *Int. J. Mass Spectrom.* **192,** 191-203 (1999).

2 K. A. Newson and S. D. Price, *Chem. Phys. Lett.* **269,** 93-98 (1997).

3 S. D. Price, S. A. Rogers, and S. R. Leone, *J. Chem. Phys.* **98,** 9455-9465 (1993).

4 S. A. Rogers, S. D. Price, and S. R. Leone, *J. Chem. Phys.* **98,** 280-289 (1993).

5 M. Manning, S. D. Price, and S. R. Leone, *J. Chem. Phys.* **99,** 8695-8704 (1993).

6 C. E. Melton and G. F. Wells, *J. Chem. Phys.* **27,** 1152 (1957).

7 Z. Herman, P. Johnathon, A. G. Brenton, and J. H. Beynon, *Chem. Phys. Lett.* **41,** 433 (1989).

8 L. Mrázek, J. Zabka, Z. Dolejsek, J. Hrusak, and Z. Herman, *Journal of Physical and Chemical A* **104,** 7294-7303 (2000).

9 Y. Y. Lee, S. R. Leone, P. H. Champkin, N. Kaltsoyannis, and S. D. Price, *J. Chem. Phys.* **106,** 7981-7994 (1997).

Chapter 9

Further work

The experimental results contained in this thesis demonstrate the power of time of flight mass spectrometry as a means of quantifying the intensity of a given channel of reaction between molecular dications and neutral collision partners, Such data provides a clearer picture and a better understanding of the dynamics of these reaction mechanisms. The use of isotopic collision partners has been demonstrated to be a useful probe of the reaction dynamics allowing more to be learnt about the reaction dynamics.[1-12]

There is an increasing interest in this field of work and there remain a large number of collision systems yet to be investigated. Work is currently underway, for example investigating, CF_3^{2+}/H_2O, CF_3^{2+}/H_2S, CF_2^{2+}/H_2O and CF_2^{2+}/H_2S collision systems. This work is prompted by work undertaken previously for the CF_2^{2+}/H_2 collision system where H^- was transferred to the dication to form HCF_2^+.[1] The investigation of these systems will determine whether this type of reactivity i.e. abstraction of OH^- or SH^- to yield $HOCF_2^+$ or $HSCF_2^+$ is applicable.

Although the apparatus discussed in this thesis provides a powerful means of studying the dynamics of collisions between molecular dications and neutral collision partners, work is currently underway in developing a two-dimensional position-sensitive coincidence (PSC) spectrometer to discover more about the dynamics of the approach of the reactant dication to a neutral molecule and the energies and relative motions of the products following these encounters. In addition the apparatus will provide data on the vibronic structure of the reactant dication.

The methodology employed in this new experiment will provide a means to study the electronic structure of fragment molecular dications, such as CF_2^{2+} and CF_3^{2+}, which cannot be probed using conventional techniques.

References

1 K. A. Newson and S. D. Price, *Chem. Phys. Lett.* **269,** 93-98 (1997).

2 K. A. Newson and S. D. Price, *Chem. Phys. Lett.* **294,** 223-228 (1998).

3 C. E. Dateo and D. C. Clary, *J. Chem. Soc. Faraday Trans.* **85,** 1685-1696 (1989).

4 P. M. Hierl, *J. Chem. Phys.* **67,** 4665-71 (1977).

5 P. B. Armentrout, *Acs Symposium Series* **502,** 194-209 (1992).

6 J. L. Elkind and P. B. Armentrout, *J. Chem. Phys.* **84,** 4862-4871 (1986).

7 R. H. Schultz and P. B. Armentrout, *J. Chem. Phys.* **96,** 1036-1045 (1992).

8 K. M. Ervin and P. B. Armentrout, *J. Chem. Phys.* **85,** 6380-6395 (1986).

9 K. M. Ervin and P. B. Armentrout, *J. Chem. Phys.* **84,** 6750-6760 (1986).

10 K. M. Ervin and P. B. Armentrout, *J. Chem. Phys.* **84,** 6738-6749 (1986).

11 R. A. Dressler, R. H. Salter, and E. Murad, *J. Chem. Phys.* **99,** 1159-1171 (1993).

12 K. Tanaka, T. Kato, P. M. Guyon, and I. Koyano, *J. Chem. Phys.* **79,** 4302-4305 (1983).